


1994

Monolayer studies of novel synthetic compounds and biological systems

Jingyuan Wang
Iowa State University

Follow this and additional works at: <https://lib.dr.iastate.edu/rtd>

 Part of the [Biophysics Commons](#), and the [Physical Chemistry Commons](#)

Recommended Citation

Wang, Jingyuan, "Monolayer studies of novel synthetic compounds and biological systems " (1994). *Retrospective Theses and Dissertations*. 10863.
<https://lib.dr.iastate.edu/rtd/10863>

This Dissertation is brought to you for free and open access by the Iowa State University Capstones, Theses and Dissertations at Iowa State University Digital Repository. It has been accepted for inclusion in Retrospective Theses and Dissertations by an authorized administrator of Iowa State University Digital Repository. For more information, please contact digirep@iastate.edu.

INFORMATION TO USERS

This manuscript has been reproduced from the microfilm master. UMI films the text directly from the original or copy submitted. Thus, some thesis and dissertation copies are in typewriter face, while others may be from any type of computer printer.

The quality of this reproduction is dependent upon the quality of the copy submitted. Broken or indistinct print, colored or poor quality illustrations and photographs, print bleedthrough, substandard margins, and improper alignment can adversely affect reproduction.

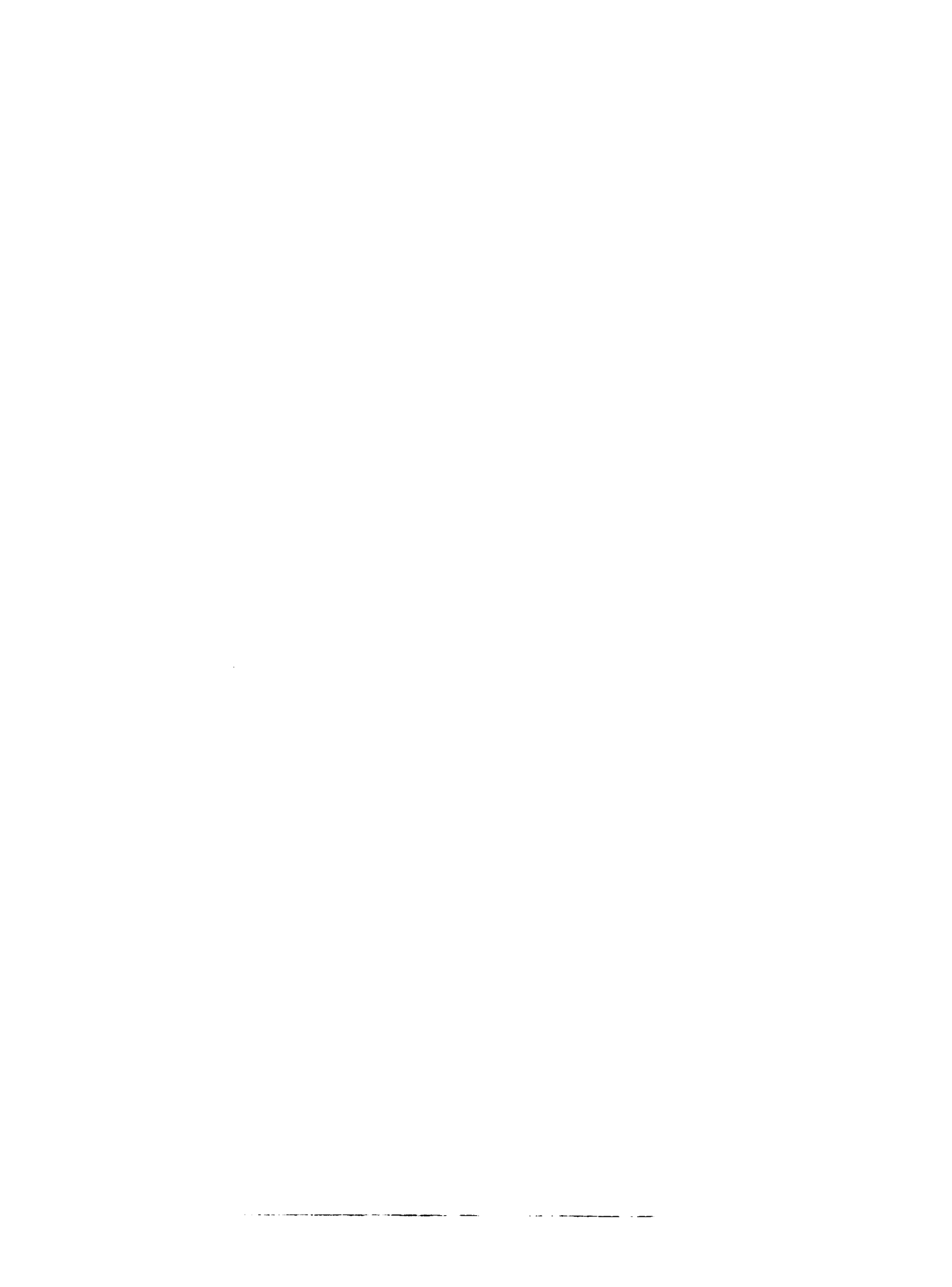
In the unlikely event that the author did not send UMI a complete manuscript and there are missing pages, these will be noted. Also, if unauthorized copyright material had to be removed, a note will indicate the deletion.

Oversize materials (e.g., maps, drawings, charts) are reproduced by sectioning the original, beginning at the upper left-hand corner and continuing from left to right in equal sections with small overlaps. Each original is also photographed in one exposure and is included in reduced form at the back of the book.

Photographs included in the original manuscript have been reproduced xerographically in this copy. Higher quality 6" x 9" black and white photographic prints are available for any photographs or illustrations appearing in this copy for an additional charge. Contact UMI directly to order.

UMI

A Bell & Howell Information Company
300 North Zeeb Road, Ann Arbor, MI 48106-1346 USA
313/761-4700 800/521-0600



Order Number 9518452

Monolayer studies of novel synthetic compounds and biological systems

Wang, Jingyuan, Ph.D.

Iowa State University, 1994

U·M·I
300 N. Zeeb Rd.
Ann Arbor, MI 48106

Monolayer studies of novel synthetic compounds and biological systems

by

Jingyuan Wang

A Dissertation Submitted to the
Graduate Faculty in Partial Fulfillment of the
Requirements for the Degree of
DOCTOR OF PHILOSOPHY

Department: Chemistry
Major: Physical Chemistry

Approved:

Signature was redacted for privacy.

In Charge of Major Work

Signature was redacted for privacy.

For the Major Department

Signature was redacted for privacy.

For the Graduate College

Iowa State University
Ames, Iowa

1994

To my parents

TABLE OF CONTENTS

GENERAL INTRODUCTION	1
Dissertation organization	5
CHAPTER 1. PREPARATION AND METHODS OF CHARACTERIZATION OF MONOLAYERS	5
Introduction	5
Formation of stable monolayers at the air-water interface	7
Surface pressure/area isotherms	8
Surface potential measurements	13
Langmuir-Blodgett films	17
Methods of characterization	19
X-ray and neutron reflection	21
Raman scattering	25
References	27
CHAPTER 2. NEUTRON AND X-RAY REFLECTION STUDY OF FULLERENE C₆₀ AND ITS DERIVATIVES AT THE AIR-WATER INTERFACE	31
Abstract	31
Introduction	32
Theory	33
Experimental details	39
Results and discussion	41

C₆₀ fullerenes	41
C₆₀-dodecylamine	48
C₆₀-propylamine	57
Conclusions	68
Acknowledgements	69
References	69
CHAPTER 3. FORMATION OF NANOSCALE SIZE PARTICLES WITHIN A CHANNEL PROTEIN MONOLAYER	72
Abstract	72
Introduction	73
Experimental details	75
Protein preparation	75
Monolayer methods	78
Formation of cadmium and zinc sulfide clusters	78
Result and discussion	79
Acknowledgement	90
References	90
CHAPTER 4. MONOLAYER STUDY OF CLEAVABLE PHOSPHOLIPIDS	92
Abstract	92
Introduction	93

Experimental details	95
Synthetic methods	95
Monolayer techniques	96
Results and discussion	97
π -A isotherms on water subphases	97
π -A isotherms on aqueous polyethylene glycol	97
Conclusions	112
Acknowledgements	113
References	113
CHAPTER 5. MONOLAYER AND SPECTROSCOPIC STUDIES OF BACTERIOCHLOROPHYLL A	115
Abstract	115
Introduction	116
Materials and methods	117
Materials	117
Methods	118
Results and discussions	119
Monolayer properties of pure components	119
Interaction of BChl <i>a</i> and DMPC in monolayer systems	125
UV-Vis absorption spectra	133
SERRS	138

Conclusions	138
References	140
SUMMARY	143
REFERENCES	146
ACKNOWLEDGEMENTS	150

GENERAL INTRODUCTION

Amphiphilic compounds have been extensively studied because of their use in a variety of applications including, for example, drug delivery, the surfactant industry, and microelectronics. The design and synthesis of novel amphiphiles also provide the possibility to prepare model biological systems, including those mimicking the cell membrane, at the air-water interface. The first step in utilizing such compounds is their characterization. A study of both the film thickness and in-plane structure at the air-water interface defines not only the aggregation properties, but also information about interaction between amphiphiles and the subphase molecules or ions. The film can be transferred from the water surface onto a solid substrate (called Langmuir-Blodgett film) and subsequently investigated by spectroscopic and imaging techniques. This approach has been used to design new diodes using the Langmuir-Blodgett technique thereby initiating the molecular computer age. Scanning tunneling microscopy (STM) and atomic force microscopy (AFM) make it possible to obtain high resolution images of these well ordered films. Recently, monolayer techniques have also been used in biomineralization studies in which specific types of crystals can be formed by controlling their nucleation at the head groups of these interfacial monolayers [1].

Fullerenes, newly discovered all carbon compounds, have attracted considerable interest because of their unusual properties. For example, electrochemical studies of C_{60} and C_{70} have confirmed that they are relatively strong oxidizing agents, similar to methyl viologen and flavin chromophores, and their first 1-electron reduction potentials are more

positive than most polycyclic aromatic hydrocarbons [2-4]. Photochemical studies have shown that the singlet and triplet excited states of fullerenes are relatively long-lived and electron transfer between C_{60} and polymers has been observed [5-15]. The chemical reactivity of C_{60} has been studied by a number of research groups [16-21] and found to be similar to that of most aromatic compounds. The aromatic character is believed to be due to the pyracylene unit [22]. There are some reports that fullerenes can be spread on a water surface to form monolayer structures [23-31]. However, it is not clear based on these studies why a hydrophobic, non-amphiphilic compound such as this is able to form stable monolayers. If C_{60} is really be able to form a stable monolayer, then it is possible to put C_{60} molecules into a mixed Langmuir-Blodgett structure with other materials like photosynthetic pigments to observe the electron transfer between the host and the guest molecules. For these reasons, additional studies of C_{60} and its derivatives at the air-water interface were carried out. The research for this part of the dissertation was undertaken using neutron and X-ray reflection techniques as well as the Langmuir trough methods.

Recently, nanoscale size particles have been extensively studied [32-33] because they can provide information concerning the physical and chemical consequences accompanying the transition from individual molecules to bulk materials. The preparation of small clusters in a controlled manner relies upon the use of methods which limit their growth by physical confinement. Many different approaches have been used to prepare particles of a desired size [34-40]. Yet, the control of the size distribution of small particles remains challenging and new methods are needed to prepare uniform particles. One such method, described in Chapter 3 of this dissertation for producing nanoscale cadmium and zinc sulfides, combines

monolayer techniques with the use of a small-cavity confinement system. A gap-junction protein called MIP-26 (major intrinsic protein) was used as the host reaction vessel. This protein has a number of advantages for this particular application: its amino acid sequence is known from cDNA cloning, it is soluble in lipid solvents but insoluble in water; it forms strong organized monolayers and it is available in large amounts.

Phospholipids are major components of cell membranes and play an important role in many biological processes. Derivatives of phospholipids capable of changing the types of structures which they form in aqueous solutions with a change in solution composition are of considerable current interest [41-43]. The ability to change from micellar or vesicular form to either a non-surfactant or alternate aggregated form, can result in entrapment or release of materials and should have many applications in process technologies and in drug delivery systems [44]. In Chapter 4 of this dissertation, the monolayer behavior of three isomeric phospholipids is described. These are new examples of vesicle-forming, cleavable surfactants. By acid-catalyzed hydrolysis, a *vic*-diol can be formed from a ketal ring located at various points along an aliphatic chain of the phospholipid. Because the phospholipids have relatively high solubilities, a polyethylene-based, non-water subphase was first used in order to obtain stable monolayers. The results obtained from the surface pressure-area isotherms were compared with that of CPK models.

Bacteriochlorophyll *a* (Bchl *a*) is the major light absorbing compound in purple photosynthetic bacteria. It plays a crucial role in the primary events of the photosynthetic process beginning with the capture of light to the subsequent energy transfer in the light-energy conversion process in the photosynthetic reaction centers where charge separation

occurs [45]. Only one previous report on monolayer properties of Bchl *a* has been published [46]. In Chapter 5, the monolayer properties of Bchl *a* were investigated at the nitrogen-water interface. This study focuses on Bchl *a* monolayers with and without phospholipids as matrix molecules. The interaction between Bchl *a* and these phospholipids at the nitrogen-water interface was investigated by both surface pressure-area and surface potential measurements.

Dissertation Organization

This dissertation is composed of an introduction to the monolayer techniques and their characterization methods (Chapter 1), four papers and a general summary. Chapter 2 was published in *Thin Solid Films*, Volume 242, page 40. Other authors listed on the paper are D. Vaknin, R. A. Uphaus, K. Kjaer and M. Lösche. Chapter 3 was published in *Thin Solid Films*, Volume 242, page 127. This work was carried out in collaboration with S. Amaeenuddin and D. A. Rintoul, Department of Biology, Kansas State University. Chapter 4 was published in *Thin Solid Films*, Volume 242, page 277. R. A. Uphaus, Jinkang Wang and D. A. Jaeger are coauthors on this paper. Chapter 5 conforms to the style for submission to *The Journal of Physical Chemistry*. References cited in the General Introduction follow the Summary.

CHAPTER 1. PREPARATION AND METHODS OF CHARACTERIZATION OF MONOLAYERS

Introduction

Considerable time has passed since the formation of oil films on water was first observed. The so-called phase boundary or interface occurs in nature and can be observed in the surrounding environment. The earliest report of the application of organic thin films is believed to be the Japanese printing art called *sumi-nagashi*, in which a dye material was spread on water surface and then transferred onto a piece of paper [1]. This technique was further developed and is now used in many applications both in industry and in academic research. This was the initial model for the development of the monolayer techniques.

Here, the contributions of some key individuals in the development of organic monolayer techniques and their applications are briefly reviewed. The first important person that should be mentioned is Benjamin Franklin. He began his experiments on the spreading of oil on various stretches of water during his visits to Europe as the principal representative of the American States. The most important experiment which Franklin carried out was the Clapham experiment in which he studied the curious effects of vibration at the interface of oil and water [2].

Before scientific research was directed towards studying the basic theory of surface phenomenon, a number of persons tried different experiments concerning the behavior of oil

on the surface of water. Among them, the independent work of John Shields and John Aitken created considerable interest [3, 4]. Lord Rayleigh was the first person to observe the effect of "contamination" on the surface tension of water and realized the possibility of obtaining a monolayer structure on the water surface [5]. Later, Agnes Pockles, by using a simple device designed by herself, measured quantitatively the change of surface tension due to the "contamination" of water [6]. The work of Irving Langmuir was very important in the development of the scientific foundation concerning monomolecular films. Langmuir realized the importance of molecular orientation and the interaction between polar molecules and the subphase and designed the very first model of the film balance [7-10]. Because of his significant contribution to the field of organic thin films, Langmuir deserves the title of the "father of monolayers". At the same time, Catherine Blodgett initiated the first experiments involving transfer of fatty acid monolayers from the water surface to a solid substrate [11]. The transferred film, later named a Langmuir-Blodgett film, made it possible to study molecular interaction and orientation in a monolayer by means of spectroscopic and many other techniques.

In this chapter, the theoretical background for the formation of monolayers is reviewed in terms of thermodynamics. Unless otherwise stated, the subphase is pure water. Next, different techniques that have been used to characterize both the Langmuir monolayers and the Langmuir-Blodgett films are described.

Formation of stable monolayers at the air-water interface

When water is placed on a waxy surface, it "beads up", forming distorted spheres. This behavior is due to an imbalance of the intermolecular forces at the surface of water. In fact, because of hydrogen bonding in the bulk liquid phase, water tends to form a loosely defined network. This network is modified at the edge of the bulk phase. This surface phenomenon is best described by the surface tension. Surface tension is the energy required to increase the surface area of a liquid by a unit amount. More precisely, it is the differential change in free energy with change of surface area at constant temperature, pressure and composition. If γ is used to indicate the surface tension, then

$$\gamma = \left(\frac{\partial G}{\partial s}\right)_{T,P,n_i} \quad (1)$$

where G is the Gibbs free energy of the system, s the surface area, the temperature T pressure P and composition n_i are held constant.

When a monolayer is present on the surface of water, it tends to reduce the surface tension of pure water. The surface pressure is then defined as the difference between the surface tension of pure water and that of monolayer covered water surface,

$$\Pi = \gamma - \gamma_0 \quad (2)$$

where Π is the surface pressure, γ the surface tension in the absence of a monolayer and γ_0

the value when the monolayer is present.

According to Langmuir, an ideal monolayer-forming material such as stearic acid should have two distinct regions, a hydrophilic head group and a hydrophobic tail. Figure 1 shows the structure of stearic acid. The interaction of the polar head group with the subphase is essential to form stable monolayers. From the thermodynamic point of view [12], a stable monolayer is formed when the interaction between the film-forming material and water are stronger than that between the molecules themselves, thus the system is in a lower energy state. Also, the hydrocarbon chain should be sufficiently long. It was determined that at least 13 carbon atoms are required in an amphiphilic compound in order that it form stable monolayers. The relative magnitude of van der Waals forces of the film forming material, as well as the interaction between the polar head groups of amphiphiles and the subphase determine the states of the monolayers. This will be discussed in the following section.

Surface pressure/area isotherms

Even though there are other methods for studying Langmuir monolayers, the surface pressure/area isotherm is the most used and has been proven to be very successful in characterizing monolayer properties. Technically, it is possible to record equilibrium surface pressure on a point to point basis, but this is very time consuming. It is more common to compress a film continuously at a constant rate. In this case, the surface pressure is not at equilibrium no matter how slowly the barrier is moved. Figure 2 shows the typical surface pressure/area isotherm of stearic acid at 20 °C.

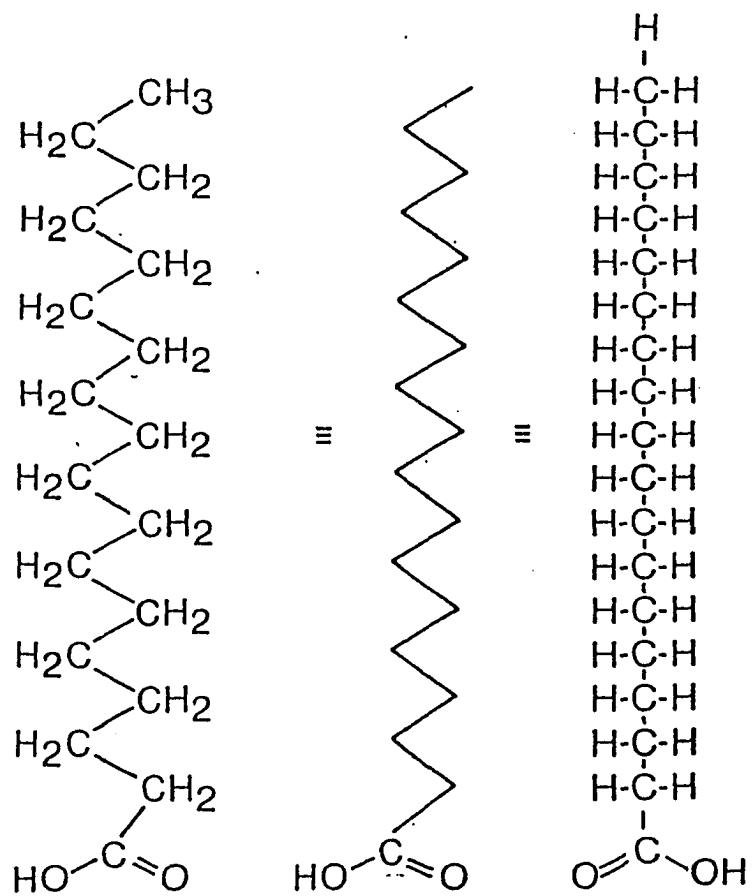
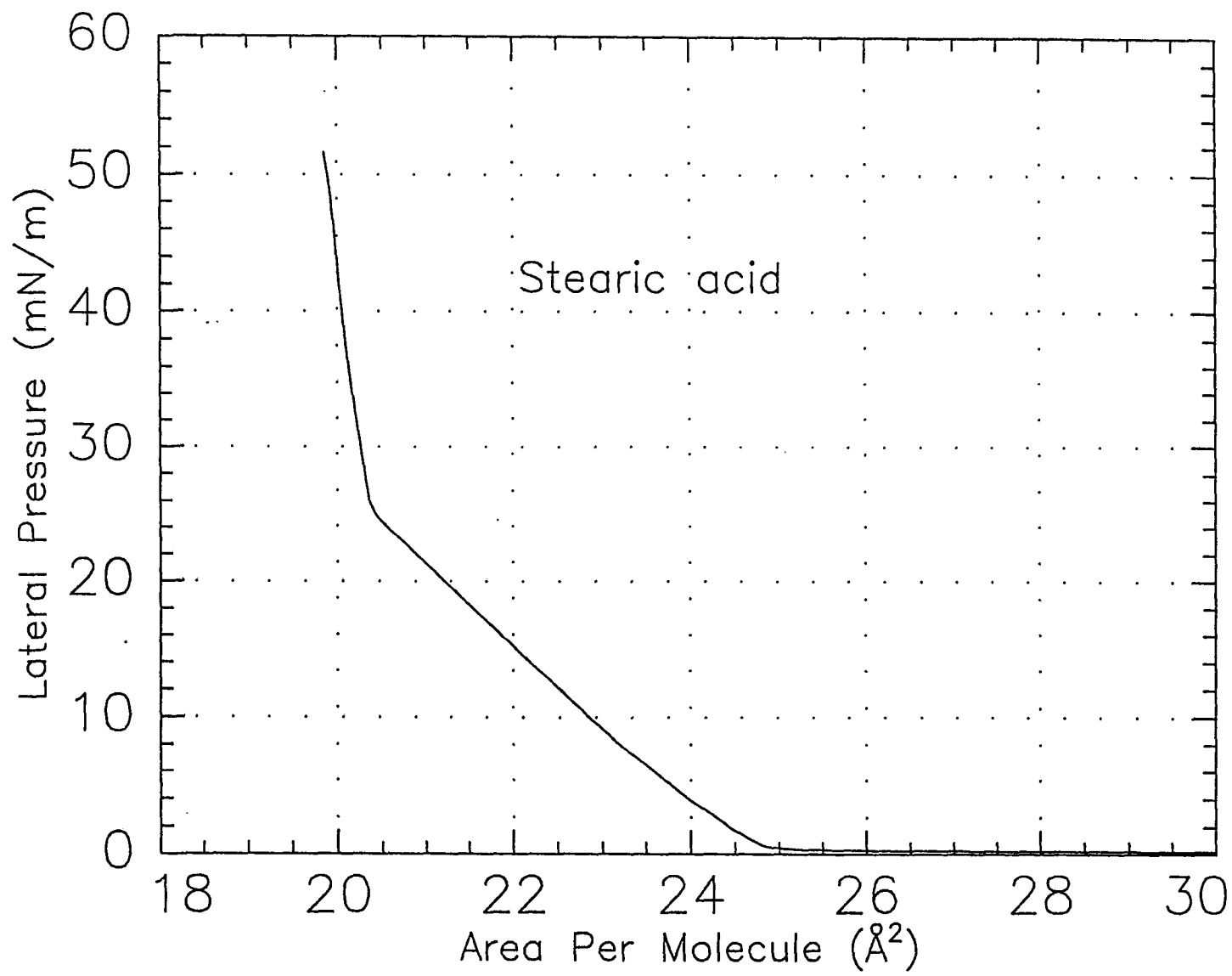


Figure 1. Various representations for the structure of stearic acid.

Figure 2. Surface pressure/area isotherm of stearic acid on pure water at room temperature.



The phase transition of two dimensional monolayers is analogous to that of three dimensional matter, although many other properties of the two systems cannot be compared. In discussing the isotherm of stearic acid, several different regions are notable. When the area per molecule is bigger than 30 \AA^2 , the surface pressure remains zero. In this region, the Van der Waals forces between the hydrophobic tails of individual stearic acid molecules are very weak and the molecules can move freely on the water surface. The molecules are considered to be in the gas phase, comparable to a three dimensional gas. When the surface area is decreased by moving the barrier, the molecular interaction becomes stronger because the molecular distance is greatly reduced and the molecules begin to orient on the water surface. As in the isotherm of stearic acid, surface pressure begins to build up when the surface area per molecule is smaller than 25 \AA^2 . Two different linear region are observed, the first is in the region between 25 \AA^2 and 20.5 \AA^2 and the second is in the region between 20.5 \AA^2 and 20 \AA^2 . The first region which has a higher compressibility is defined as a "liquid phase" and the second region a "solid phase". At a surface pressure of 25.6 mN/m , there is a sharp change in the slope of the isotherm and this is defined as the phase transition point of the two dimensional monolayer systems. It should be mentioned that the compressibility of a monolayer as defined by the following equation:

$$c = -1/A \left(\frac{\partial A}{\partial \Pi} \right)_{T,P,N_i} \quad (3)$$

is approximately constant in both the liquid and solid regions of the isotherm, where A is

the surface area per molecule, Π is the surface pressure, and the temperature T , Pressure P and composition n_i are held constant.

The liquid phase of stearic acid monolayer is known as "liquid-condensed" phase [13] and the stearic acid monolayer is often described as "liquid-condensed" film, in which there is a sharp phase transition. A totally different type of isotherm is often observed, in which there is no clear phase transition and the surface area per molecule remains at a larger value as compared with that of the closed packing model. The linear region of these isotherms are defined as a "liquid expanded" phase. This type of isotherm is observed when the disruption of the hydrocarbon chains of an amphiphilic compound causes difficulty in packing. The isotherm of oleic acid at room temperature represents a typical example of this kind of compounds.

Further compression of the monolayer will result in breaking of the film. In the case of stearic acid, the collapse of the monolayer occurs when the area per molecule is smaller than 20 \AA^2 . The collapse state of monolayers is not well defined and is generally believed to result in disordered multilayers. The collapse points are not unique for a given amphiphile and depend on the conditions under which the material is compressed.

Surface potential measurements

In addition to surface pressure-area isotherms, surface potential measurements provide another useful method for characterizing Langmuir monolayers. The surface potential at a given interface will change if a highly oriented monolayer is present on the surface. A change

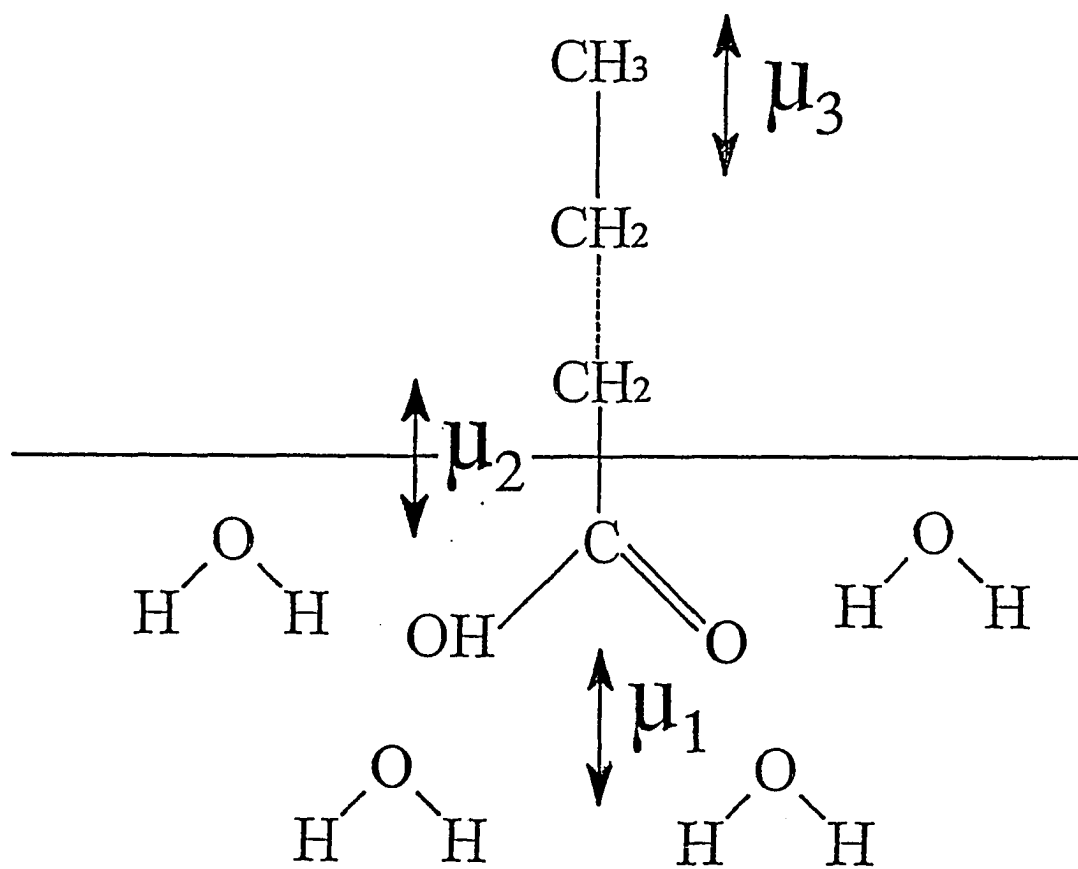


Figure 3. Orientations of dipoles of amphiphilic molecules at the air-water interface, e.g., subphase water (μ_1), polar (μ_2), and alkyl chain (μ_3) part of the film forming material.

in the orientation of the molecules at the air-water interface will result in a change in the dipole moment at the interface.

Different models have been developed for estimating the group dipole moments at the air-water interface. In the Helmholtz model, it is assumed that the surface potential change at the interface is due to the uniform orientation of the film forming molecules. This has been shown to be an improper model because a) the orientation of molecules in the monolayer is not always uniform; b) the polarizabilities of different regions across the air-water interface may be significantly different, which contributes to the overall group dipole moments [14].

Vogel and Möbius [15] treated the monolayer as a two-layer capacitor, one accounting for dipoles at the monolayer-air interface and the other for dipoles at the monolayer-water interface. The second capacitor includes the dipole moment of the headgroup, the polarization of the subphase and any contribution from the double layer. This VM approach introduces, for the first time, a partial dipole compensation technique in which the two effective dipole moments are estimated. Using this model, Vogel and Möbius have evaluated the headgroup dipole moments of two phospholipids, i.e. DPPC and DPPE [15b].

Based on the ideas of Davies and Rideal [16], Demchack and Fort [17] assigned local permittivities to different regions across the air-water interface. Figure 3 shows the orientation of different dipoles at the air-water interface. In this model, the surface potential change comes from three contributions:

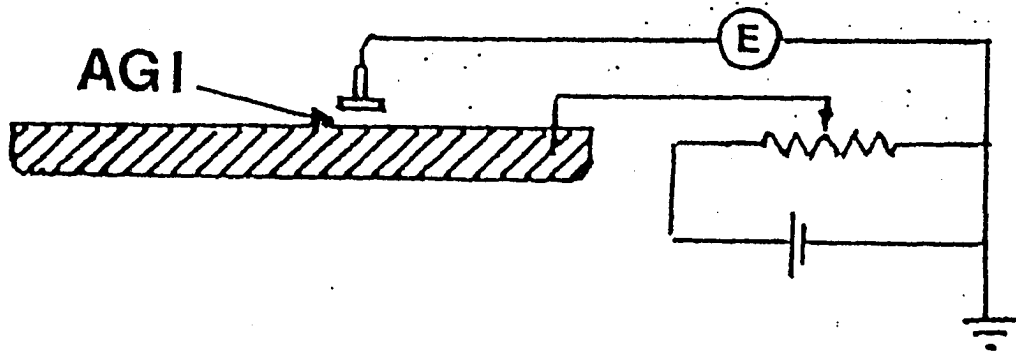


Figure 4. Simple schematic diagram for measuring surface potential change ΔV , AGI is the gap ionized α -emitter, E is the voltmeter.

$$\Delta v = \Delta v_1 + \Delta v_2 + \Delta v_3 \quad (4)$$

$$= 4\pi n(\mu_1 + \mu_2 + \mu_3) \quad (5)$$

where μ_1 is the dipole moment of subphase water, μ_2 the dipole moment of polar group and μ_3 the dipole moment of alkyl chains of the film forming material. A number of aliphatic compounds have been evaluated using this model [14].

Compared with the surface pressure-area isotherm measurement, surface potential measurements provide much more sensitive information about the orientation of the monolayers. Figure 4 shows a simple apparatus for measuring the surface potential. The electrode that has been used in the course of this dissertation is based on this simple circuit. The working electrode which is held about 5 mm above the water surface is coated with an α emitter (polonium or americium). The ionization of air makes the gap between the electrode and the water surface sufficiently conducting so that the potential difference can be measured by a high-impedance ($>10^{16}\Omega$) voltmeter [12, 18 and 19].

Langmuir-Blodgett films

When Langmuir monolayers are transferred from the subphase to solid substrates, they are termed Langmuir-Blodgett (L-B) films. L-B films can be characterized by a variety of spectroscopic and imaging techniques, and therefore are very important in the study of monolayer properties, especially the molecular interaction in two dimensional systems.

The most commonly used method of monolayer transfer is vertical dipping and

lifting. A substrate is first dipped into a monolayer-covered subphase and then withdrawn. The surface pressure is kept constant during the process of monolayer transfer. It is always best to transfer a monolayer in the "solid" region of the isotherms, but not essential to achieve a good quality L-B film. Repeated dipping and lifting steps produce a multilayer structure. Several factors need to be considered in obtaining good L-B films: (1) The film forming molecules themselves determine whether a tightly packed, uniform 2-D monolayer can be formed at the air-water interface. Some materials (e.g. glycerol and some lipids) are liquid at room temperature and highly viscous. It is extremely difficult for these molecules to orient at the air-water interface so as to maintain a homogeneous film even at high compression. These kinds of materials usually cannot be deposited on a solid substrate [20, 21]. An alternate way to transfer a highly viscous film is to lower temperature so that the film becomes more rigid and behaves like a "solid" film. Uniaxial materials (e.g. fatty acids, azo compounds, some dyes) readily form homogeneous two dimensional liquid-crystal-like structures and the L-B films of these materials are easily characterized [12,22-24]. Some other materials, such as chlorophylls, related porphyrins and proteins can be transferred to a solid substrate, but do not readily form well-organized homogeneous films [25]. Large domain structures are usually present in the monolayer of these materials and defects often occur when these materials are deposited onto a substrate. (2) Pure, deionized water is usually used as subphase. It has been shown that ions in the subphase can stabilize Langmuir monolayers [26] and therefore may be used to get better L-B films. For example, CdCl_2 is often added in the subphase when fatty acid monolayer is transferred, since the Cd^{2+} ion has

been shown to stabilize these monolayers. (3) Optically smooth substrates are often used for deposition of L-B films. The quality of the substrate is an important factor for obtaining satisfactory L-B films. The surface of substrate can either be hydrophilic or hydrophobic. Fresh cleaved mica surfaces are usually used for obtaining high resolution microscope images of L-B films. Optical and quartz glasses are examples of other substrates that are often used. Metal surfaces are also appropriate, especially if a roughened surface is required. Among the metals, silver and gold are the most commonly used. When a hydrophobic surface is needed, a hydrophilic surface is usually treated with ferric stearate or with silanes [27]. (4) Finally, the rate that a substrate can be withdrawn from the subphase is typically 1 mm per second. Even though an L-B film can be sometimes deposited very rapidly [28, 29] (1 cm per second), a slower lifting speed is preferred in order to produce good quality films.

Three possible multilayer structures can be formed when a continuous dipping and lifting mode is used to prepare L-B films. These are generally referred to as X, Y and Z type. Figure 6 shows the three multilayer structures.

Horizontal lifting is another way to deposit Langmuir monolayers on a solid slide, and is referred to as the Langmuir-Schaffer(L-S) transfer technique. L-S deposition does not always result in good films and therefore is only used for limited purposes [30].

Methods of characterization

X-ray and neutron scattering techniques have been used recently to characterize

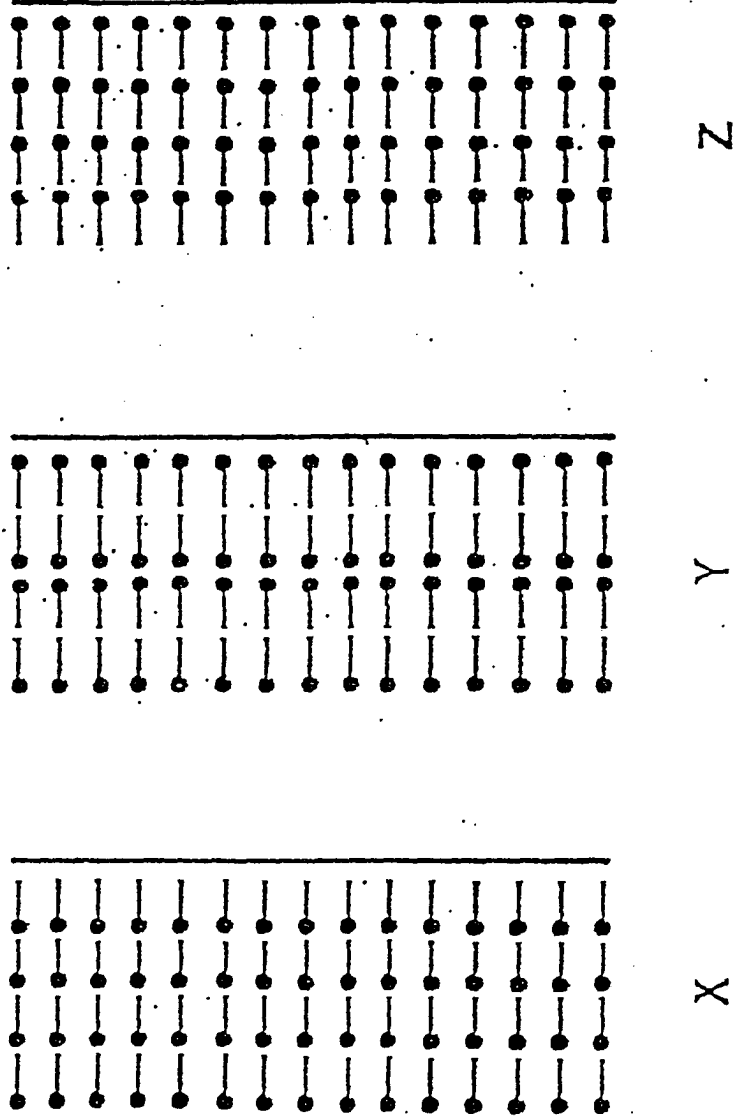


Figure 5. Structures of X, Y and Z type multilayers.

Langmuir monolayers and Langmuir-Blodgett films [31-38]. X-ray and neutron reflection techniques are particularly interesting because of their abilities to reveal structural information of a monolayer on a molecular level. An description of these two techniques and their application to Langmuir monolayers is given in this section. A brief introduction to Raman spectroscopy is also included. There are many other methods that have been used to characterize monolayers, i.e. dichroism, ellipsometry, infrared spectroscopy, atomic force microscopy (AFM) and scanning tunneling microscopy (STM). Applications of these techniques have been reported [2] but will not be discussed here.

X-ray and neutron reflection

X-ray and neutron reflection have been extensively applied to the study of Langmuir monolayers recently [39-43]. The optics of X-ray and neutron reflectivities at the air-water interface have been treated in detail elsewhere [38, 40] and only a simple case is discussed here to indicate the reflectivity principles.

Whereas X-ray reflection probes the variation of electron density normal to the interfacial plane, neutron reflection detects the variation in scattering length density across the interface. The average density across the surface varies from the air above the surface to the liquid-bulk density below the surface. The simplest approximation is to assume a discontinuous jump in density across the surface, *i.e.*, the change of the density is described by a step function. The corresponding reflectivity is known as the Fresnel reflectivity. In practice, the change of density across the interface is gradual and the reflectivity is modified

correspondingly.

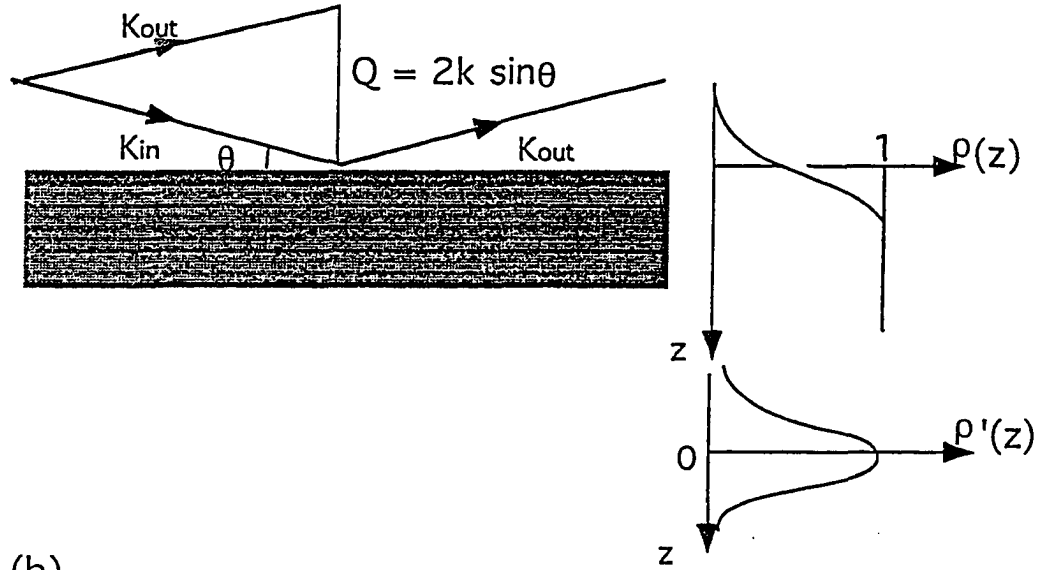
In Figure 6, a monochromatic X-ray or neutron beam with wavevector k_{in} , incident at an angle θ_0 is specularly reflected (i.e., exit angle $\theta_r = \theta_0 \equiv \theta$) with wave vector k_{out} . The wavevector transfer $Q \equiv k_{out} - k_{in}$ is used here as the independent variable and is strictly parallel to the surface normal n . By monitoring the incident and the reflected X-ray or neutron intensities, the reflectivity is reported as a function of Q . The density profile across the interface is also sketched in the right-hand side of Figure 6, in which $\rho(z)$ denotes the density and $\rho'(z)$ is the gradient of the density. If we consider the density $\rho(z)$ is a step function, the reflectivity is Fresnel reflectivity and can be described by the following equation

$$R_F = [Q_c / (Q_0 + Q_1)]^4 \quad (6)$$

where Q_c denotes the wavevector transfer corresponding to total reflection, Q_0 the wave vector transfer which correlates the incident and the reflected wavevectors, and Q_1 the wavevector transfer that associates with the incident and the refractive wavevectors. In the limit of $Q_0 \gg Q_c$, the refraction of the transmitted beam is negligible and this result is readily expanded to give an even simpler result

$$R_F \approx [Q_c/2Q_0]^4 \quad (7)$$

(a)



(b)

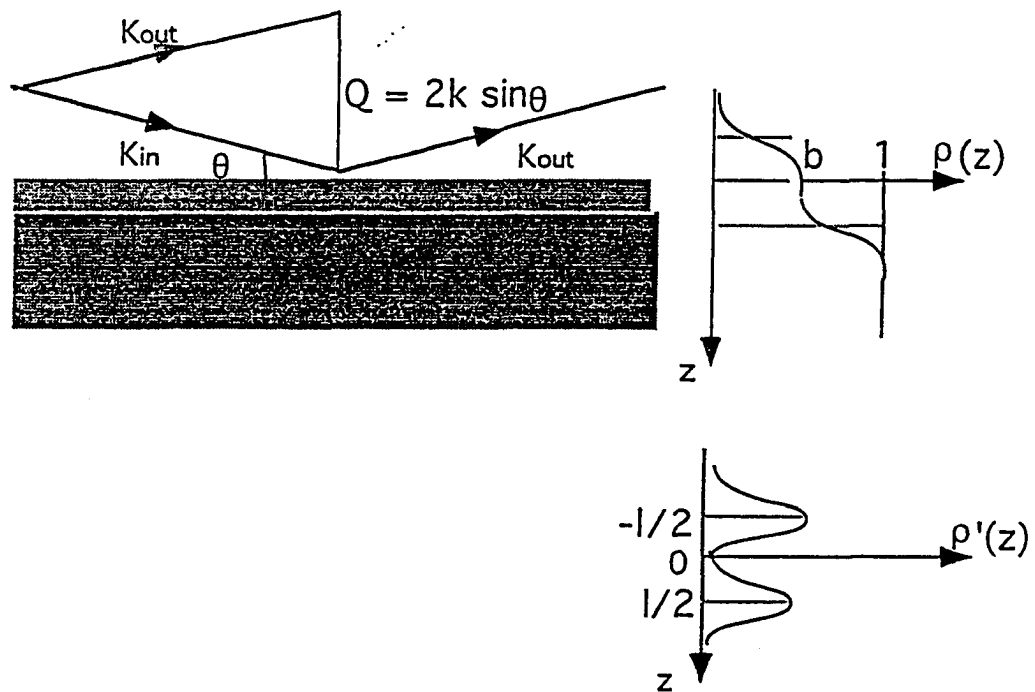


Figure 6. Specular reflection of a monochromatic beam on a pure substrate (a) and a monolayer covered substrate (b). The density profile is on the right-hand side. The reflectivity versus wavevector transfer is related to the Fourier transform of the gradient of the density. See text for detail.

So far, the reflectivity of a sharp and flat surface in which the scattering density is described by a step function has been considered. Because the change of scattering density across the interface is always gradual, it is necessary to consider the surface roughness. As a simple example, the ideal discontinuity in density at the surface, $z = 0$, is smeared by a Gaussian function (see right-hand side of Figure 6a) $(2\pi)^{-1/2}\sigma^{-1}\exp(-z^2/2\sigma^2)$. The Fourier transform of a normalized Gaussian is itself a Gaussian,

$$G(Q) = \int_{-\infty}^{\infty} C \exp\left(\frac{-z^2}{2\sigma^2}\right) \exp(iQz) dz = \exp\left(-\frac{1}{2}Q^2\sigma^2\right) \quad (8)$$

where C is the normalization constant $(2\pi)^{-1/2} \sigma^{-1}$. The reflectivity, relative to the Fresnel reflectivity, is the square of $G(Q)$,

$$R(Q)/R_F(Q) = \exp(-Q^2\sigma^2) \quad (9)$$

The application of reflectivity theory to Langmuir monolayers or Langmuir-Blodgett films is now considered. If a flat monolayer is deposited on a substrate, the Fresnel reflectivity is then the result of the interference between the singly and multiply reflected waves. Equations (6) and (7) are modified accordingly (result not given here). If we assume the monolayer is homogeneous and has a different density compared with that of the substrate, then the density profile of the monolayer-covered surface can be treated as the Gaussian smearing of two discontinuities (see Figure 6b). The Fourier transform of the $\rho'(z)$

can be written as:

$$G_1(Q) = \exp(-Q^2\sigma^2/2)[b(-2i) \sin(Ql/2) + \exp(iQl/2)] \quad (10)$$

where b is the height of the density profile of the monolayer. In practice, a sinusoidal modulation of the density profile is often made in order to fit the experimental data. Once the scattering density profile is known, the reflectivity of the monolayer-covered surface can be calculated and best fit parameters that are used to describe the properties of the monolayer are available.

Because the scattering length density varies from element to element, the isotope effect is significant in neutron scattering experiments. Deuterated compounds and heavy water (D_2O) are often used in order to resolve the conformation of the underlying monolayers. In addition to specular reflection as discussed above, the grazing incidence diffraction (GID) technique is also used to obtain the transverse component Q_x and Q_y that contain the in-plane structural information regarding the monolayers.

Raman scattering

Raman scattering is another powerful tool for the study of L-B films. Normal Raman spectroscopy is usually not sufficiently sensitive to obtain high signal-to-noise ratio spectra and signal enhancement techniques are necessary. However, recent advances in detector technology (CCD) have made it possible to measure Raman spectra of single monolayers

under non-enhanced conditions. The use of the CCD has been limited to fatty acids and their salts [44]. Signal enhancement is usually achieved in several ways: resonance Raman scattering (RRS), surface enhanced Raman scattering (SERS), surface enhanced resonance Raman scattering (SERRS) and surface plasmon enhanced Raman scattering.

Resonance Raman scattering has been widely used because of its ability to increase the scattering cross section. The change in molecular polarizability under resonance conditions give rises to an enhancement of the Raman scattering intensity by as much as 6 orders of magnitude over normal Raman scattering. Resonance Raman scattering spectra for single and multilayer L-B films of cumylphenoxy-phthalocyanine derivative and stearyl alcohol were reported by D.P. Dilella et al [45]. Polarized RRS can be used to determine the orientation of the molecules in L-B films [46].

The first RRS study of a single monolayer at the liquid-liquid interface and L-B films were reported by Takenaka and coworkers [47-48]. The RR spectra of porphyrin LB films were calculated [46] and measured experimentally [49]. These authors claimed that a signal to noise ratio of better than 100 can be reached. The aggregation state of cyanine and merocyanine dyes were also studied by the RRS technique [50-52].

In some cases, even RRS is not sufficient for obtaining good quality spectra from 2-D monolayer systems. Surface Enhanced Raman Scattering (SERS) is therefore has to be exploited in this situation. The so called SERS phenomenon is observed when molecules are adsorbed on certain metal surfaces (Ag, Au). The Raman scattering intensity is as much as 10^7 (or higher) times stronger than normal Raman scattering. The most commonly used

substrates in SERS experiments are silver and gold. Copper is also applicable but the enhancement is not as good as in the case of silver and gold. The metal surfaces are usually roughened by either an electrochemical method or by vacuum deposition of island-like structures which are essential in order to obtain SERS signal. It is generally accepted that the enhanced Raman scattering signal is due mainly to the field enhancement of the incident and scattered radiation [53]. The SERS technique has a tremendous advantage over RRS and normal Raman and has been widely used for studying L-B films of different compounds.

References

- 1 T. Terada, R. Yamamoto, and T. Watanabe, *Sci. Pap. Inst. Phys. Chem. Res. (Tokyo)*, **23** (1984) 173.
- 2 C. H. Giles, S. D. Forrester and G. G. Roberts in Gareth Roberts(Ed), *Langmuir Blodgett Films*, Plenum Press, New York, 1990, p. 1.
- 3 C. H. Giles, *Chem. Ind. (London)*, (1990) 1616.
- 4 J. Aitken, *Proc. R. Soc. Edinburgh*, **12** (1882-4) 56.
- 5 (a) L. Rayleigh, *Phil. Mag.*, **48** (1890) 337. (b)L. Rayleigh, *Phil. Mag.*, **48** (1890) 321.
- 6 A. Pockels, *Nature*, **43** (1891) 437.
- 7 I. J. Langmuir, *J. Am. Chem. Soc.*, **39** (1917) 1848.
- 8 D. A. Buchwald, D. M. Gallagher, C. P. Harkins, E. M. Thatcher and P. A. Zahl, *Proc. Natl. Acad. Sci.*, **24** (1938) 204.

- 9 H. H. Race, S. J. Reynolds, *J. Am. Chem. Soc.*, *61* (1939) 1425.
- 10 P. A. Thiessen, D. Beischer, H. V. Gillhausen, *Naturwiss*, *28* (1940) 265.
- 11 K. B. Blodgett, *J. Am. Chem. Soc.*, *57* (1935) 1007.
- 12 G. L. Gaines, Jr, *Insoluble Monolayers at Liquid-Gas Interface*, Wiley-Interscience, New York, London, Sydney (1966).
- 13 W.D. Harkins, T. F. Young and E. Boyd, *J. Chem. Phys.*, *8* (1940) 954.
- 14 D. M. Taylor, O. N. De Oliveira, Jr. and H. Morgan, *J. Colloid Interface Sci.*, *139* (1990) 508.
- 15 (a) V. Vogel and D. Möbius, *J. Colloid Interface Sci.*, *126* (1988) 408. (b) V. vogel and D. Möbius, *Thin Solid films*, *159* (1988) 73.
- 16 J. T. Davis and E. K. Rideal, *Interfacial Phenomena*, Academic Press, New York, 1966.
- 17 R. J. Demchak and T. J. Fort, Jr., *J. Colloid Interface Sci.*, *46* (1974) 191.
- 18 A. W. Adamson, *Physical chemistry of Surfaces*, 4th ed., John Wiley, New York, 1982.
- 19 D. K. Chattoraj and K. S. Birdi, *Adsorption and the Gibbs Surface Excess*, Plenum Press, New York, 1984.
- 20 M. R. Buhaenko, J. W. Goodwin, R. M. Richardson and M.F. Daniel, *Thin Solid Films*, *134* (1985) 217.
- 21 B. R. Malcolm, *Thin Solid Films*, *134* (1985) 201.
- 22 B. M. Abraham, J. B. Ketterson, K. Miyano and A. Kueny, *J. Chem. Phys.*, *75* (1981) 3137.
- 23 P. A. Chollet, *Thin Solid Films*, *52* (1978) 343.

- 24 J. F. Rabolt, F. C. Burns, W. E. Schlatter and J. D. Swalen, *J. Chem. Phys.*, **78** (1983) 946.
- 25 J. Y. Wang and R. A. Uphaus, Unpublished data.
- 26 R. A. Hann, in Gareth Roberts (ed.), *Langmuir-Blodgett Films*, Plenum Press, New York, 1990, p.17.
- 27 K. B. Blodgett and I. Langmuir, *Phys. Rev.*, **51** (1937) 964.
- 28 I. R. Peterson, G. J. Russell and G. G. Roberts, *Thin Solid Films*, **109** (1983) 371.
- 29 I. R. Peterson and G. J. Russell, *Thin Solid Films*, **134** (1985) 143.
- 30 I. Langmuir and V. J. Schaefer, *J. Am. Chem. Soc.*, **60** (1938) 1351.
- 31 C. Holley, *Phys. Rev.*, **51** (1937) 1000.
- 32 V. K. Srivastava and A. R. Verma, *Solid State Commun.*, **4** (1966) 367.
- 33 G. L. Clark, R. R. Sterrett and P. W. Leppa, *J. Am. Chem. Soc.*, **52** (1935) 330.
- 34 D. C. Bisset and J. Iball, *Proc. Phys. Soc. London A*, **67** (1954) 315.
- 35 W. Lesslauer, *Acta Crystallogr., sect. B* **30** (1974) 1932.
- 36 M. Pomerantz and A. Segmüller, *Thin Solid Films*, **68** (1980) 33.
- 37 T. P. Russel, *Material Science Reports*, **5** (1990) 171.
- 38 R. M. Nicklow, M. Pomerantz and A. Segmüller, *Phys. Rev. B*, **23** (1981) 1081.
- 39 J. Als-Nielsen and P. S. Pershan, *Nucl. Instrum. Methods*, **208** (1983) 545; *Risø-R-660(EN)*, 1992, pp. 130-131.
- 40 J. Als-Nielsen and K. Kjaer, in T. Riste and D. Sherrington, (eds.), *Phase Transition in Soft Condensed Matter*, Plenum Press, New York, 1989, p. 113.

- 41 D. Vaknin, K. Kjaer, J. Als-Nielsen and M. Lösche, *Biophys. J.*, *59* (1991) 1352.
- 42 D. Vaknin, J. Als-Nielsen, M. Piepenstock and M. Lösche, *Biophys. J.*, *60* (1991) 1545.
- 43 D. Vaknin, J. Als-Nielsen, M. Piepenstock and M. Lösche, in H. Zabel and I. K. Robinson, (eds.), *Springer Proceedings in Physics*, *61* (1992) 155.
- 44 S. B. Dieker, C. A. Murray, J. D. Legrange and N. E. Schlotter, *Chem. Phys. Lett.*, *137* (1987) 453.
- 45 D. P. Dilella, W. R. Barger, A. W. Snow and R. R. Smardzewski, *Thin Solid Films*, *133* (1985) 207.
- 46 P. Lesieur, M. Vandevyver, A. Ruaudel-teixier and A. Barraud, *Thin Solid Films*, *159* (1988) 315.
- 47 T. Takenaka and T. J. Nakanaga, *J. Phys. Chem.*, *80* (1976) 475.
- 48 T. Takenaka and H. J. Fukuzaki, *J. Raman Spec.*, *8* (1979) 151.
- 49 G. A. Schick, I. C. Schreiman, R. W. Wagner, J. S. Lindsey and D. F. Bocian, *J. Am. Chem. Soc.*, *111* (1989) 1344.
- 50 D. L. Akins, *J. Colloid Interface Sci.*, *90* (1982) 373.
- 51 J. -H Yang and R. H. Callender, *J. Raman Spec.*, *16* (1985) 319.
- 52 Y. Ozaki, K. Iriyama, T. Iwasaki and H. Hamaguchi, *Appl. Surf. Sci.*, *33/34* (1988) 1317.
- 53 C. A. Murray, in B. A. Garetz and J. Lombardi, eds., *Recent Adv. Laser Spectrosc.*, *4*, John Wiley, New York, 1983.

CHAPTER 2. NEUTRON AND X-RAY REFLECTION STUDY OF FULLERENE

 C_{60} AND ITS DERIVATIVES AT THE AIR-WATER INTERFACE

A paper published in *Thin Solid Films*

J. Y. Wang, D. Vaknin and R. A. Uphaus

Abstract

Neutron and X-ray reflection measurements and surface pressure isotherms of spread films of fullerene-dodecylamine adduct C_{60} - $[NH_2(CH_2)_{11}CH_3]_x$ and fullerene-propylamine adduct C_{60} - $[NH_2(CH_2)_2CH_3]_x$ all indicate that these materials may form monomolecular layers on water surface. The reflection data sets (neutron on both H_2O and D_2O) can be accounted for by a single model structure defined in terms of the dimensions of an average cell and its chemical composition.

For the dodecylamine adduct, this model ascribes a total thickness of about 29 Å to the molecular interface layer with the following internal structure. The fullerenes (with several alkyl chains attached) form a central stratum and the remainder alkyl tails are located close to both the air and the water interfaces. The alkyl moieties close to the aqueous substrate are hydrated. The reflection experiments and the isotherms suggest that on average 8 ± 3 dodecylamine molecules are present per fullerene, consistent within error, with elemental analysis 5 ± 2 . For the propylamine derivative, the isotherm indicates that a phase transition may exist in a two dimensional closed packed monolayer. The thickness of the

film changes from 12 to 15 Å as extracted from the reflectivity data. The adduct is elevated by alkyl chains over the water, and the alkyl moieties close to the aqueous subphase are hydrated.

By contrast, neutron reflection and surface pressure *vs.* area data of spread films of C₆₀ fullerene on aqueous surfaces indicate the formation of inhomogeneous multilayer films with a thickness and a surface roughness exceeding the molecular size. These underivatized fullerenes thus do not form monomolecular films.

Introduction

Recent studies probing all physical and chemical aspects of fullerenes have indicated that the C₆₀ species is a very strong electron acceptor, comparable to or even stronger than viologens. Fullerenes therefore could be attractive candidates as elements in L-B assemblies serving as biomimetic models. Extensive studies of spread films of C₆₀ and C₇₀ fullerenes on aqueous surfaces indicate that the films are multilayered [1-11], presumably owing to fullerene aggregation. In fact, Brewster angle microscopy shows inhomogeneity and clustering of the material on the micron length scale immediately after spreading from the solvent [8]. Such clustering is anticipated, since the fullerenes lack amphiphilic character; attractive forces between fullerene molecules are most likely stronger than those between water and fullerene molecules. It is therefore unlikely that monomolecular films of the material will be stable at the air-water interface.

We have recently derivatized fullerenes with amines [11] in an attempt to reduce the strong cohesive forces operative between individual fullerene molecules, thus reducing aggregation. It was also anticipated that the presence of amine groups introduce amphiphilic character to the adduct. In a similar approach, the fullerene molecules have been placed in the nitrogen-rich hydrophilic cavities of azacrown compounds and resulted in the formation of a monomolecular layer of the complex [10]. Amines with varying number of carbons react with fullerenes in a two-step nucleophilic addition [12, 13]. It was also reported [13] that the number of amine molecules that react with each fullerene molecule varies with the hydrocarbon chain length. The present study compares the film structure of pure C_{60} with that of the fullerene-amine adducts at the air-water interface using neutron and X-ray scattering techniques. Two different fullerene-amine adducts have been studied in this paper.

Theory

A brief discussion on the theory of neutron and X-ray reflectivity is given here. While X-ray reflectivity probes the variation of electron density, neutron reflectivity detects the variation in scattering length density as function of depths across the interface. Since neutron and X-ray reflection are the same in principle, only the X-ray reflection is discussed. At the X-ray wavelengths the energy of photon is very high and the electrons from the X-ray source can be treated as free electrons. The elastic scattering of light with a wavelength λ is described by refractive index n [14]:

$$n = 1 - \delta + i\beta \quad (1)$$

where $\delta = \rho(\lambda^2/2\pi)r_0$ in which ρ is the electron density and r_0 the radius of the electrons. β describe the possible absorption in the medium. In practice, we will ignore the effect of absorption because we mainly are concerned with the region where the glancing angle is much bigger than the critical reflection angle.

Figure 1 (top) shows the reflection measurement at a sharp and flat surface. A plane wave with wavelength λ_0 and associated with k_0 , where $k_0 = 2\pi/\lambda_0$, incident at angle θ_0 on a sharp, flat interface between two media with refractive indices n_0 and n_1 . The incoming beam will be reflected as well as refracted/transmitted at the interface. The reflectivity R is defined as the ratio of the intensities of the reflected and incoming beam and is often expressed in terms of wave vector transfer $Q_0 = k_0' - k_0$. For specular reflection ($\theta_0 = \theta_0'$) Q_0 is normal to the interface and R is given by the Fresnel equation:

$$R = |r_{01}|^2 = [(Q_0 - Q_1) / (Q_0 + Q_1)]^2 \quad (2)$$

in which,

$$r_{ij} = (Q_i - Q_j) / (Q_i + Q_j) \quad (3)$$

$$Q_\alpha = 2k_\alpha \sin\theta_\alpha \quad (4)$$

The angles are related via Snell's law:

$$n_0 \cos \theta_0 = n_1 \cos \theta_1 \quad (5)$$

If the change in wavelength across the interface is neglected, Snell's law can be rewritten as:

$$Q_1 = (Q_0^2 - Q_c^2)^{1/2} \quad (6)$$

then the reflectivity is given by:

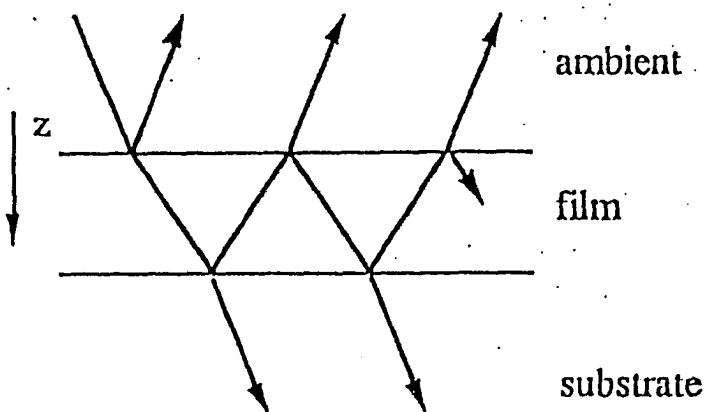
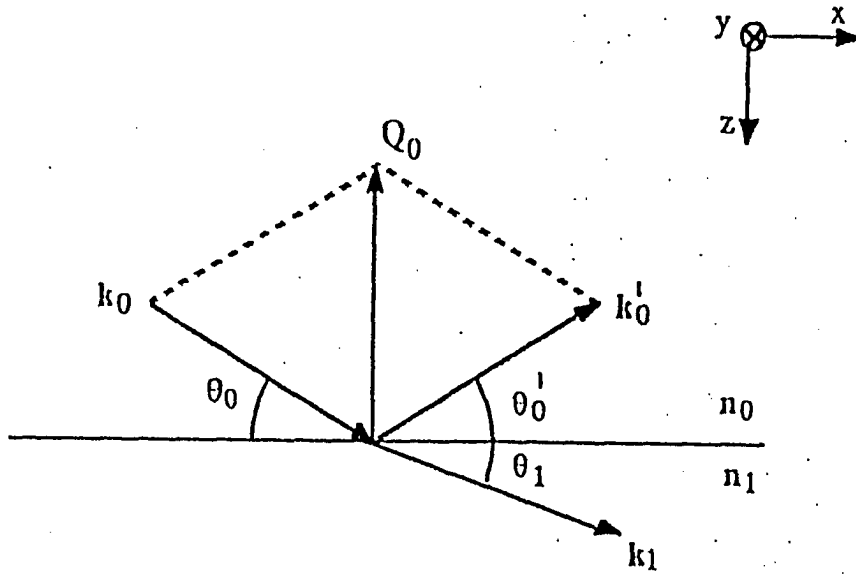
$$\begin{aligned} R_F &= \left\{ \left[1 - \left[1 - (Q_c/Q_0) \right] \right]^{1/2} / \left[1 + \left[1 - (Q_c/Q_0) \right] \right]^{1/2} \right\}^2 \\ &= [Q_c / (Q_0 + Q_1)]^4 \end{aligned} \quad (7)$$

This equation is called Fresnel law and the reflectivity described by this equation is referred to the Fresnel reflectivity. When $Q \gg Q_c$, equation (7) is readily condensed to give the much simpler result:

$$R_F = (Q_c/2Q_0)^4 \quad (8)$$

Now consider a monolayer of thickness d on a substrate in contact with an ambient as shown in figure 1 (bottom). The reflected wave is then the result of the interference

Figure 1 X-ray reflection at (top): a sharp and flat surface and (bottom): a monolayer covered surface.



between the singly and multiply reflected waves, which add up to give the standard optical result:

$$r = [r_{01} + r_{12}\exp(-iQ_1d)] / [1 + r_{01}r_{12}\exp(-iQ_1d)] \quad (9)$$

where r_{ij} and Q_i are given in equation (3) and (4) respectively. In this case, the reflectivity profile contains a series of maxima and minima [15] which characterize the thickness of the monolayer.

In actual experiment, the interface under investigation always has a roughness and therefore will have off-specular reflection. Real examples may be the thermal fluctuations of a liquid surface. The reflectivity of a rough surface depends on the lateral scale of the roughness [16]. Lateral coherence length l_c is introduced here to discriminate between roughnesses of different length scales. The coherence length is the maximum separation distance in the scattering object from which the waves still interfere coherently at the detector. The macroscopic roughness of a surface is referred to the situation that the interface is locally flat and the waves will still be specularly reflected. The total scattering of the interface is obtained by adding incoherently the reflections for the different orientations and positions of the interface. The microscopic roughness is true when the variations take place on a scale smaller than l_c . The specular reflection is much weaker in this case because light is also scattered in non-specular reflections. Considering the roughness of an interface, the reflectance described by eq.(3) is modified by:

$$r_{ij} = [(Q_i - Q_j)/(Q_i + Q_j)] \exp[(-1/2)Q_i Q_j < \sigma_{ij} >^2] \quad (10)$$

where σ_{ij} is the surface roughness.

Experimental details

The fullerenes investigated were purchased from the Texas Fullerene Corp., Houston, TX (purity 99.9%) and used as received. N-propylamine and n-dodecylamine were purchased from the Aldrich Chemical Co. Chloroform (HPLC grade), methanol(reagent grade) and benzene(reagent grade) were purchased from Fisher Scientific and were used as received. The amine adducts were prepared in a similar procedure described somewhere else [13] and summarized as following. For $C_{60}(NH_2C_3H_7)_x$, 15 mg of C_{60} was mixed with 20 ml of freshly opened n-propylamine. A dark green solution was formed upon mixing of these two compounds. The mixture was stirred for 24 hours at room temperature under air condition. The green colored solution gradually turned brown. The n-propylamine was evaporated and the product was dried under vacuum. Further purification was made by dissolving the product in toluene and the solution was passed through a silica column using toluene as mobile phase, the brown color product stayed at the top of the column and the unreacted C_{60} was flushed out of the column. The product was then washed out of the column using toluene + isopropyl alcohol (9:1). The solvent was evaporated and the product was dried under vacuum for 24 hours. For $C_{60}(NH_2C_{12}H_{25})_x$, 20 mg of C_{60} was mixed with 1 ml of

dodecylamine. A green suspension was formed upon mixing and turned brown gradually. The mixture was stirred for 30 hours at room temperature. The suspension became clear after an hour. Then methanol was added to the mixture and the precipitate was centrifuged and washed twice with methanol. The product was dried under vacuum. Addition reactions between fullerenes and amines do not result in single product, because the extent of addition cannot be controlled and thus result in multiple products. Fast atom bombardment mass spectroscopy (FAB-MS) of the products confirmed multiple chain additions with no unique stoichiometry. Elemental analysis (Desert Analytics, Tucson, AZ) indicated that an average of 12 ± 2 propylamine and 5 ± 2 dodecylamine molecules reacted per fullerene to yield $C_{60}(CH_3CH_2CH_2NH_2)_{12}$ and $C_{60}[CH_3(CH_2)_{11}NH_2]_5$ respectively.

Surface pressure-area isotherms were determined on a conventional Teflon Langmuir trough with a Wilhelmy sensor, using benzene and chloroform as the spreading solvents for the pure fullerenes and for the amine adducts respectively. Monolayers were spread on Milli-Q water or on D_2O triply distilled from $D_2O-KMnO_4$.

For pure C_{60} and the dodecylamine adduct, neutron reflection measurements of spread films were carried out on the liquid surface reflectometer at the DR3 reactor at Riso National Laboratory (Denmark). X-ray reflection experiments were performed on the BW1 liquid surface reflectometer at HASYLAB (Hamburg, Germany). Both facilities have been described previously [17, 18]. For propylamine adduct, reflectivity measurements of spread films were carried out on a novel liquid-surface X-ray reflectometer recently constructed at Ames Laboratory, U.S. DOE. The apparatus is similar to the one described above with the

additional degree of freedom that allows second order correction the 2θ monochromator arm that ensures a constant wavelength ($\lambda = 1.5404\text{\AA}$, $\text{CuK}\alpha$) at all scattering angles.

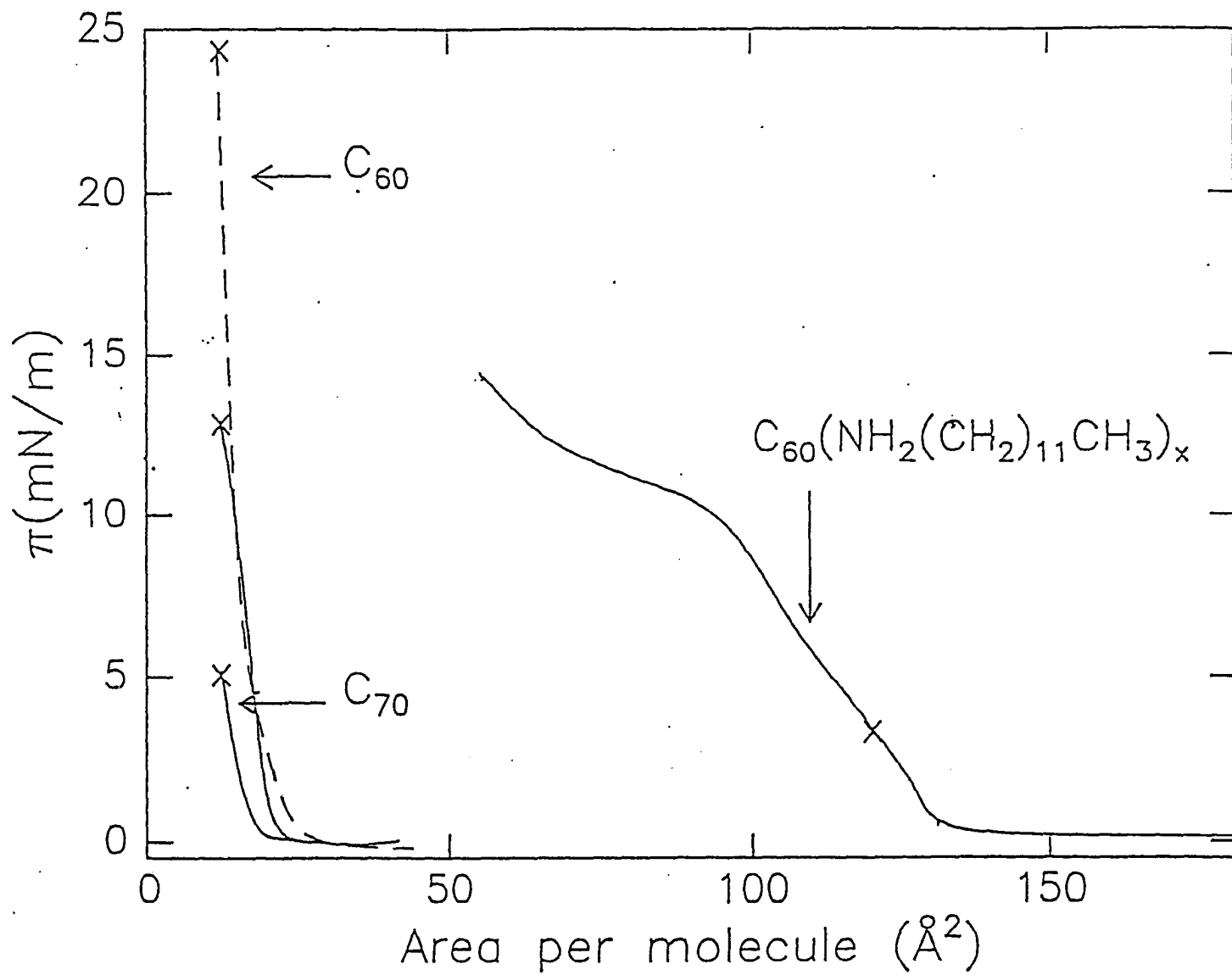
Results and discussion

C₆₀ fullerenes

π -A isotherms of pure C_{60} on H_2O and D_2O of prepared for the neutron scattering experiments are shown in figure 2. Typical curves show a limiting area per molecule in the range $10\text{-}40\text{ \AA}^2$, depending on the size of the sample, the concentration of the solution and the rate of compression. This area range is much smaller than that predicated from X-ray diffraction studies of polycrystalline C_{60} (about 87 \AA^2 [19]). In general it was noticed that the isotherms were not reproducible and that upon decompression the surface pressure dropped to zero rapidly and expansion of the floating film did not occur.

Figure 3(a) and 3(b) show the neutron reflectivities vs. the momentum transfer Q_z from pure C_{60} films on H_2O and D_2O at pressure of 12.5 and 24 mN/m respectively. The solid curves are the reflectivity curves calculated from the nuclear scattering length densities across the interface shown in the inset of each figure. The distribution of the molecules across the interface is modeled assuming two boxes [20-21] incorporating one fullerene and interpenetrating water molecules. One box includes a fraction f of the fullerene at the water interface (thickness d_1) with N_w water molecules closely packed and the other box at the air interface incorporates the other $1-f$ (thickness d_2). The average area per one fullerene plus N_w water molecules, A_0 , is common to the two boxes. Volume constraints to fitting the

Figure 2. Surface pressure vs. area per molecule of C_{60} on H_2O (solid curve) and D_2O (dashed curve) and of C_{60} -dodecylamine spread films. The crosses indicate the pressures at which the reflectivity measurements were performed.



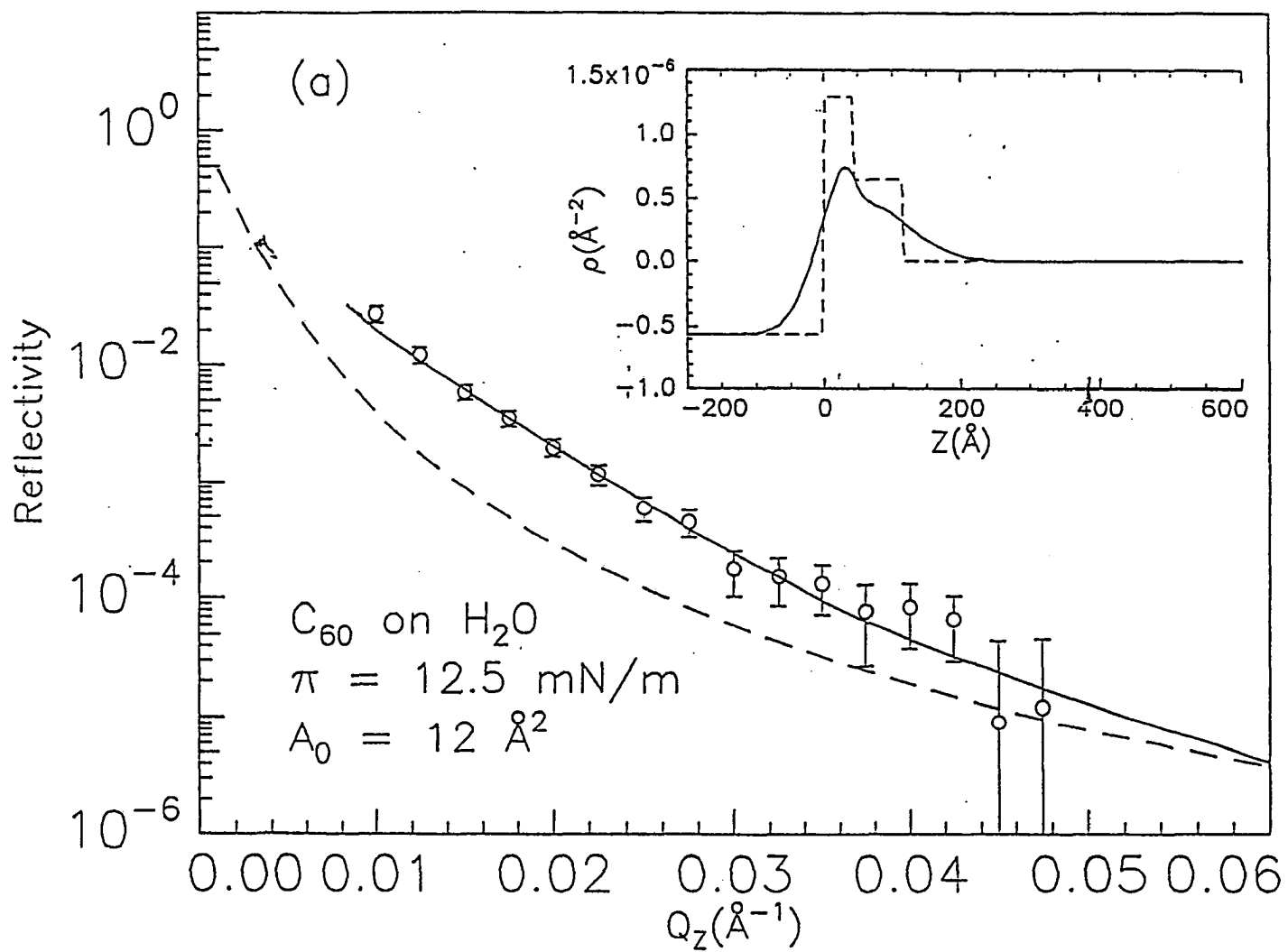
molecules in each box were applied. In the fitting procedure it was ensured that the volume of the box in the vicinity of the air interface $V_2 = A_0 d_2$, is equal to or greater than the partial volume of the fullerene present, $(1-f)V_{C60}$ ($V_{C60} = 713.5 \text{ \AA}^3$ [19]). The volume of the lower box, $V_1 = A_0 d_1$, is completely filled with the f fraction of the fullerene, fV_{C60} , and with N_w water molecules ($V_w = 30 \text{ \AA}^3$). The scattering length density across the interface is determined from the dimensions of each box and its chemical content. Thus the scattering length density profile is constructed as a sum of three step functions representing three interfaces. To account for the surface roughness as discussed earlier, it is convoluted with gaussians representing the diffuseness of the interface [20-21]:

$$\rho(z) = \sum \Delta b(i) P[z-z(i)/\sigma(i)_{rms}] \quad (11)$$

where $P(w)$ is the normalized probability integral [ref. 22, eqn. 26.2.2], $z(i)$ is the position of interface i and $\Delta b(i)$ is the difference in scattering length density across $z(i)$. The surface roughness values $\sigma(i)_{rms}$ (R.M.S interfacial widths) may differ at different interfaces. For calculating the reflectivity, the scattering length density function is dissected into thin slices to form a histogram (typically consisting of about 100 slices) and the reflectivity is calculated by a recursive method applying continuity conditions to the wavefunctions and their derivatives at each interface of the histogram [23].

Structural parameters obtained from a non-linear least-squares fit to the data sets shown in Figure 3 are listed in Table 1. The most prominent features in the scattering length

Figure 3. Neutron reflectivity vs. momentum transfer Q_z from films of C_{60} on (a) H_2O and (b) D_2O . The solid curves are the calculated reflectivities obtained from the scattering length density profiles shown with solid curves in the insets. The dashed line in each inset corresponds to the box model that is smeared by gaussian to give the solid curve. The area per molecule, A_0 , is extracted from the isotherm in Figure 1.



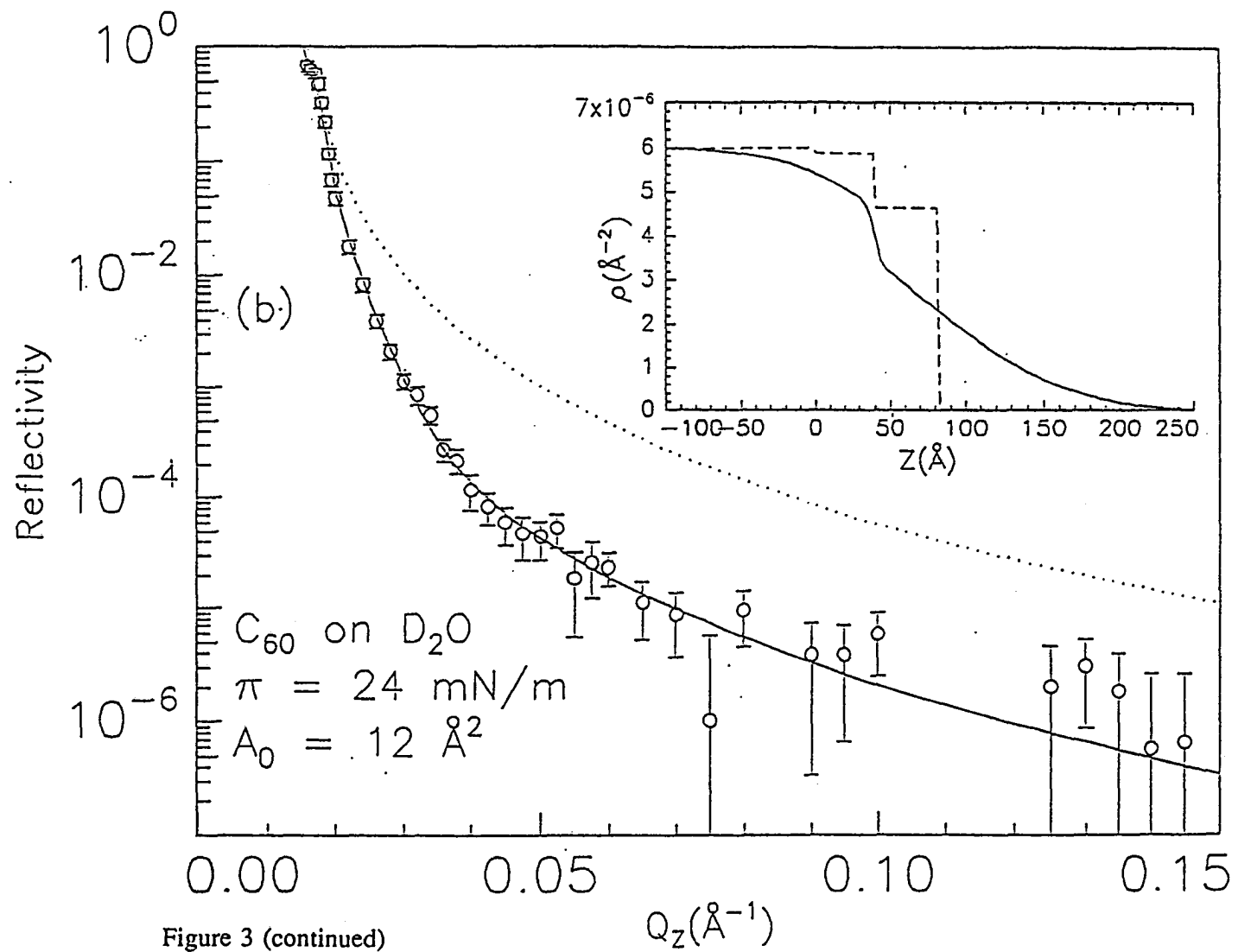


Figure 3 (continued)

densities extracted from the reflectivity data are the large values of the surface roughness. Both data sets show surface roughness values at some interfaces that exceed the molecular size of the constituents. These values should be compared with typical surface roughness values of amphiphilic monolayers, which are on the order of 3-5 Å [21-22] and are conformal for all interfaces. The area per molecule for each fullerene in the films on H₂O and D₂O is 33.4 and 12 Å² respectively and the total thickness of the films is on the order of 100 Å. The thickness of the film and the large surface roughness values suggest that the film consists of large ridges and depressions as depicted in Figure 4. The area per molecule deduced in the case of H₂O is inconsistent with that obtained from the isotherms. It is possible that remnant solvent (benzene) in the film may bring about this discrepancy.

C₆₀-dodecylamine

Figure 1 shows the surface isotherm for C₆₀-dodecylamine on H₂O; similar isotherms were obtained on D₂O. The area per molecule is calculated on the basis of the stoichiometry determined in the elemental analysis. Compared with the π -A curves of the pure fullerene C₆₀, the adduct exhibits a much large limiting area per molecule. A gradual increase in the surface pressure starts at an area per molecule larger than 150 Å². From the isotherm we infer that the adduct molecules are already densely packed at an area values of about 130 Å² per molecule. At surface pressure below 10 mN/m the film exhibits a well-reproducible isotherm which does not depend on the size of the sample or the concentration of the solution. Above $\pi = 10$ mN/m the isotherm is indicative of a collapsed monolayer.

Table 1. Structural parameters used to calculate the reflectivity curves of C_{60} films on H_2O and on D_2O shown in Figures 3(a,b). See text for a detailed description of the model.

	Dimensions	C_{60} on H_2O	C_{60} on D_2O
A_0	\AA^2	12	12
$\rho_{substrate}$	(\AA^{-2})	$-5.60 \cdot 10^{-7}$	$6.0 \cdot 10^{-6}$
σC_{60} -Water	(\AA)	22.8	43.5
d_1	(\AA)	61.7	40.0
f (fraction in water)		0.25	0.42
N_w		18.8	6.0
σC_{60} - C_{60}	(\AA)	282.8	3.5
ρ_1	(\AA^{-2})	$9.0 \cdot 10^{-7}$	$5.87 \cdot 10^{-6}$
d_2	(\AA)	50.0	41.5
f (fraction in air)		0.75	0.58
σC_{60} -air	(\AA)	282.8	67
ρ_2	(\AA^{-2})	$5.0 \cdot 10^{-6}$	$4.7 \cdot 10^{-6}$

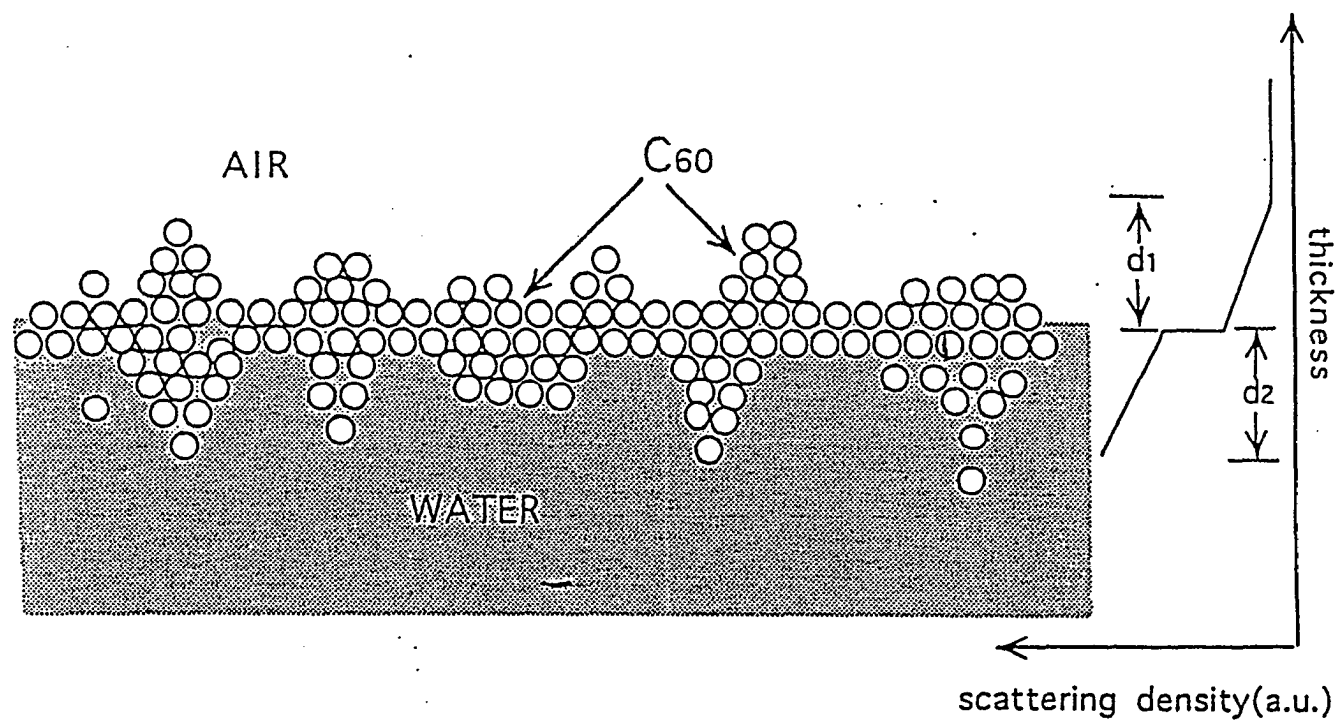
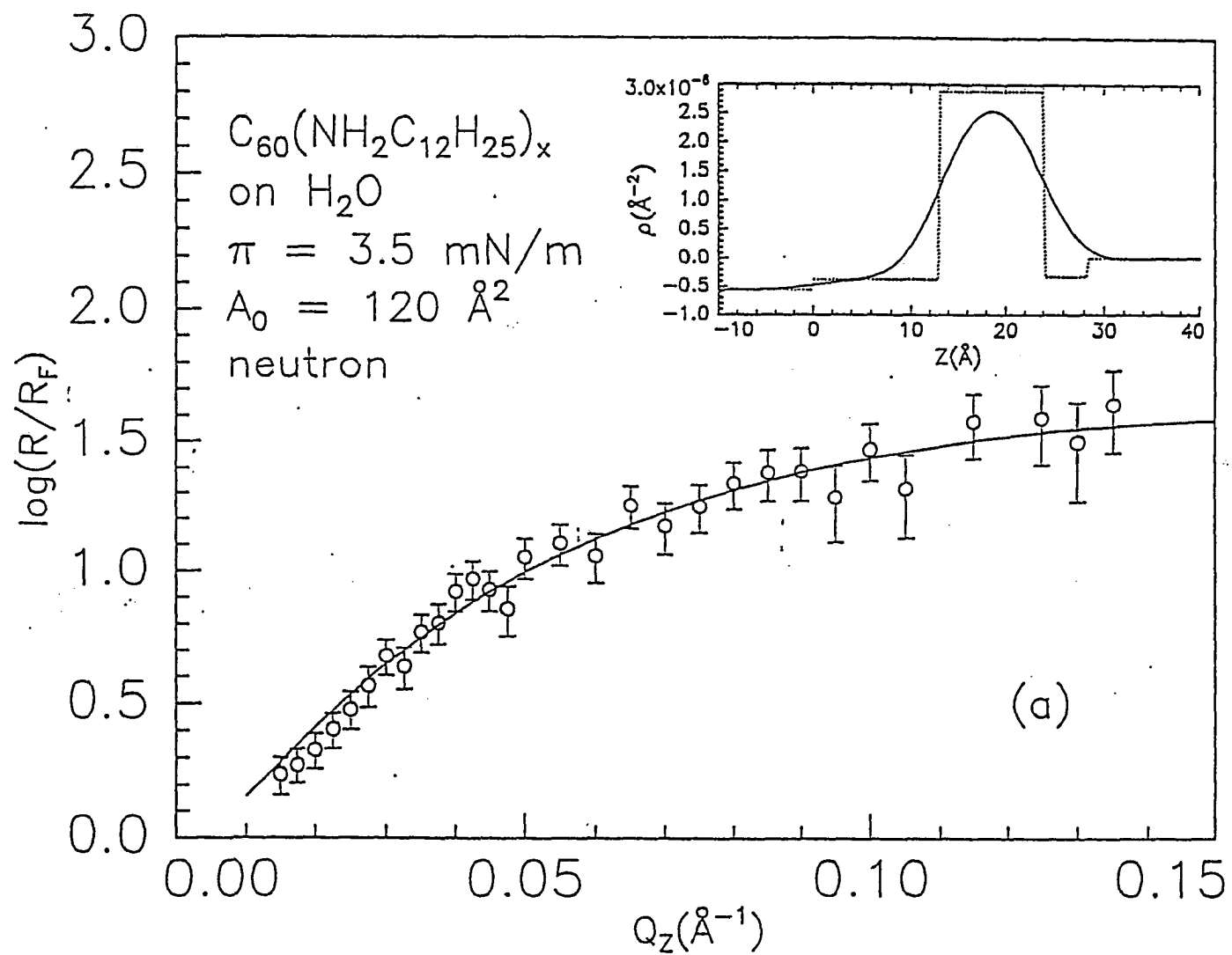


Figure 4. Illustration of the morphology of C₆₀ on the surface of water. The surface roughness is much larger than the diameter (about 8.2 Å) of a fullerene molecules.

Figure 5 shows the (a, b) neutron and (c) X-ray reflectivities of C_{60} -dodecylamine on (a, c) H_2O and (b) D_2O normalized to the Fresnel reflectivity of the bare subphase R_F . The solid curves are calculated from the scattering length densities shown in the insets using the Parratt recursion formalism [23]. In refining a global model [17] to all these data sets (neutron on H_2O and D_2O and X-ray on H_2O), it is assumed that the interface consists of three boxes [20-21] of homogeneous scattering length densities [17] (see figure 6). One box consists of one fullerene and a variable number of alkyl chains, N_F . Two boxes are located on either side of the fullerene slab, both filled with the hydrocarbon chains of the amines. One box adjacent to the water interface contains N_{CW} alkyl chains and N_W water molecules, while the other at the air interface contains N_{CA} alkyl chains. A_0 denotes the area per one fullerene plus $N_{CA} + N_F + N_{CW}$ alkyl chains plus N_W water molecules. The dimensions of these boxes and their chemical content in terms of the number of moieties or molecules are the free variables. The best fit free parameters of the model are listed and defined in Table 2. The X-ray reflectivity data in Figure 5(c) show a subtle ripple which could not be accounted for in the model.

Figure 6 shows schematically the conformation of the molecules on the surface of water and the corresponding scattering length densities. The thickness of the fullerene slab is 11 \AA , which is larger than the value expected from a smoothly distributed fullerene layer, 8.2 \AA . Alternatively, a model that assigns a thickness of 8 \AA to this slab yields a similar fit to the data but associates a total of 10 alkyl chains with each fullerene, which is beyond the uncertainty of the analysis determination of the composition. Such a thickness, 11 \AA , implies

Figure 5. Neutron and X-ray reflectivity (normalized to the Fresnel reflectivity R_F) from the surface of (a, c) H_2O and (b) D_2O covered with a single layer of C_{60} -dodecylamine. The solid curves are calculated from the scattering length density profiles shown in the insets. All scattering length densities correspond to the same interfacial model structure. The area per molecule, A_0 , is deduced from the amount of material deposited (see Figure 1).



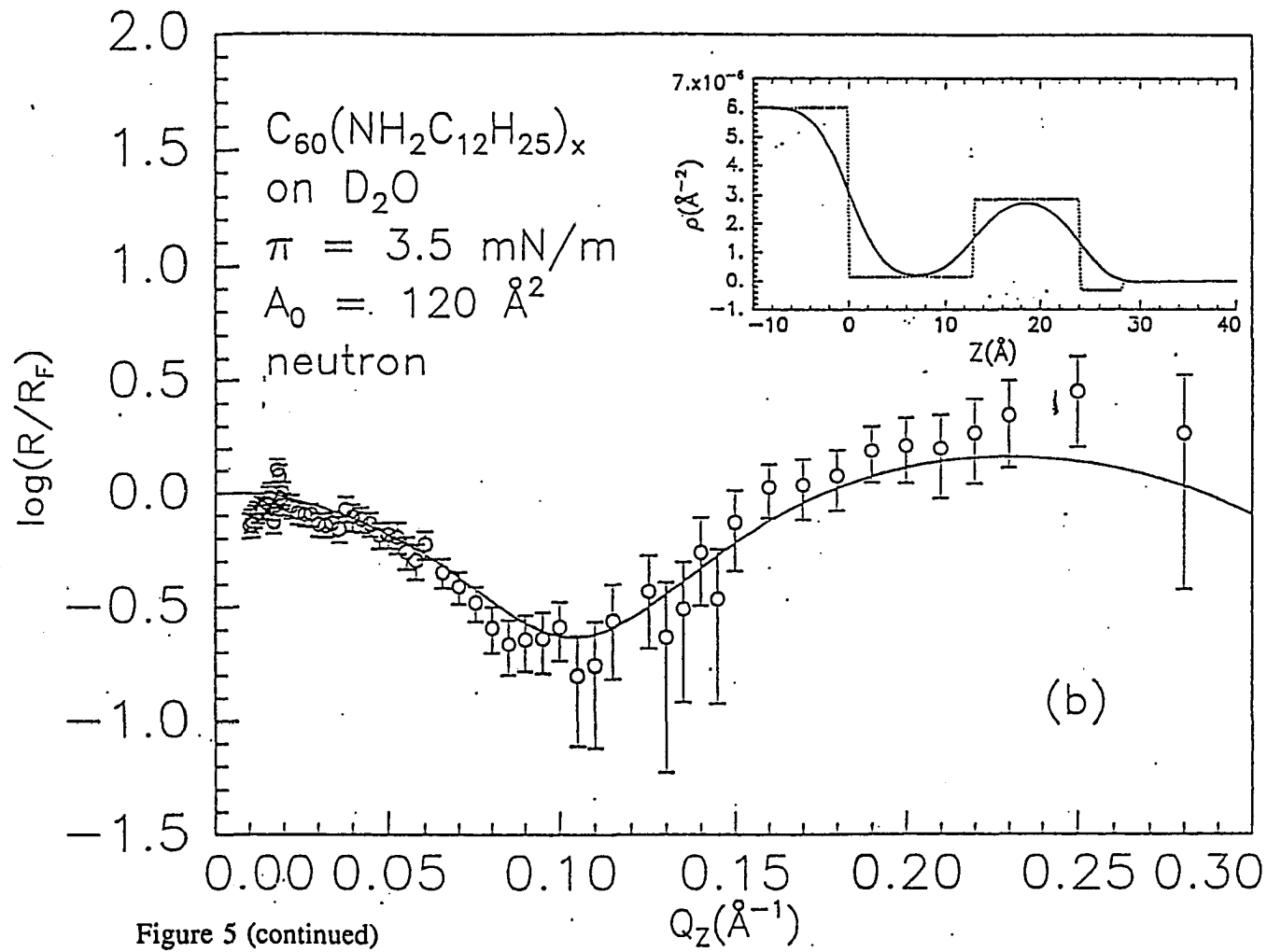


Figure 5 (continued)

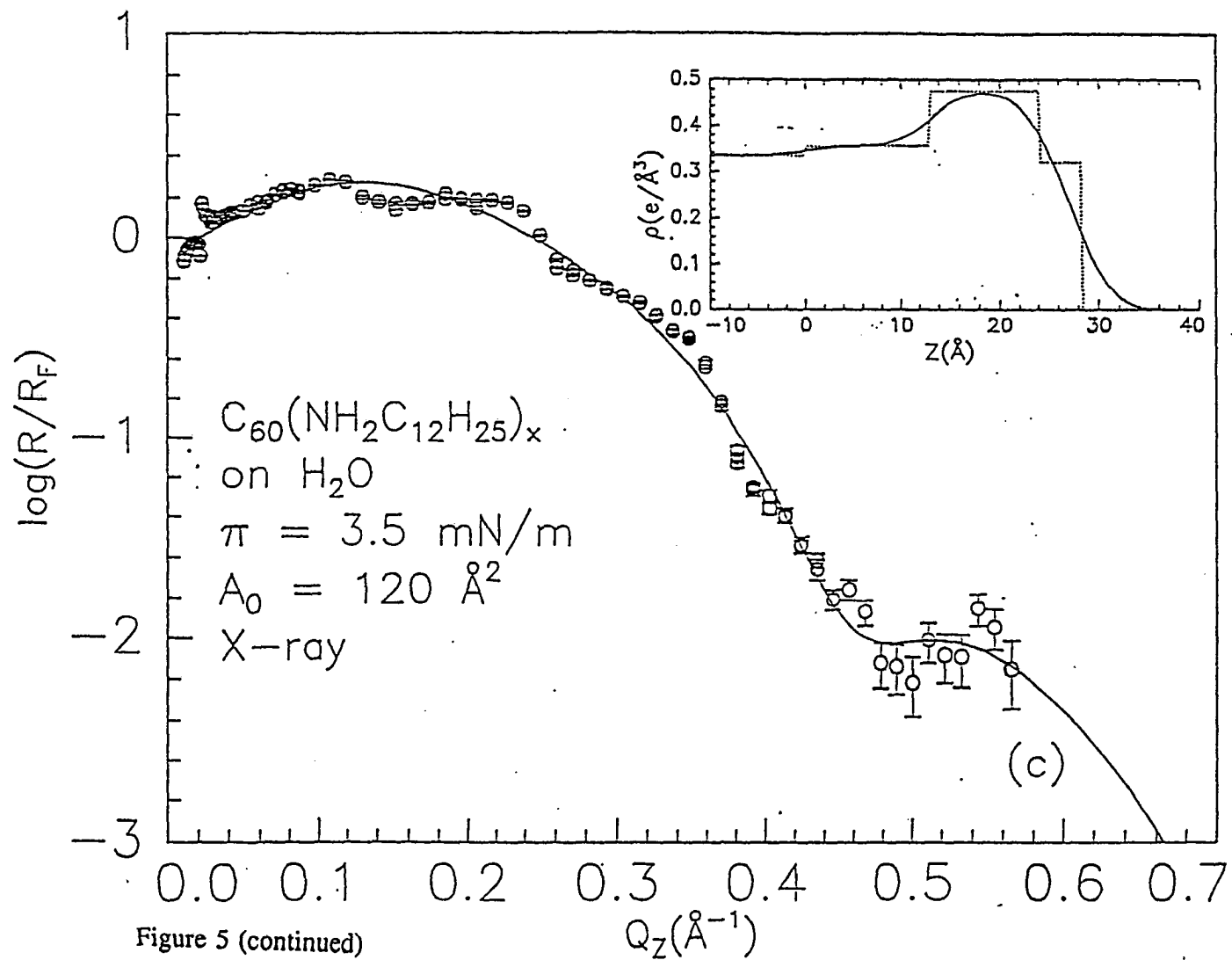


Figure 5 (continued)

Table 2. Structural parameters of $C_{60} - [N H_2 (C H_2)_{11} C H_3]_x$ monolayer at the air-water interface, as obtained from fitting one model to the combined data sets in Figure 5.

A_0	117. Å ²	Average area per molecule
d_1	13.1 Å	thickness of lower hydrocarbon chain
N_{CW}	4.6	number of chains at water interface
N_W	4.1	number of water molecules in chain region
d_F	11.0 Å	thickness of C_{60} -Fullerene slab
N_F	2.3	number of chains in Fullerene slab
d_u	4.1 Å	thickness of upper hydrocarbon chain
N_A	1.4	number of chains at air-interface
σ_N	4.8 Å	surface roughness, neutron on H_2O
σ_N	3.9 Å	surface roughness, neutron on D_2O
σ_X	3.9 Å	surface roughness, X-ray on H_2O

a distribution in the height of the fullerenes, resulting in a large surface roughness. The surface roughness in the present study, about 4 Å, is slightly larger than the expected surface roughness for classical amphiphilic monolayers at this temperature ($T = 20\text{ }^{\circ}\text{C}$, about 3.3 Å [20-21]).

The area per molecule, $117\text{ }\text{Å}^2$, is very close to the area per molecule obtained from the isotherm, $120\text{ }\text{Å}^2$. It is, however, larger than that expected for closely packed fullerenes (about $87\text{ }\text{Å}^2$) and is consistent with a picture in which the fullerenes are entangled with alkyl chains. Our structural model suggests that 8 ± 3 amine molecules react with each Fullerene molecule, consistent with the value of 5 ± 2 extracted from elemental analysis. Wudl et al. however, reported only one amine per fullerene in this adduct [16].

C₆₀-propylamine

Figure 7 shows the surface isotherm for C₆₀-propylamine on the surface of water. The area per molecule is calculated based on the stoichiometry determined in the elemental analysis. Compared with the isotherm of pure fullerene C₆₀, the adduct exhibits a much larger limiting area per molecule. The isotherm of this adduct is very similar to that of C₆₀-dodecylamine adduct discussed above except this adduct monolayer can stand much higher lateral pressure. Gradual increase in the surface pressure starts at area per molecule larger than $200\text{ }\text{Å}^2$. From the isotherm we infer that the molecules are already densely packed at area values of $\sim 150\text{ }\text{Å}^2$ per molecule. At surface pressure below 15 mN/m the film exhibits a well reproducible isotherm which does not depend on the size of the sample or the

Figure 6. Depiction of the model structure of C₆₀-dodecylamine on aqueous surfaces.

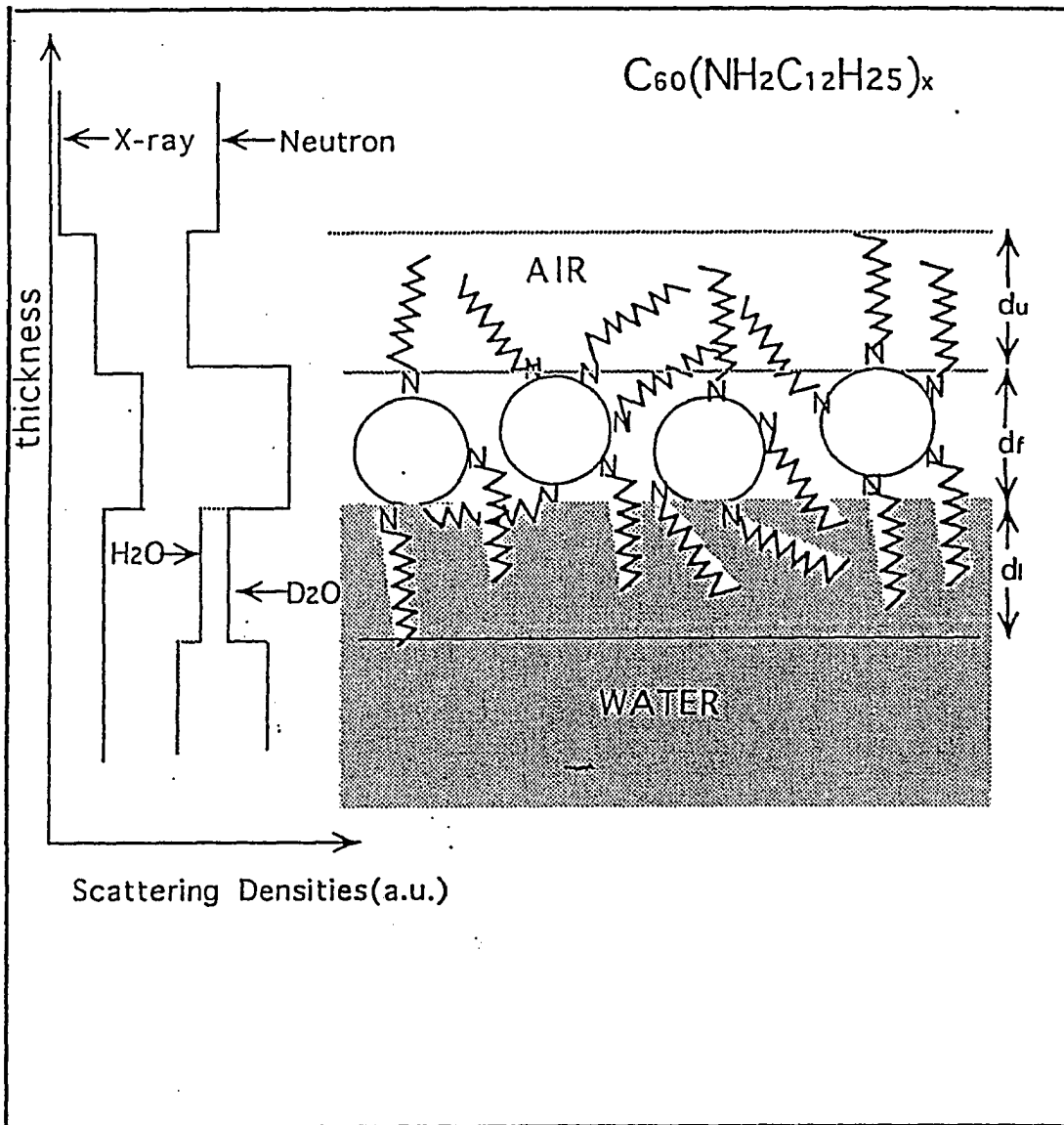
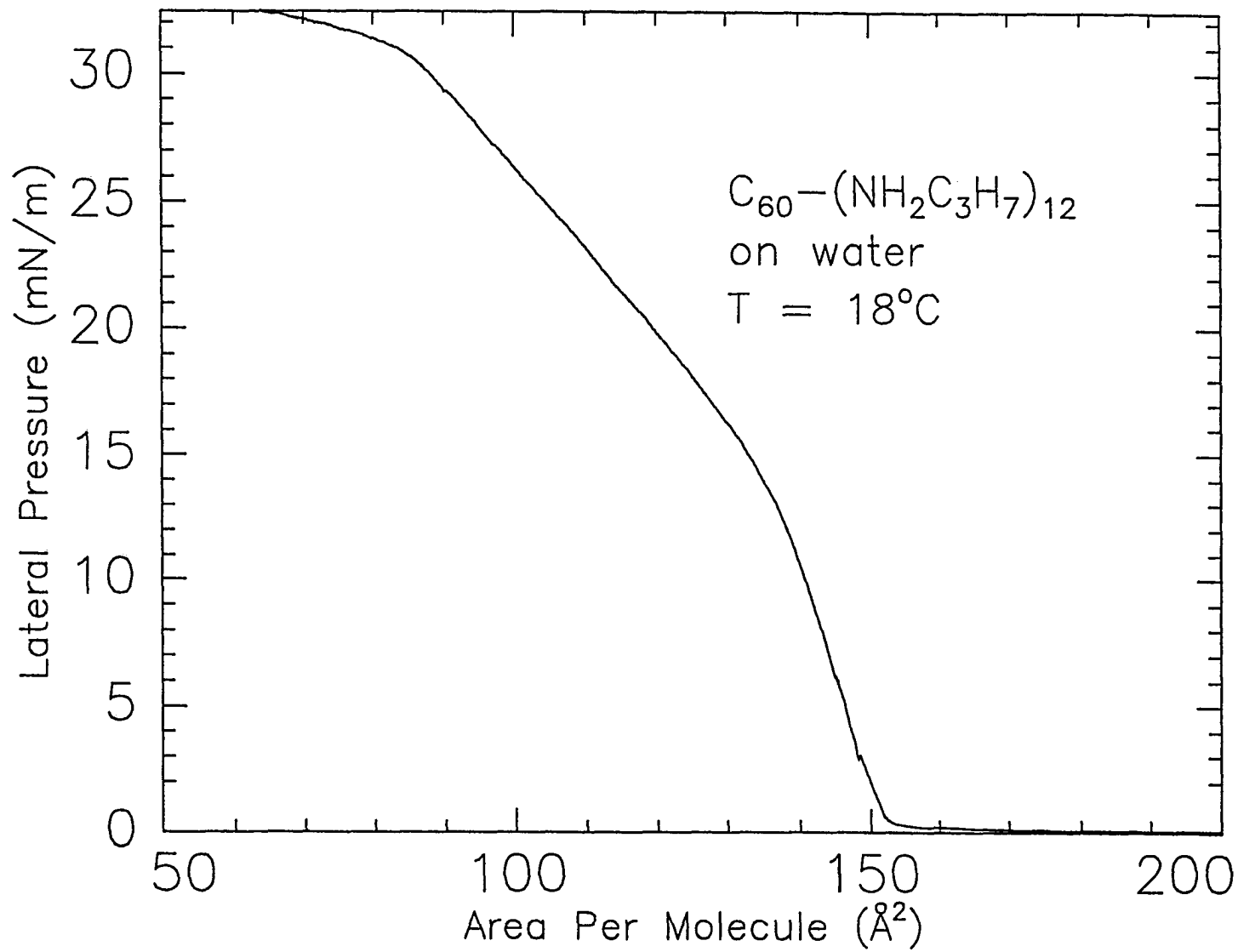


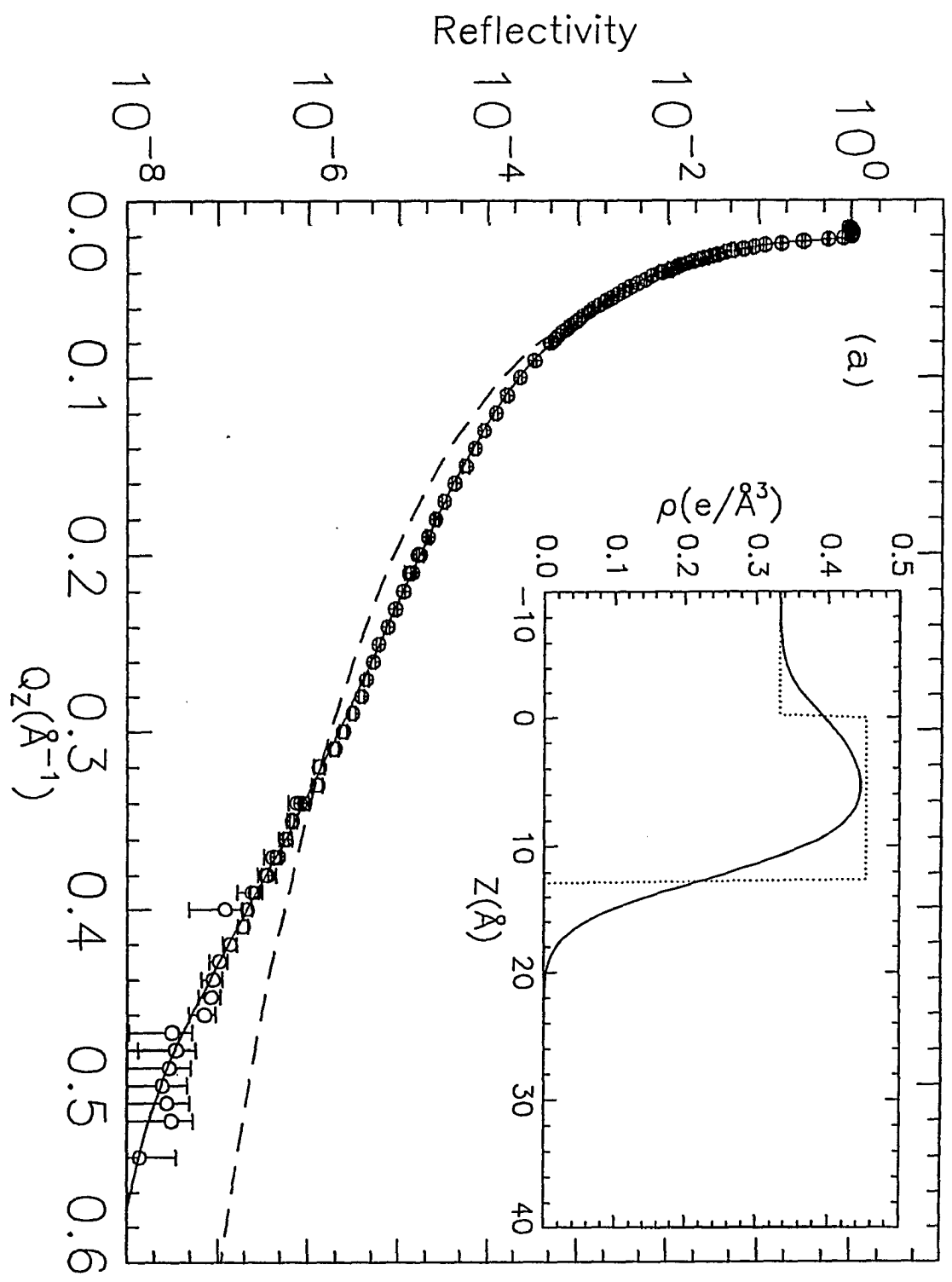
Figure 7. Surface pressure vs. area per molecule of C₆₀-propylamine spread film.



concentration of the solution. Above $\pi \sim 15$ mN/m the isotherm is indicative of a phase transition, possibly from square to triangle lattice. Above 30 mN/m the film consists of a bilayer of the amine adduct.

Figure 8 shows the X-ray reflectivity (a) of C_{60} -propylamine on water and the reflectivity normalized (b) to the Fresnel reflectivity of the bare subphase, R_F at lateral pressure, $\pi = 6.7$ mN/m. The solid lines are calculated from the scattering length densities shown in the insets, using the Parratt recursion formalism [23]. In refining a global model to the data it was assumed that the interface consists of a single box of homogeneous scattering length densities [17]. The box contains one fullerene and a variable number of water molecules, N_w . A_0 denotes the area per fullerene plus 12 propylamine, plus N_w water molecules. The dimensions of this box, area A_0 , the thickness d and the N_w are the free variables. The best fit free parameters of the model are listed and defined in Table 3 for several values of lateral pressure. Figure 9 shows schematically the conformation of the molecule on the surface of water and the corresponding scattering length densities. The average thickness of the adduct monolayer is 12 \AA , larger than the expected value from a smoothly distributed fullerene layer, 8.2 \AA , however much smaller than the expected end to end length of the adduct (about 20 \AA). The limiting area per molecule obtained by extrapolating the isotherm is about 150 \AA^2 and this value suggests that the neighbor molecules interpenetrate one another in the amine chain region. It is, however, larger than that expected for closely packed fullerene (about 87 \AA^2) and is consistent with a picture in which the adducts are entangled with alkyl chains.

Figure 8. X-ray reflectivity (a) of C₆₀-propylamine spread film on water and the reflectivity normalized (b) to the Fresnel reflectivity of the bare subphase, R_F at lateral pressure $\pi= 6.7$ mN/m.



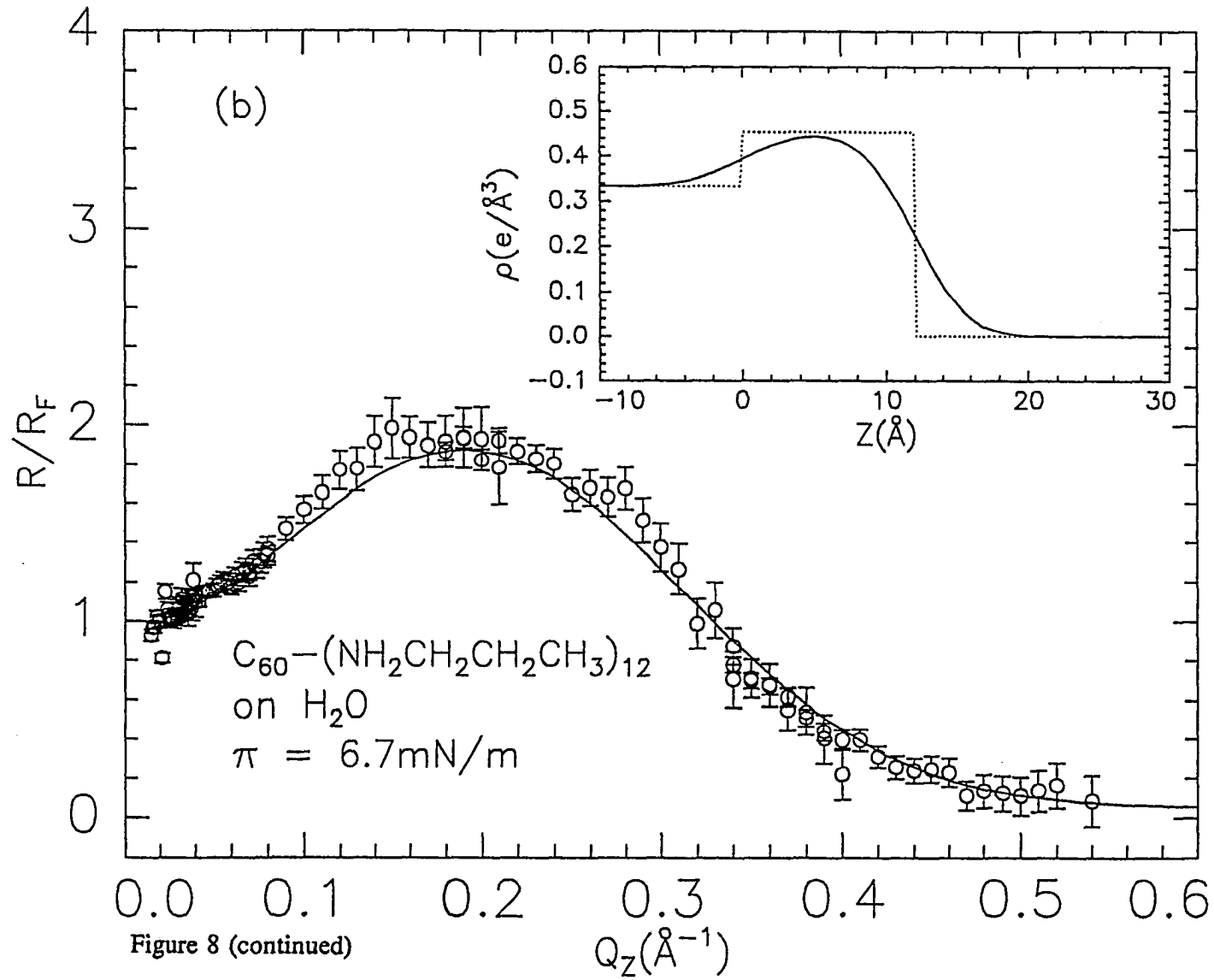


Figure 8 (continued)

Table 3. Structural parameters of C_{60} - $[NH_2(CH_2)_2CH_3]_x$ monolayers at the air-water interface, as obtained from fitting one model to the data sets in Figure 8.

A_0	148.0 Å ²	Average area per molecule
d	12.0 Å	Thickness of the monolayer
N_{cw}	12.0	Number of chains per molecule
N_w	4.8	Number of water molecules in the chain region
σ	3.0 Å	Surface roughness

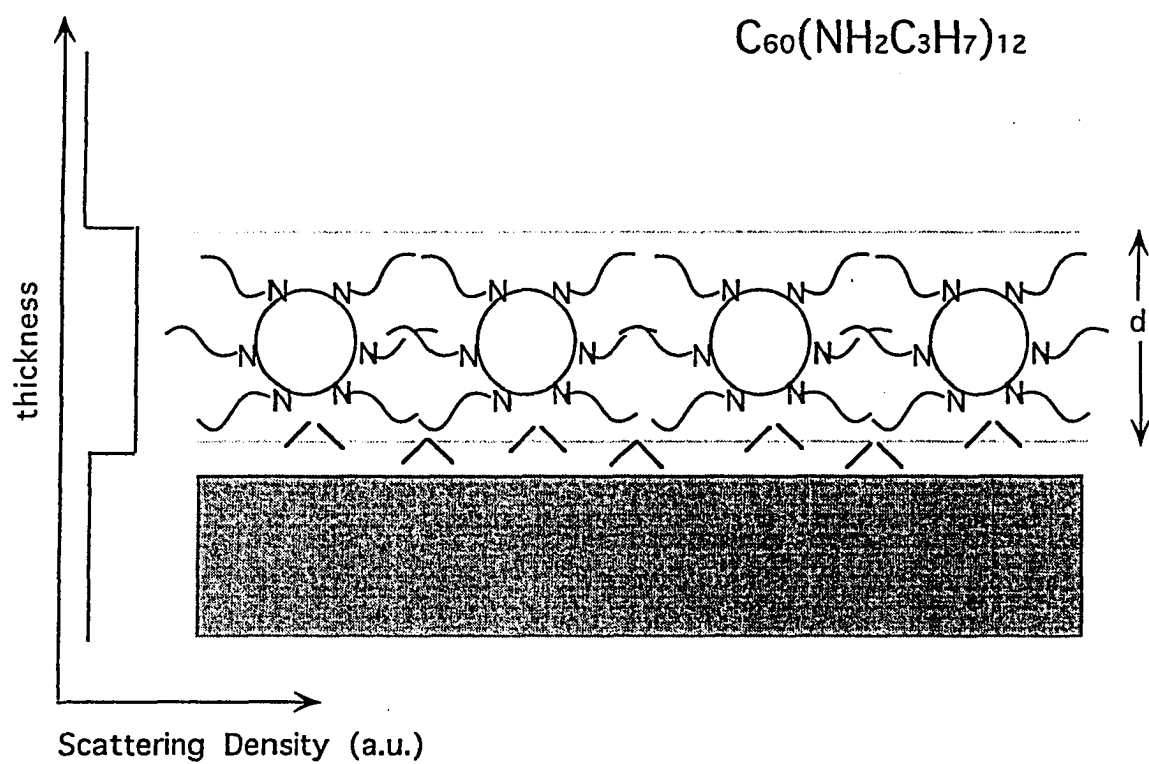


Figure 9. Depiction of the model structure of C_{60} -propylamine monolayer on water surface.

Conclusions

It is widely appreciated that fullerenes possess unique combinations of chemical and physical properties. The present study confirms this view in the specific case of spread monolayers of fullerenes and their derivatives. Although the parent fullerenes can be spread as a film at the air-water interface, the vast majority of studies to date have indicated that these are not homogeneous, monomolecular films. The present scattering data together with the π -A isotherms confirm these conclusions.

Derivatization of the parent C_{60} molecule by forming an adduct with either a long or a short hydrocarbon chain produces a species with a considerably reduced tendency to aggregate. Neutron and X-ray scattering results as well as surface isotherms indicate the formation of monolayers. In addition, the self-consistent model proposed for the detailed structure of the monolayer of the adduct indicates a unique distribution of the submolecular components. The alkyl chains of the amine are randomly distributed over the fullerene surface. In a closely packed monolayer it appears that some alkyl chains contribute to the levitation of the fullerene over the water interface, some chains are laterally entangled with chains of neighboring molecules and some chains are directed into the monolayer-air interface.

Acknowledgments

The author would like to thank Riso National Laboratory for the hospitality extended during the performance of neutron scattering studies. This work was funded in part by Ames Laboratory which is operated for the US Department of Energy by Iowa State University under contract W-7405-Eng-82, supported by the Office of Basic Energy Sciences, by the German Bundesministerium für Forschung and Technologie under contract 05 433 FA I9 and by the NOVO and Carlsberg foundation and the Danish SNF. We are indebted to HASYLAB at DESY, Hamburg, Germany for synchrotron X-ray beam time at beam line BW1.

References

- 1 Y. S. Obeng and A. J. Bard, *J. Am. Chem. Soc.*, **113** (1991) 6279.
- 2 G. Williams, C. Pearson, M. R. Bryce and M. C. Petty, *Thin Solid Films*, **209** (1992) 150.
- 3 J. Milliken, D.D. Dominguez, H. H. Nelson and W. R. Barger, *Chem. Mater.*, **4** (1992) 252.
- 4 T. Nakamura, H. Tachibana, M. Yumura, M. Matsumoto, R. Azumi, M. Tanaka and Y. Kawabata, *Langmuir*, **8** (1992) 4.
- 5 J. Guo, Y. Xu, Y. Li, C. Yang, Y. Yao, D. Zhu and C. Bai, *Chem. Phys. Lett.*, **195** (1992) 625.

- 6 P. Ganguli, D. V. Paranjape, K. R. Patil, S. K. Chaudhary and T. Kshrsagar, *Indian J. Chem.*, **31** (1992) F42.
- 7 R. Back and R. B. Lennox, *J. Phys. Chem.*, **96** (1992) 8149.
- 8 Brewster angle microscope pictures of spread films at the onset of compression show macroscopic clusters (with sizes on the order of microns); data courtesy of Nanofilm Technologie, Göttingen, German using the BAM-1 system.
- 9 M. Iwahashi, K. Kikuchi, Y. Achiba, I. Ikemoto, T. Arki, T. Mochida, S. Yokoi, A. Tanaka and K. Iriyama, *Langmuir*, **8** (1992) 2980.
- 10 F. Diederich, J. Effing, E. Jones, L. Jullien, T. Plesniviy, H. Ringsdorf, C. Thilgen and D. Weinstein, *Angew. Chem.. int. Ed. Engl.*, **31** (1992) 1599
- 11 J. Y. Wang, D. Vaknin and R. A. Uphaus, unpublished.
- 12 T. Suzuki, Q. Li, K. Khemani, F. Wudl and Ö. Almarsson, *Science*, **154** (1991) 1186.
- 13 F. Wudl, A. Hirsch, K.C. Khemani, T. Suzuki, P.-M. Allemand, A. Koch, H. Eckert, G. Srdanov and H. M. Webb, in G.S. Hammond and V.J. Kuck(eds.), *Fullerenes, Synthesis, Properties, and Chemistry of Large Carbon Clusters*, American Society, Washington, D. C., 1992, p. 161.
- 14 R. W. James, *The Optical Principles of the Diffraction of X-rays*, G. Bell and Sons Ltd., London (1948).
- 15 H. Kiessig, *Ann. Phys. (Leipzig)* **10** (1931) 769.
- 16 S. K. Sinha, E. B. Sirota, S. Garoff and H. B. Stanley, *Phys. Rev. B* **38** (1988) 2297.

- 17 D. Vaknin, K. Kjaer, J. Als-Nielsen and M. Lösche, *Makromol. Chem., Macromol. Symp.*, 46 (1991) 383; *Biophys. J.*, 59 (1991) 1352.
- 18 J. Als-Nielsen and P. S. Pershan, *Nucl. Instrum. Methods*, 208 (1983) 545; *Risø-R-660(EN)*, 1992, pp. 130-131.
- 19 J. E. Fischer, P. H. Heiney and A.B. Smith III, *Acc. Chem. Res.*, 25 (1992) 112, and references cited therein.
- 20 J. Als-Nielsen and K. Kjaer, in T. Riste and D. Sherrington (eds), *Proc. NATO ASI Ser. B, Phase Transitions in Soft Condensed Matter*, Plenum, New York, 1989, p. 113.
- 21 J. Als-Nielsen and H. Möhwald, In S. Ebashi, M. Koch and E. Rubenstein (eds.), *Handbook on Synchrotron Radiation*, Elsevier, Amsterdam, 1991, p. 1.
- 22 M. Abramowitz and I.A. Stegun(eds.), *Handbook of Mathematical Functions*, National Bureau of Standards, Washington, D.C., 1992.
- 23 L.G. Parratt, *Phys. Rev.*, 95 (1954) 359.

CHAPTER 3. FORMATION OF NANOSCALE SIZE PARTICLES
WITHIN A CHANNEL PROTEIN MONOLAYER

A paper published in *Thin Solid Films*

J. Y. Wang and R. A. Uphaus

Abstract

The size, structure and ease of manipulation of organized monolayer structures have been used to control reaction pathways for the formation of semiconductor particle clusters of cadmium sulfide and other semiconductors. The size and particle distributions are determined by the specific monolayer structure chosen. The present study reports a new technique for the formation of small clusters of cadmium and zinc sulfides. It combines monolayer methods with techniques based on inclusion formation in restricted volumes. Cadmium and zinc sulfides are formed within the cavity of a channel protein by a simple process in which a close-packed monolayer of the channel protein is formed on a neutral subphase, transported to a cadmium-chloride-containing subphase, transferred to a slide by Langmuir-Blodgett transfer and exposed to hydrogen sulfide. The channel protein is a membrane-bound entity with hydrophobic exterior walls and a hydrophilic inside channel (12 Å diameter). It is cylindrical and in compressed monolayers is oriented normal to the interface with the channel mouth in communication with the subphase. Small water soluble ions are rapidly taken into the channel interior. The size of the cluster formed is limited by

the small number of ions capable of assimilation into the channel and, because each group of ions is compartmentalized, there is no possibility of spontaneous aggregation to produce macroscopic particulate inside of the protein channel. The cadmium and zinc sulfides were produced in the "quantum dot" size range as evidenced by their markedly blue-shifted optical spectra.

The results of this study indicate more general potential application of channel protein structures as nanoscale reactors; in the case of the protein used here the channel opening and closing can be modulated by pH changes, affording the possibility of sealing or encapsulating reactants or products in small defined volumes. Other types of channel structure are closed by changes in potential, specific small ions or biogenic messenger molecules. Some of these have significantly larger channel volumes than the protein used here. These too may be likely future systems for specific small-scale reaction.

Introduction

In recent years, intense activity in various fields of physics and chemistry has been directed to studies of clusters and small particles. The state of subdivision of these materials (roughly 1-10 nm size) is thus intermediate between single atoms and the bulk materials; in this size range, quantum effects are manifest. Many general reviews are available (see, for example, ref. 1). The problem in regard to preparation of small clusters in a controlled manner devolves into the use of preparative systems which have restraints on growth by the control of physical confinement. The following systems, among others, have been used to

prepare clusters of the desired size: vesicles [2]; reverse micelles [3]; polymers [4]; glasses [5]; zeolites [6]; bulk solution [7] and solid-phase thermolysis [8]. The size scale and the structural organization of monolayers and vesicles suggest themselves as suitable types of systems for *in-situ* synthesis of small clusters and many of these efforts have been reviewed [9]. Cadmium sulfide thus was made by simple reaction of hydrogen sulfide with multilayers of cadmium arachidate [10]. The use of monolayer systems was more fully exploited in the studies of Fendler and coworkers [11] who investigated a range of techniques to produce cadmium sulfide in these structures.

A method is here described for producing nanoscale cadmium and zinc sulfides which combines monolayer techniques with the use of a small-cavity confinement system. Particulates are formed inside the hydrophilic channel of the gap-junction channel protein MIP-26 (major intrinsic protein; molecular weight, 26kD). MIP-26 is found in the cells of mammalian eye lenses; because by necessity the eye lens must be optically clear and free of blood vessels, all metabolites must diffuse throughout the lens structure and the channel protein system forms an interconnecting network of conduits throughout the entire lens. The protein has a number of advantages for monolayer studies: its amino acid sequence is known from cDNA cloning; it is soluble in lipid solvents but insoluble in water; it forms strong (60 mN/m) organized monolayers and it is available in large amounts, unlike most other channel protein systems. One bovine eye lens provides 1 mg of pure material, a consequence of the fact that about 30% of the total protein in the lens is bound up in MIP-26 structures.

Preliminary monolayer characterization has been reported [12], together with Raman

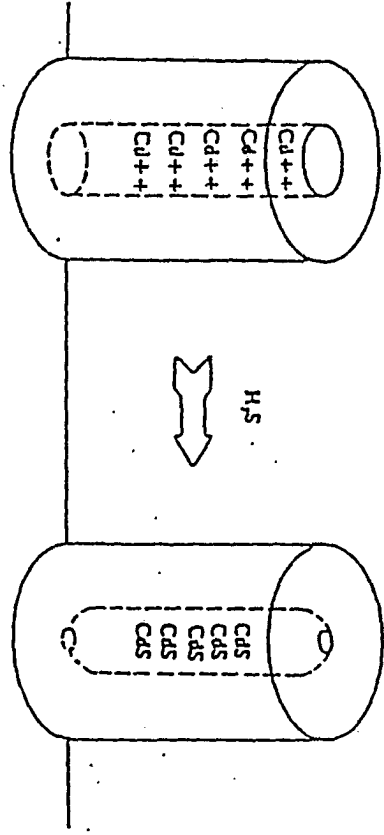
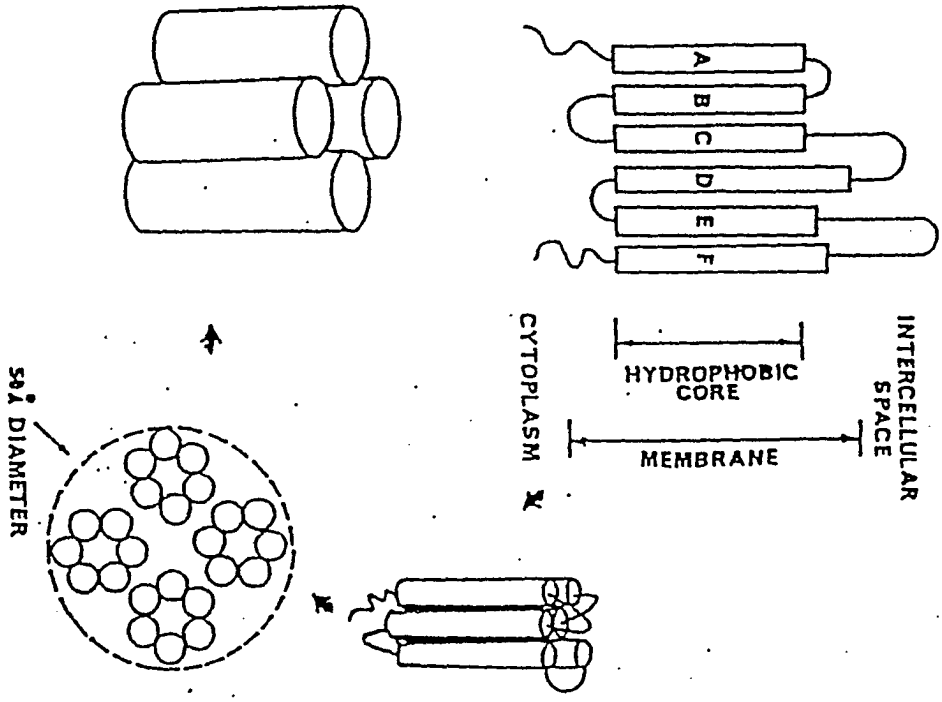
and electrochemical data which indicate that the channel function and its accessibility can be manipulated while in monolayer form. The apparent area per functional unit is around 19 nm² which agree with other data, indicating that the functional unit is a cylinder made up of a tetramer of bundles each made up from five to six α -helical bundles; the channel is formed as a void between contacting bundles. Figure 1 shows schematically the spontaneous formation of the functional system from four separate 240-residue linear peptides, together with the mode of formation of cadmium sulfide on the inside of a channel. The channel is closed upon deviation of the ambient pH from physiological values. The previous monolayer data indicate that the channel stand normal to the interface when in a close-packed monolayer; therefore the ends are accessible to the subphase and water soluble materials can pass readily into the hydrophilic channel interior. Reviews are available describing the biochemical and biophysical characteristics of MIP-26 [13].

Experimental details

protein preparation

MIP-26 was prepared and purified by a modification of a method using organic solvents [14] and the final purified product was present in a chloroform-methanol solution (chloroform:methanol = 1:1) which was used directly as the spreading solution.

Figure 1. Structure of the MIP-26 channel protein and model of formation of the sulfide particles within the channel.



Monolayer methods

A circular multicompartiment trough (Meyer Feintechnik, Göttingen, German) was used to measure surface pressure-area isotherms and to facilitate transport of monolayers from one subphase to another. Optical spectra of a transferred multilayers were measured with a Perkin-Elmer Lambda 6 UV-visible spectrophotometer. The water used to prepare subphases was produced from the tap water by an initial treatment with carbon and particulate filter and reverse osmosis; this was the feed water for a Milli-Q (Millipore Corporation) purification system. The cadmium and zinc chlorides were analytical grade.

Formation of cadmium sulfide and zinc sulfide clusters

A close-packed ordered monolayer of MIP-26 was formed in one compartment of the multiple sector trough and compressed to 50 mN/m. The subphase was maintained close to PH 7 using TES (N-tris[Hydroxymethyl]-methyl-2-aminoethane-sulfonic acid) buffer solution, at which value the channel is open. The monolayer was translated to the adjacent compartment, the subphase of which contained cadmium chloride (10^{-3} M) and allowed to stand for 30 minutes. The film was then moved to the compartment from which it could be transferred by Langmuir-Blodgett dipping (2 mm/min) to a quartz glass slide. In some initial experiments it was thought that excess cadmium sorbed at random in regions other than the channel interior could be removed by transport of the monolayer to intermediate subphases of cadmium-free water. However, such a procedure never subsequently produced the desired cadmium sulfide end product because evidently cadmium ions could diffuse out of channels

quite rapidly and be lost into the washing subphase. The optical spectrum of the protein covered quartz slide was then recorded as background signal. The slide was then exposed to an atmosphere of hydrogen sulfide for 60 min and the difference spectrum was recorded. The same procedure was used to produce zinc sulfide.

Results and discussion

Surface isotherms of the MIP-26 at two pH values are shown in Fig. 2. These isotherms are highly reproducible in several independent experiments. From the isotherms we can see that the MIP-26 can form very stable monolayers, no evidence was seen that the film collapsed at pressures of 50 mN/m or higher. Fig. 2 also indicated that a somewhat smaller limiting area per molecule was obtained at pH 6 than that of pH 7. If the orientation of the protein at the air-water interface was such that the long axis of the system were normal to the interface, the variation of molecular size at the different pH values can be attributed to a diameter decrease at lower pH values. This is consistent with the independent measurements of Gooden et al. [15], who measured material flux through the system, reconstituted into vesicles, as a function of pH. Material throughput (i.e. channel diameter) was maximal at around pH 7.

Clusters of cadmium sulfide on a nanoscale size scale were formed inside the channels of MIP-26, as evidenced by the marked blue shift in the optical spectrum of transferred monolayers. Figure 3 represents the optical spectra of pure protein MIP-26 in chloroform-

Figure 2 Surface pressure /are isotherm of MIP-26 at room temperature, solid curve: pH=6, dashed curve: pH = 7.

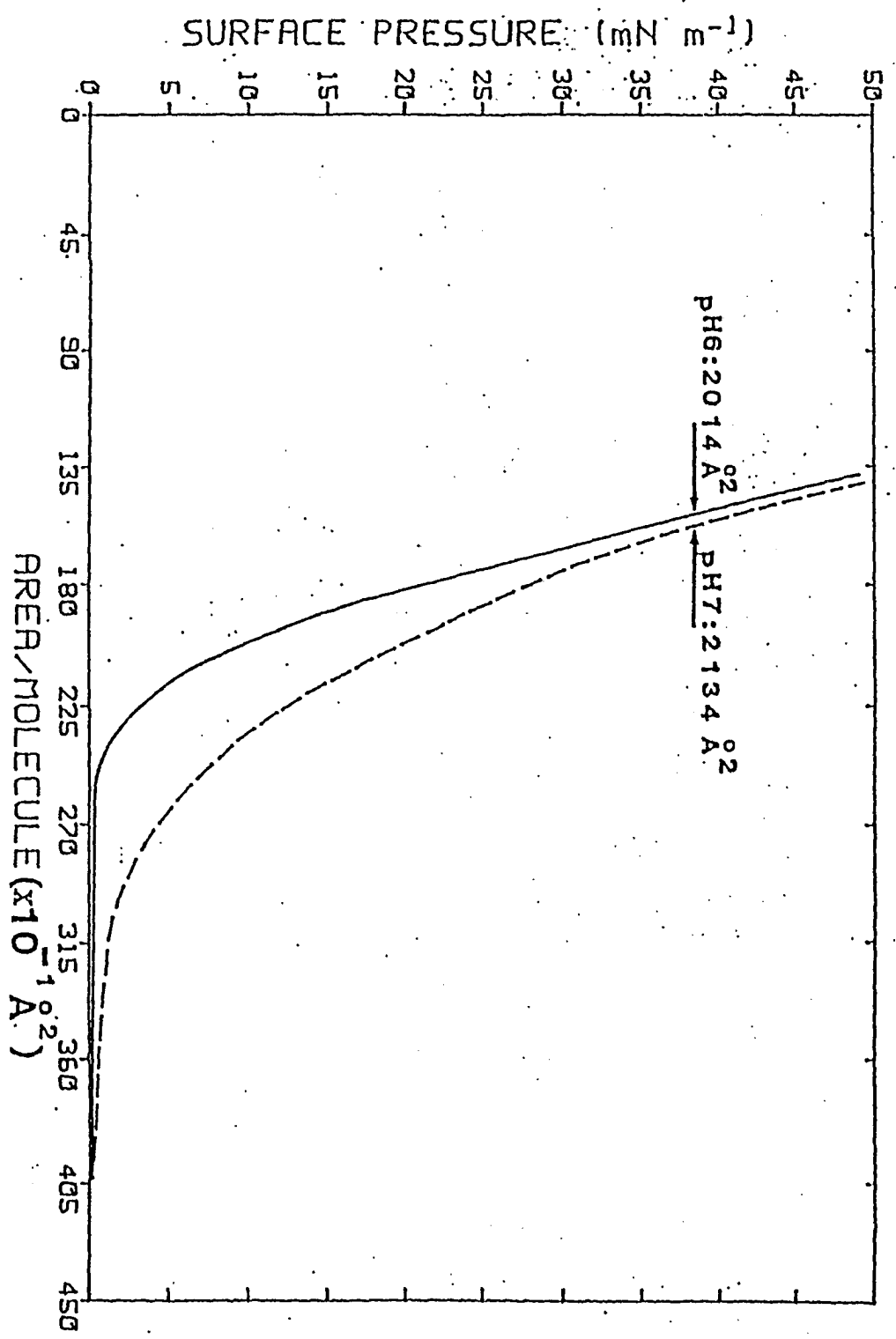
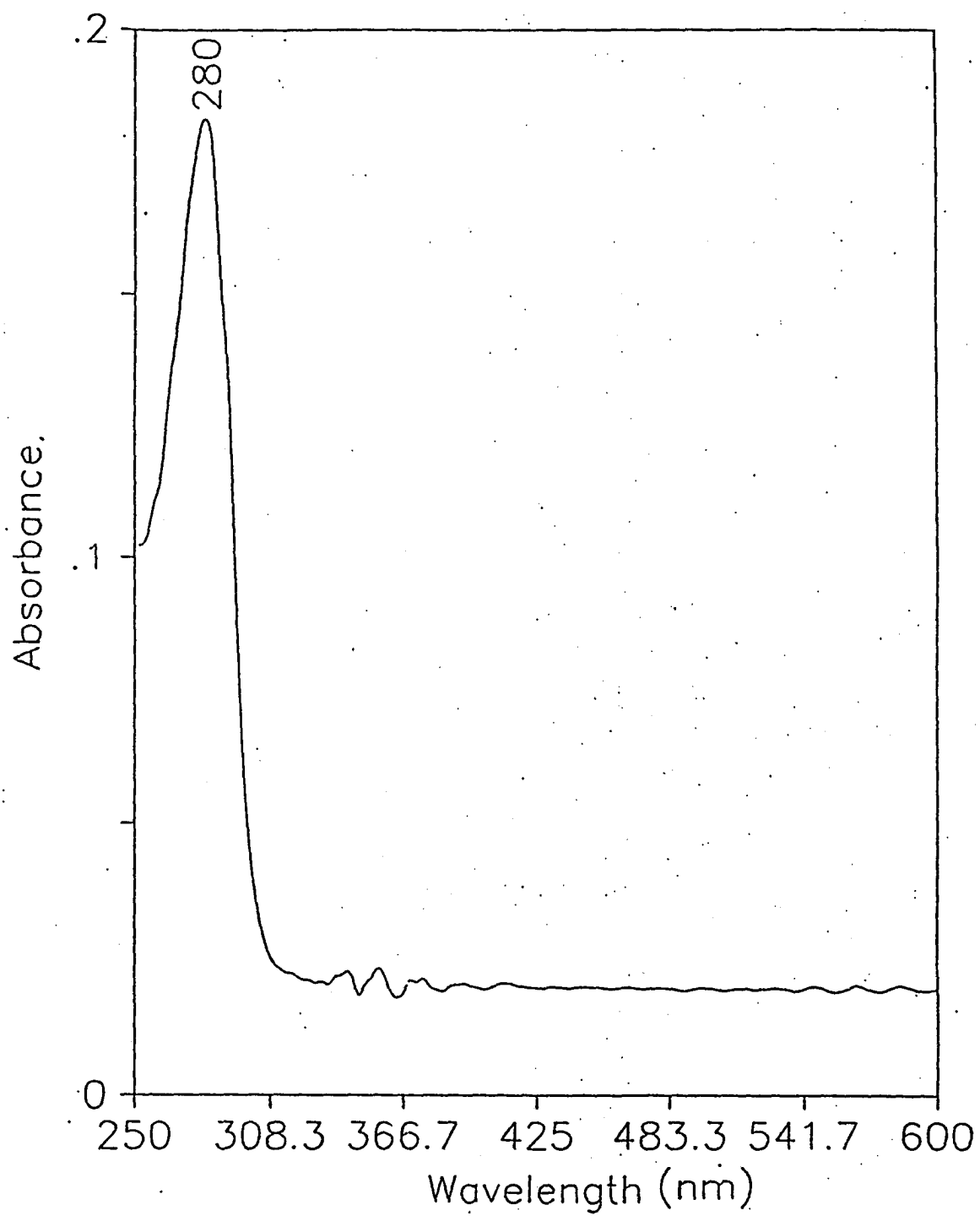


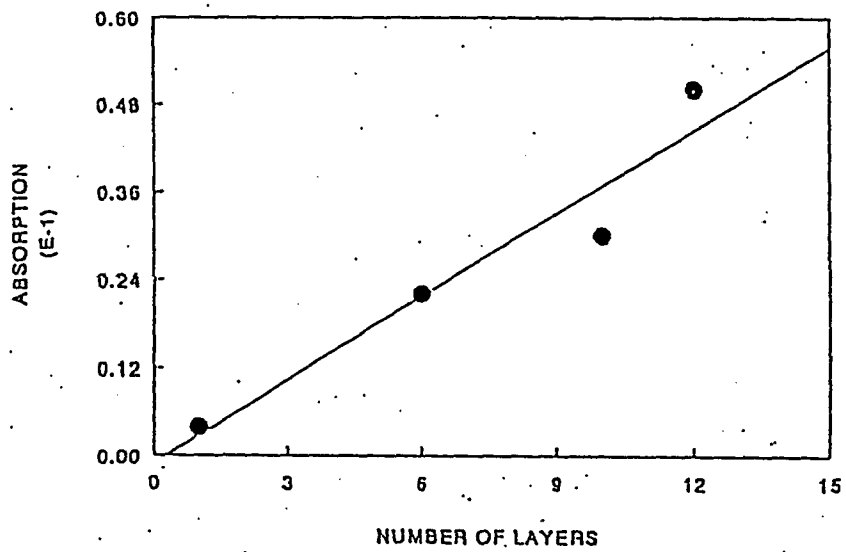
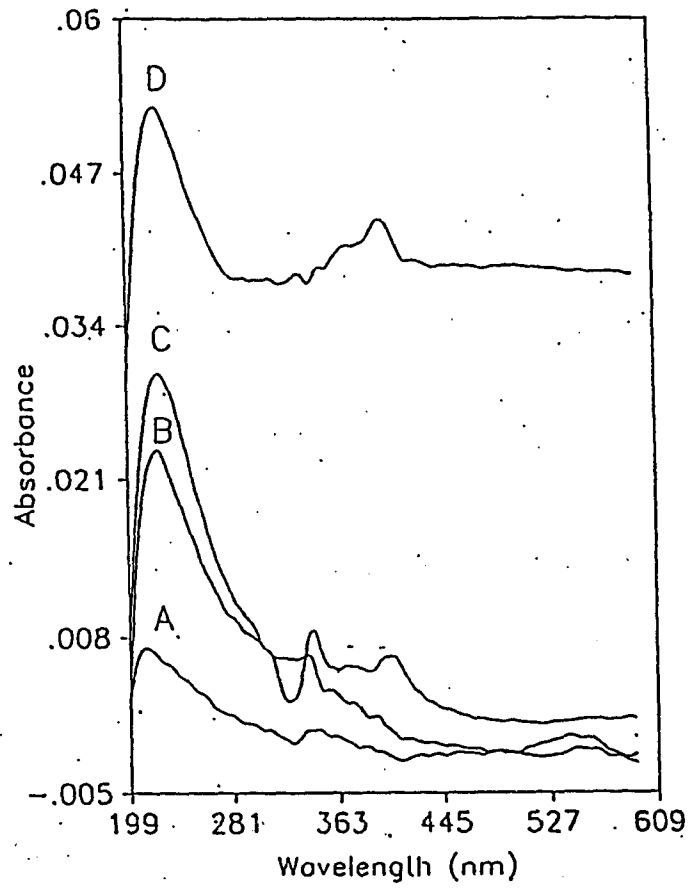
Figure 3. Optical spectra of MIP-26 in chloroform-methanol (chloroform:methanol =1:1) (concentration, 268 $\mu\text{g ml}^{-1}$).

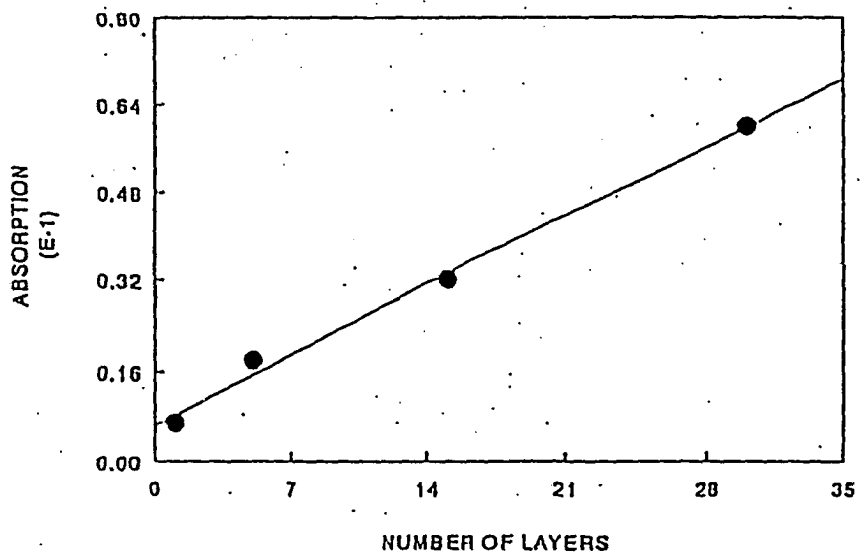
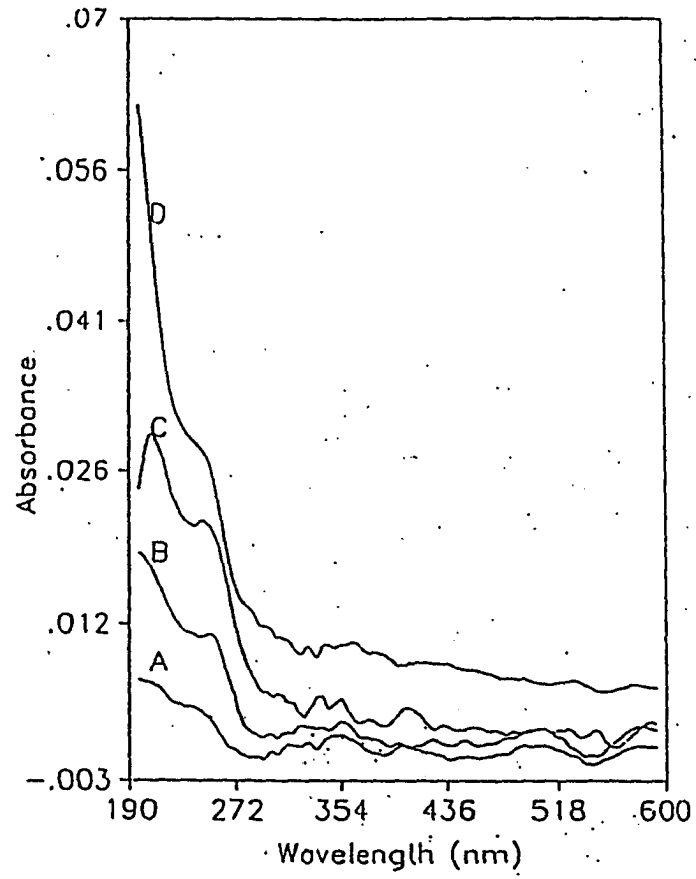


methanol (chloroform:methanol = 1:1). Like many other proteins, MIP-26 absorbs only in the UV region. Figure 4 shows this shift for various number of multilayers and also indicates the linearity of the intensity of the absorption peak with increasing number of layers transferred. Figure 5 show the corresponding results for zinc sulfide particles. All spectra are corrected for background absorption of the protein monolayer before exposure to hydrogen sulfide. It is noteworthy that most of the sulfide appears to form within the channels rather than forming large aggregates around the perimeters or outside the monolayer systems. However, the appearance of absorption maxima at longer wavelengths in some of the spectra indicates that large particulates may sometimes be formed from cadmium ions outside the channels, perhaps sorbed near the hydrophilic ends of the channels. The spectra do not indicate that bulk material is coprecipitated during the formation of the sulfides. The other product of the reaction, HCl, may actually have an enhancing effect on containment, since reduction in pH will cause closure of the channel. However, MIP-26 channels have a closure mechanism at one end only (the end normally projecting outwards into the periplasm) and, until future studies may establish with certainty the up-down orientational sense of individual units in the monolayer, it must be assumed that there is a random 50:50 mixture of up-down orientations. In this case, only half of the channel mouths in contact with the subphase would be affected by the presence of HCl.

It may be concluded tentatively that the MIP-26 channel protein system can be regarded as a true nanoscale reactor vessel. This capability should invite diverse future applications where very small reaction volumes are required. Still to be explored are the

Figure 4. (a) Optical spectra of CdS formed with the MIP-26 channel: curve A, one transferred layer; curve B, six transferred layers; curve C, ten transferred layers; curve D, twelve transferred layers. (b) Absorbance at 230 nm as a function of number of layers transferred.





potential for chemical modification of the inside wall of the hydrophilic channel surface by specific chemical reagents. These could include compounds reacting with specific sites or specific amino acid residues. In addition, a close-packed monolayer of MIP-26 might be made more stable and mechanically stronger if treated with cross-linking agents such as glutaraldehyde. The extent of stabilization would depend upon the frequency and distribution of lysine residues on the exposed outer walls of the protein; such information is not yet available.

The present results suggest that other channel protein systems can be exploited as nanoscale containment vessels. Several hundred channel protein systems have been described to date, with various degree of completeness in regard to their structural and compositional character. However, most of these systems occur at very low concentrations *in vivo* and are moreover usually designed for highly specific functions concerned with regulations and recognition. Most would not be suitable for the application suggested here, but there appear to be some candidates which could be seriously considered for further study. They must meet the requirement of availability in finite amounts (about 1 mg or more) and must have been characterized rather well by various biochemical and physical methods. Two such appear to be the so called VDAC channel [16] and the porin channel systems. The former can be produced in quantity from baker's yeast and the latter from *Escherichia coli* into which the gene-spliced sequence for porin synthesis has been inserted. In both cases, channel closure is mediated by transmembrane potential changes ("voltage gating"). The porin channel is larger than the channel of MIP-26, 2-3 nm in diameter.

The present study has indicated a method for producing semiconductor particles inside a protein structure without, however, indicating how the particulate can be produced free of the protein matrix if this were thought desirable. Stabilization by phosphate followed by enzymatic digestion of the protein structure appears a feasible route; work to that end is in progress.

Acknowledgment

Work performed in part under Contract W-7405-Eng-82, Basic Energy Science, US Department of Energy.

References

- 1 A. Henglein, *Chem. Rev.*, *89* (1989) 1861 and references cited therein.
- 2 S. Mann, A. J. Skarnulis and R. J. P. Williams, *Isr. J. Chem.*, *21* (1982) 3.
- 3 L. Motte, C. Petit, L. Boulanger, P. Lixon, and M. P. Pileni, *Langmuir*, *8* (1992) 1049.
- 4 Y. Wang and W. Mahler, *Opt. Commun.*, *61* (1987) 233.
- 5 A. J. Ekimov and A. Onushchenko, *JETP Lett.*, *40* (1984) 1136.
- 6 Y. Wang and N. Herron, *J. Phys. Chem.*, *91* (1987) 257.
- 7 R. Rossetti, R. Hull, J. M. Gibson and L. E. Brus, *J. Chem. Phys.*, *82* (1985) 552.
- 8 J. G. Brennan, T. Siegrist, P. J. Carrol, S. M. Stuczynski, L. E. Brus and M.L. Steigerwald, *J. Am. Chem. Soc.*, *111* (1989) 4141.

- 9 J. H. Fendler, *Chem. Rev.*, 87 (1987) 877.
- 10 E. S. Smotkin, C. Lee, A. J. Bard, A. Campion, M. A. Fox, T. E. Mallouk, S. E. Weber and J. M. White, *Chem. Phys. Lett.*, 152 (1988).
- 11 S. Xu, X. K. Zhao and J. H. Fendler, *Adv. Mater.*, 2 (1990) 183; K. C. Y. Yi and J. H. Fendler, *Langmuir*, 6 (1990) 1519; X. K. Zhao, Y. Yuan and J. H. Fendler, *J. Chem. Soc., Chem. Commun.*, (1990) 1248; X. K. Zhao and J. H. Fendler, *J. Phys. Chem.*, 95 (1991) 3716; X. K. Zhao, L. D. McCormick and J. H. Fendler, *Langmuir*, 7 (1991) 1255; X. K. Zhao, S. Xu and J. H. Fendler, *Langmuir* 7 (1991) 520; X. K. Zhao and J. H. Fendler, *Materials*, 3 (1991) 168.
- 12 J. H. Kim, D. M. Schufeldt, T. M. Cotton and R. A. Uphaus, in F. T. Hong (ed.) *Molecular Electronics*, Plenum, New York, 1989, p. 329.
- 13 C. Peraccia (ed.), *Biophysics of Gap-junction Channels*, CRC Press, Boca Raton, FL, 1990.
- 14 R. M. Broekhuys, E. D. Kuhlmann and A. L. H. Stols, *Exp. Eye Res.*, 23 (1976) 365.
- 15 M. M. Godden, L. J. Takemoto and D. A. Rintoul *Curr. Eye Res.* 32 (1981) 511.
- 16 C. M. Jones, D. M. Taylor, H. Morgan, J. Lonsdale and R. Southgate, *Proc. 4th Eur. Conf. on Organized Thin Films, Bangor, 1992*, Abstract BP9.

CHAPTER 4. MONOLAYER STUDY OF CLEAVABLE PHOSPHOLIPIDS

A paper Published in *Thin Solid Films*

J. Y. Wang and R. A. Uphaus

Abstract

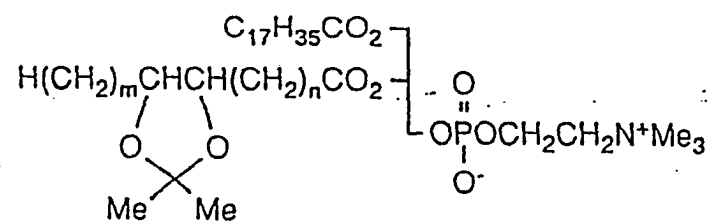
Monolayer characteristics were determined for three isomeric phospholipids containing a ketal group on one of the alkyl chains: 1-octadecanoyl-2-[trans-[2,2-dimethyl-5-octyl-1,3-dioxolan-4-yl]octanoyl]-*sn*-glycero-3-phosphatidylcholine (**1a**); 1-octadecanoyl-2-[16-(2,2-dimethyl-1,3-dioxolan-4-yl)methanoyl]-*sn*-glycero-3-phosphatidylcholine (**1b**); and 1-octadecanoyl-2-[*trans*-Z1-(2,2-dimethyl-5-pentadecyl-1,3-dioxlan-4-yl)methanoyl]-*sn*-glycero-3-phosphatidylcholine (**1c**). The monolayer characteristics were also determined for two of the daughter surfactants in which a *vic*-diol group replaces the ketal group: 1-octadecanoyl-2-(*threo*-9,10-dihydroxyoctadecanoyl)-*sn*-glycero-3-phosphatidylcholine (**2a**) and 1-octadecanoyl-2-(17,18-dihydroxyoctadecanoyl)-*sn*-glycero-3-phosphatidylcholine (**2b**). Surfactants **1a-c** displayed surprisingly high solubility in the water subphase; stable monolayers could not be formed even at 7-8 °C. Reproducible surface pressure isotherms were obtained for **1a-c**, **2a** and **2b** using a subphase of a aqueous 30% polyethylene glycol. The apparent areas/molecule were larger than expected based on estimates fromCPK models, even assuming that all alkyl chains are flat on the interface and are never elevated above it to any appreciable degree, even at high compression. Surface potential measurements

generally remained constant throughout the range of compression. The disparities between measured and estimated molecular areas are probably due to two effects: chirality in the systems and occlusion of void areas present in many of the planar conformational states.

Introduction

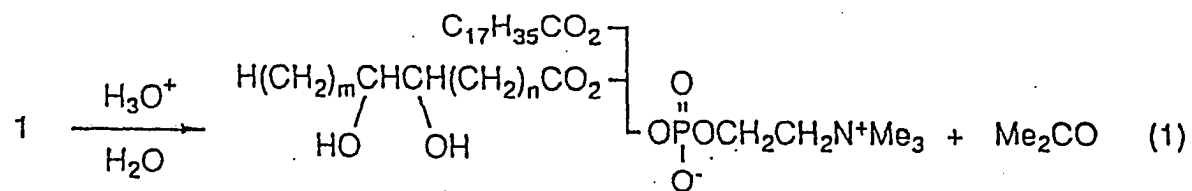
Cleavable surfactants can be converted into daughter surfactants or nonsurfactants [1-3]. Their ability to undergo a change from micellar or vesicular form to an alternate aggregated or nonsurfactant form should have many applications in process technologies, including chemical reagent storage and release. Rinsdorf *et al.* have addressed some of these possibilities [4]. The subject of the present study are the isomeric phospholipids **1a-c**, new examples of vesicle-forming, cleavable surfactants, and the daughter surfactants **2a** and **2b** (Fig. 4.1). Surfactants **1** and **2** contain ketal and *vic*-diol groups, respectively, on one of the alkyl chains. The former are expected to give the latter on acid-catalyzed hydrolysis of the ketal groups. (eqn. 1 in Fig. 1). The parent phospholipid, 1,2-dioctadecanoyl-*sn*-glycero-3-phosphatidylcholine, and chain-substituted analogues (alkyl and phenyl) have been studied in monolayer form [5], as have the analogues having keto or hydroxy substituents at various points along the alkyl chains [6].

The present study was undertaken for several reasons: to compare, if possible, the monolayer behavior of the present compounds to that of the previously studied parent



1

a, m = 8, n = 7; b, m = 0, n = 15; c, m = 15, n = 0



2

Figure 1. Structure of phospholipid isomers and the acid hydrolysis which yields daughter diols.

systems [5, 6]; to determine the changes in hydrophilic/hydrophobic balance from isomer to isomer as reflected in monolayer behavior; and to determine the feasibility of the compounds not as vesicle-forming materials, but as possible components for monolayer-based membrane model systems.

In addition, another intriguing application of these compounds could be in the preparation of membrane-bound proteins or similar compounds, for which it is usually necessary to employ surfactants. After initial extraction, manipulation of the milieu could destroy the detergent and replace it with a different solubilizing agent more amenable to physicochemical studies.

Experimental details

Synthetic methods

The three isomeric phospholipids were prepared as reported elsewhere [5, 6]. Final purification was by column chromatography on silica gel. The appearance of the three compounds at room temperature was as follows: **1a**, a heavy paste; **1b**, a sticky powder; **1c**, a freely flowing powder; **2a**, a sticky powder and **2b**, a granular, free-flowing powder. The last two diols had the same appearance as their corresponding ketal-containing parents. These states appear to arise as a consequence of the position of the ketal/*vic*-diol group and appear to have a qualitative correlation with the observed monolayer behavior of each of these groups.

Monolayer techniques

All water was purified by passage through a Milli-Q system, following a prepurification step using carbon and particulate filtration and reverse osmosis treatment of tap water. Surface isotherms were determined in a thermostated Teflon trough using a (filter paper) Wilhelmy plate and LVDT electrical transducer. Subphase temperature was measured by a teflon covered thermocouple (Yellow Springs Instrument Co., Yellow Springs, OH). Surface pressure measurements made on 30% polyethylene glycol aqueous subphase were uncorrected for the absolute surface tension of such solution. Surface potentials were determined with a specially designed ionization type surface electrode [7]. The entire trough system was enclosed in a grounded Faraday cage because of the sensitivity of the surface potential electrode to minor ambient electrical fluctuations. Background determinations of the surface potential on pure water subphase indicated a base line drift with the compression barrier at different positions in the compression cycle, and the error in surface potential determination is estimated at ± 5 mV. Signals for all variables were digitized and computer-stored. All solvents were analytical grade and all other chemicals at least reagent grade. The polyethylene glycol (Sigma Chemicals) had an average molecular weight of 200 and was used without additional treatment. In all cases the compression rate was $0.42 \text{ \AA}^2 \text{ min}^{-1} \text{ molecule}^{-1}$.

Results and discussion

π -A isotherms on water subphases

The previous monolayer studies of related phospholipids [5, 6], which contained either hydrophobic aromatic substituents or hydroxy/keto functions in the alkyl chains, rather than the hydrophilic ketal and *vic*-diol groups of the present compounds, indicated that stable monolayers were formed, with little tendency to desorb into the subphase. However, surfactant **1** and **2** are much more water soluble. Repetitive compression/expansion cycles with **1a-c** indicated progressive loss of material and smaller and smaller apparent molecular areas (data not shown). Compounds **1a** showed the most extreme behavior in this regard, consistent with the generalization that substituent groups near the center of a long alkyl chain will cause the maximum disruption of packing and the greatest perturbation of monolayer structure. The previous study of monolayers of the related phospholipids indicated that even the presence of a methyl group causes measurable disruption of the monolayer structure [5]. Reduction of subphase temperature to 7-8 °C resulted in considerable improvement in surface isotherm reproducibility, especially for isomer **1b**, which showed about 5% area loss between successive compression/expansion cycles. Overall results indicated the unsuitability of a pure water subphase for surface isotherm determination.

π -A isotherms on aqueous polyethylene glycol

In order to decrease desorption of the monolayers into the subphase it was necessary

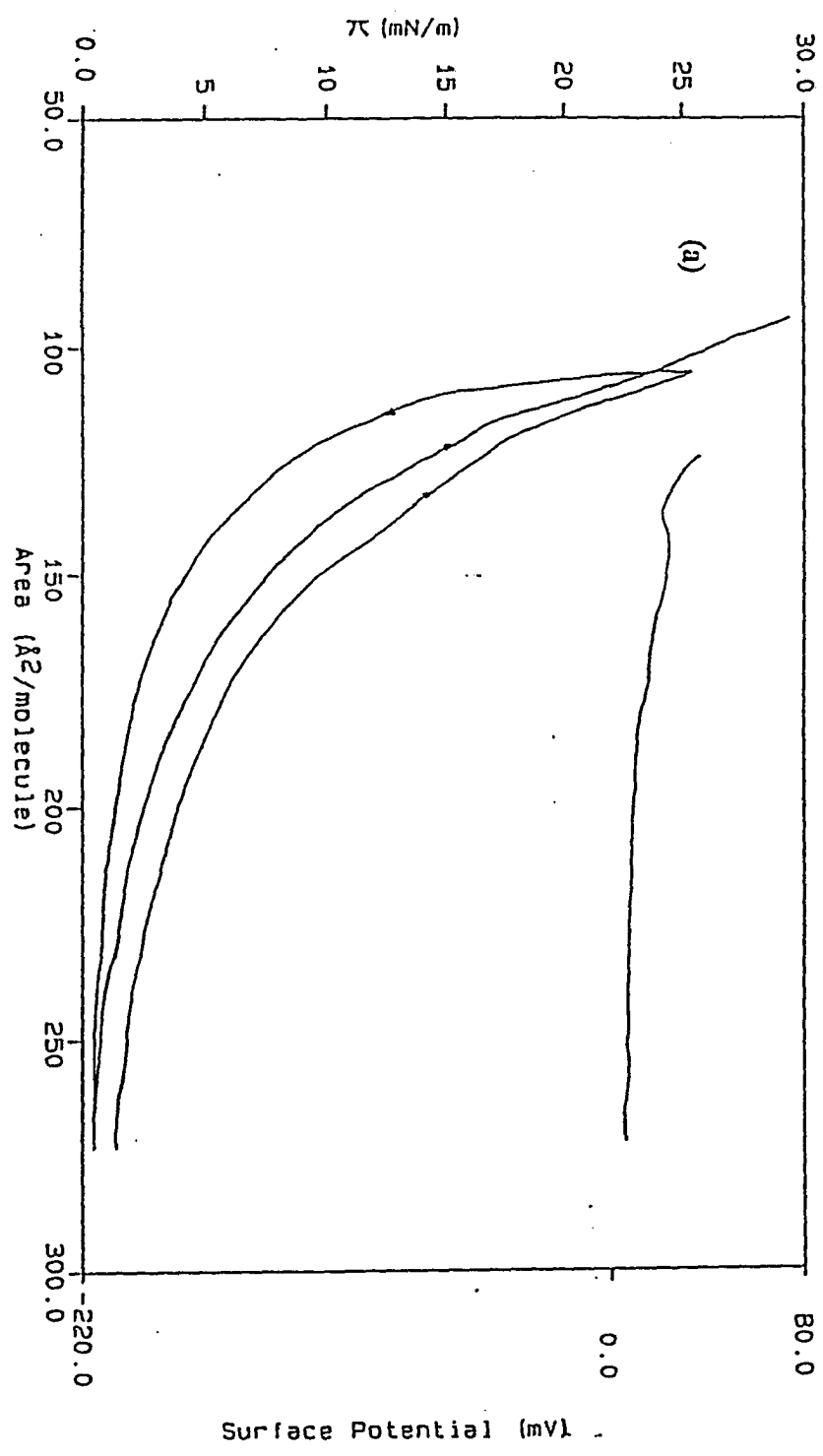
to change to a subphase composition which reduced the activity of water but still provided hydrophilic character and a hydrogen bonding network. Aqueous polyethylene glycol appeared suitable for this purpose. The lowest average molecular weight polymer commercially available (about 200 mol. wt) was used at 30% concentration by volume. A similar compound, e.g. glycerol has been used to advantage as a subphase for spread monolayers [8]. The glycol concentration was a compromise between the increased subphase viscosity taking place with increasing glycol concentration, and the decreased solubility of the monolayers with increased glycol content.

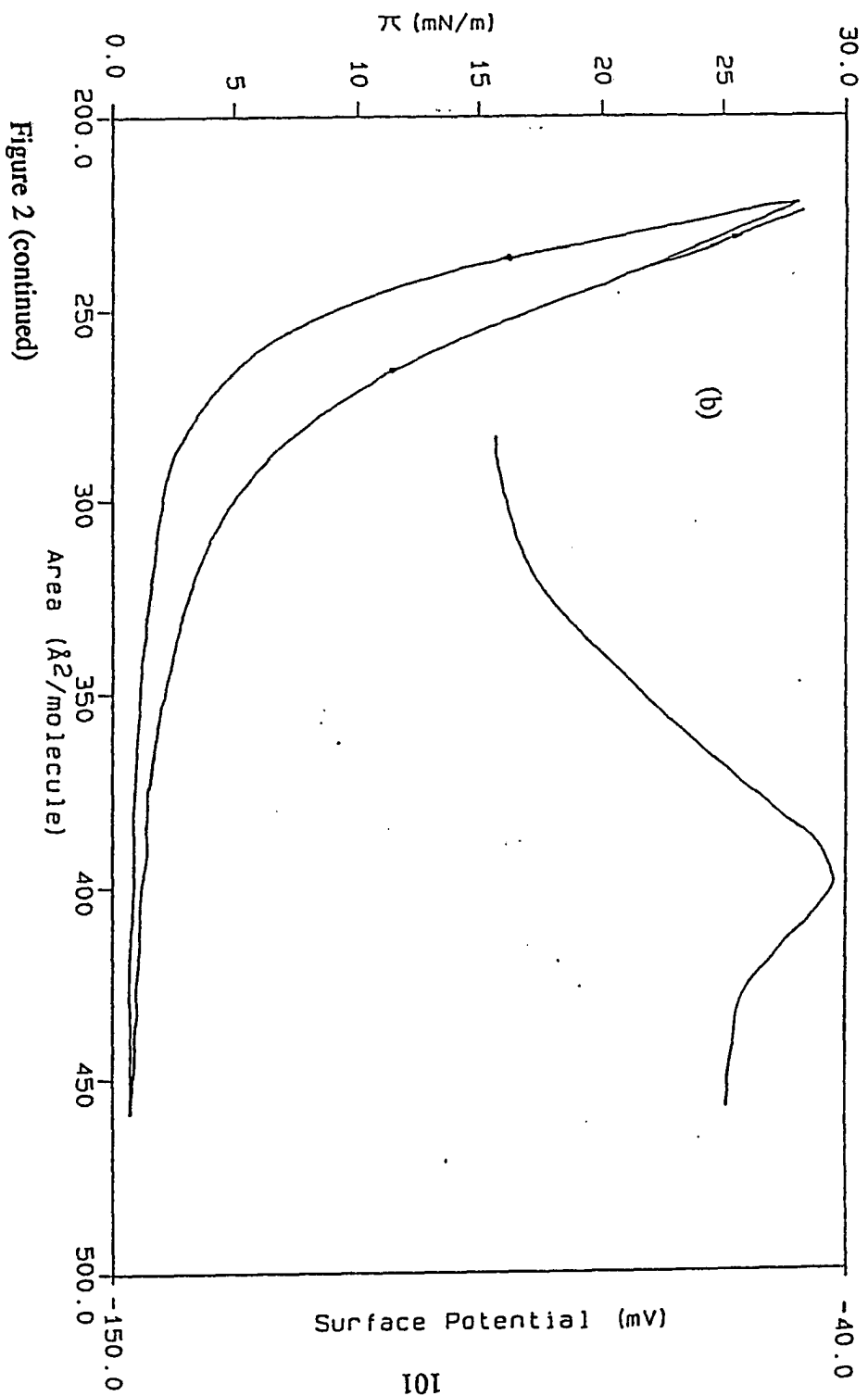
On replacement of pure water with the aqueous glycol subphase the surface potential changed about 300 mV in a positive sense, evidently because of restructuring of hydrogen bonds and the changed net dipole field. However, for purposes of comparison this is not considered of consequence, in the absence of prior data or some theoretical model which might indicate that the phospholipid/subphase interaction is qualitatively different for pure water as compared to the glycol-bearing subphase.

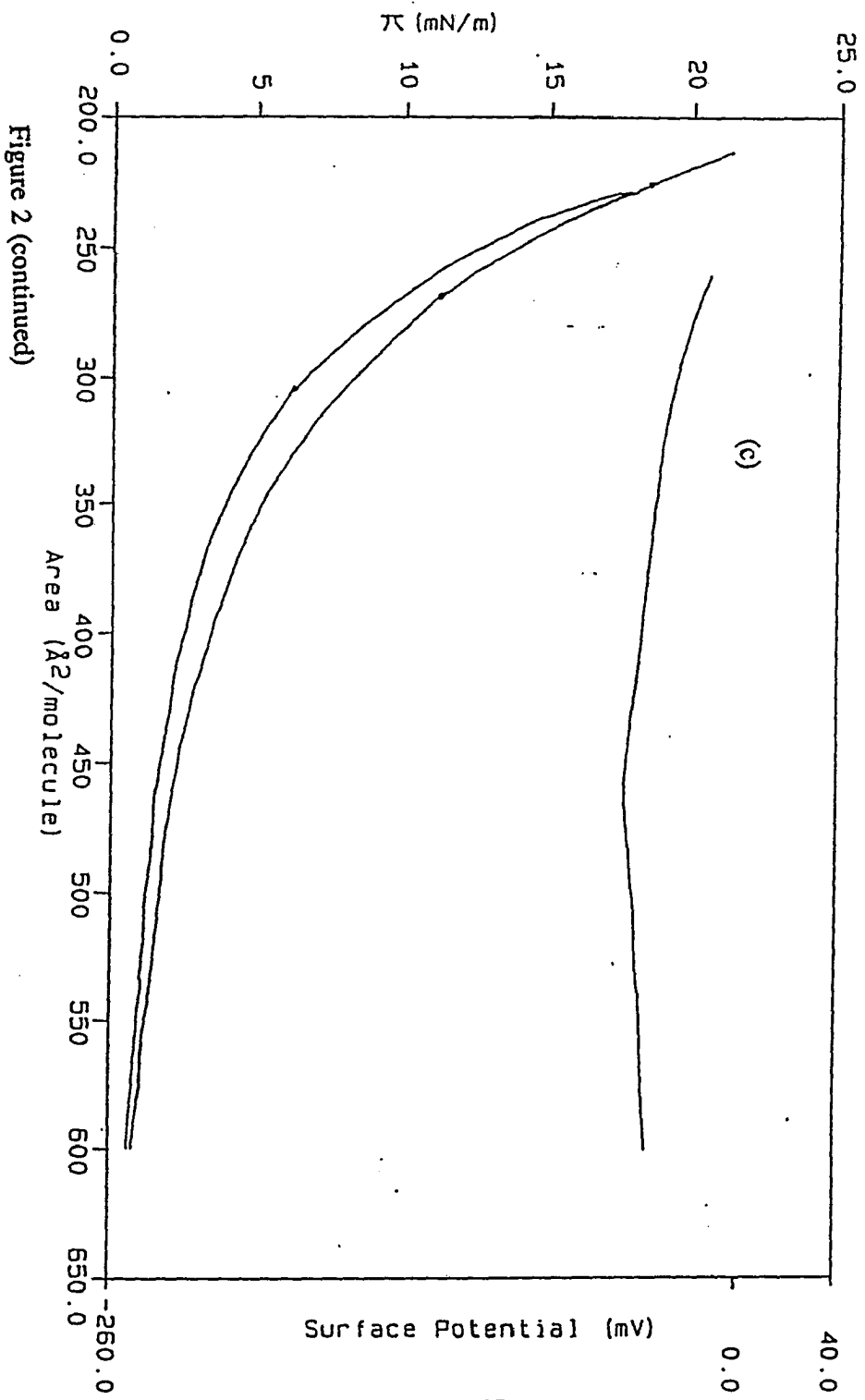
At ambient temperature (21-23 °C) even the use of a glycol subphase did not entirely solve the problem of desorption. Table 1 gives the apparent molecular areas found after the first and the second compression cycles, together with the change in surface potential taking place during compression.

Surface isotherms and surface potential changes are shown in figure 2 for compounds 1a-c and corresponding measurements for compounds 2a and 2b are shown in figure 3. With

Figure 2. Surface isotherms and surface potential changes for phospholipids isomers 1a-c: (a), (b), (c) 1a, 1b, 1c respectively at 23 °C; (d) 1a at 7 °C.







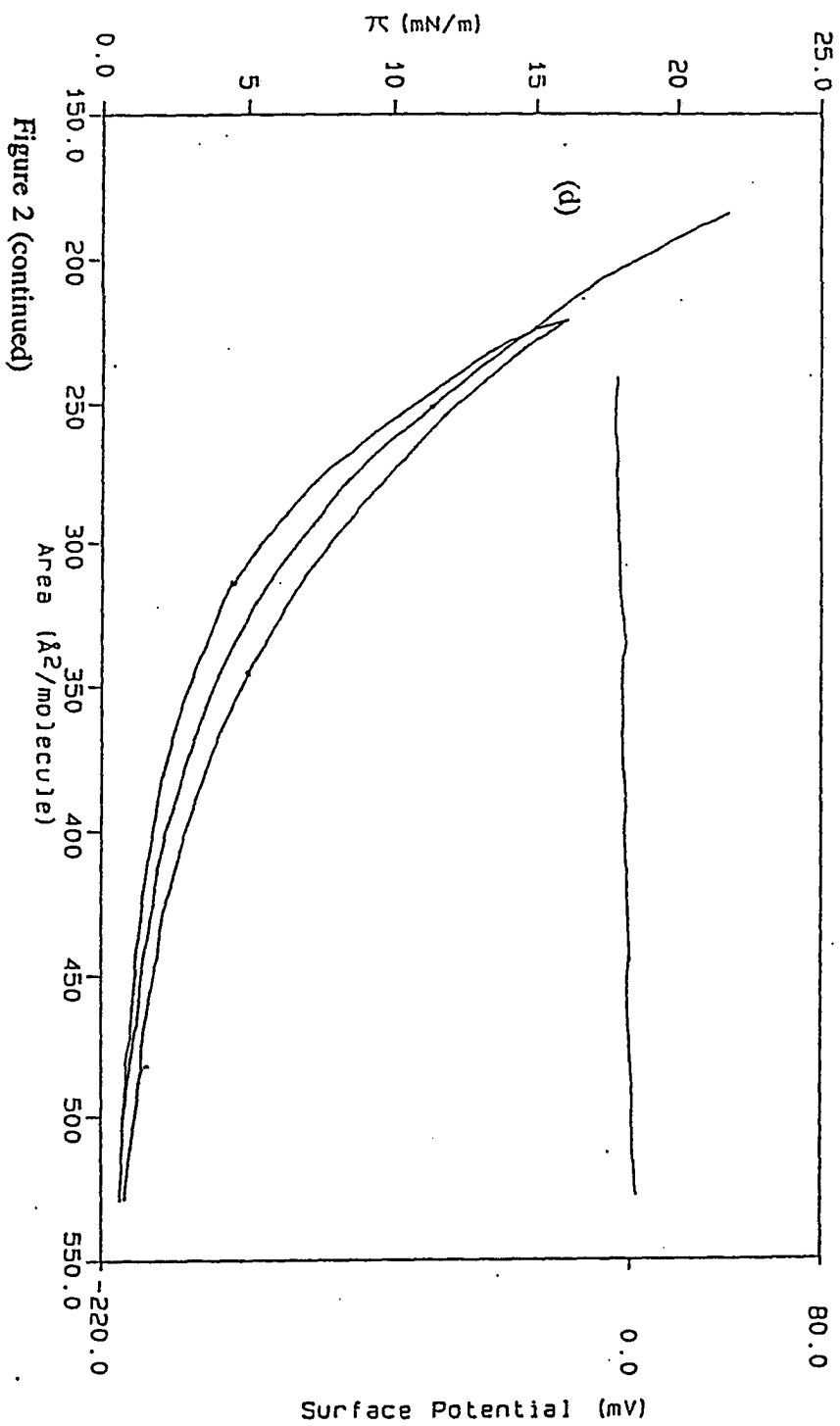


Figure 2 (continued)

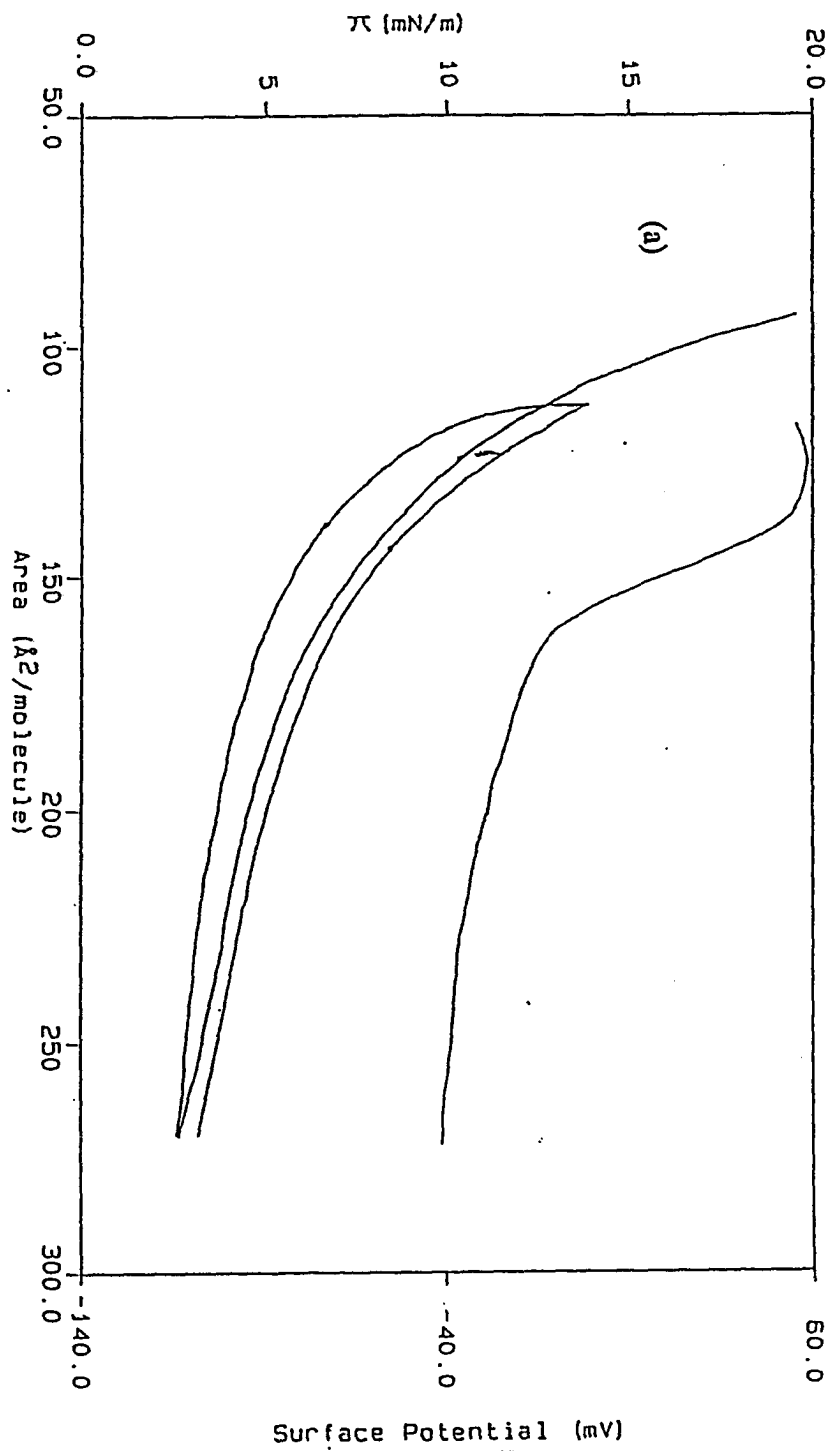
Table 1. Molecular areas and surface potential changes for phospholipids isomers

Compound	Area		Δ Surface potential	
	23°	7°	23°	7°
1a	170	325	+5	-8
	≤ 100	290		
1b	290		+87	
	260			
1c	310		+22	
	290			
2a	170	325	+100	+29
	135	290		
2b	210		-14	
	175			

two exceptions, no pronounced changes in surface potential are evident with increasing states of compression. The observed changes are considerably smaller than those seen in *e.g.*, compression of stearic acid monolayers, which have changes of hundreds of millivolts after the onset of the orientation of alkyl chains normal to the surface and approaching a close-packed state. The small changes observed are taken as indication of little structural reorganization.

In only two instances are the surface potential changes of appreciable magnitude at room temperature (but not at 7 °C). Compound **1b** has a large positive surface potential change at moderate states of compression, later declining to negative values lower than the initial value; compounds **2a** shows a surface potential increase at slightly more advanced stages of compression; however, this is monotonic in later stages of compression. It is tentatively suggested that in the case of **1b**, with the ketal rings at the extreme distal position relative to the main hydrophilic region, compression at ambient temperatures will force the alkyl chain up and above the plane of the interface, much as is the case with compressional changes taking place with long-chain α - ω dicarboxylic acids. At higher compression this chain then falls over back into the plane of the interface. At very high states of compression the chain tends to be drawn downwards into the subphase. This "liftoff" effect was present to a more marked degree in studies of the related phospholipids [6] which contained hydroxy groups along one chain. The mechanism producing the surface potential changes seen with compounds **2a** may be different, but it is again proposed that here the chain carrying the diols is lifted upwards above the interface and maintains this orientation even at high

Figure 3. Surface isotherms and surface potential changes for diols **2a** and **2b**: (a) **2a** at 21 °C; (b) **2b** at 22 °C; (c) **2a** at 7 °C.



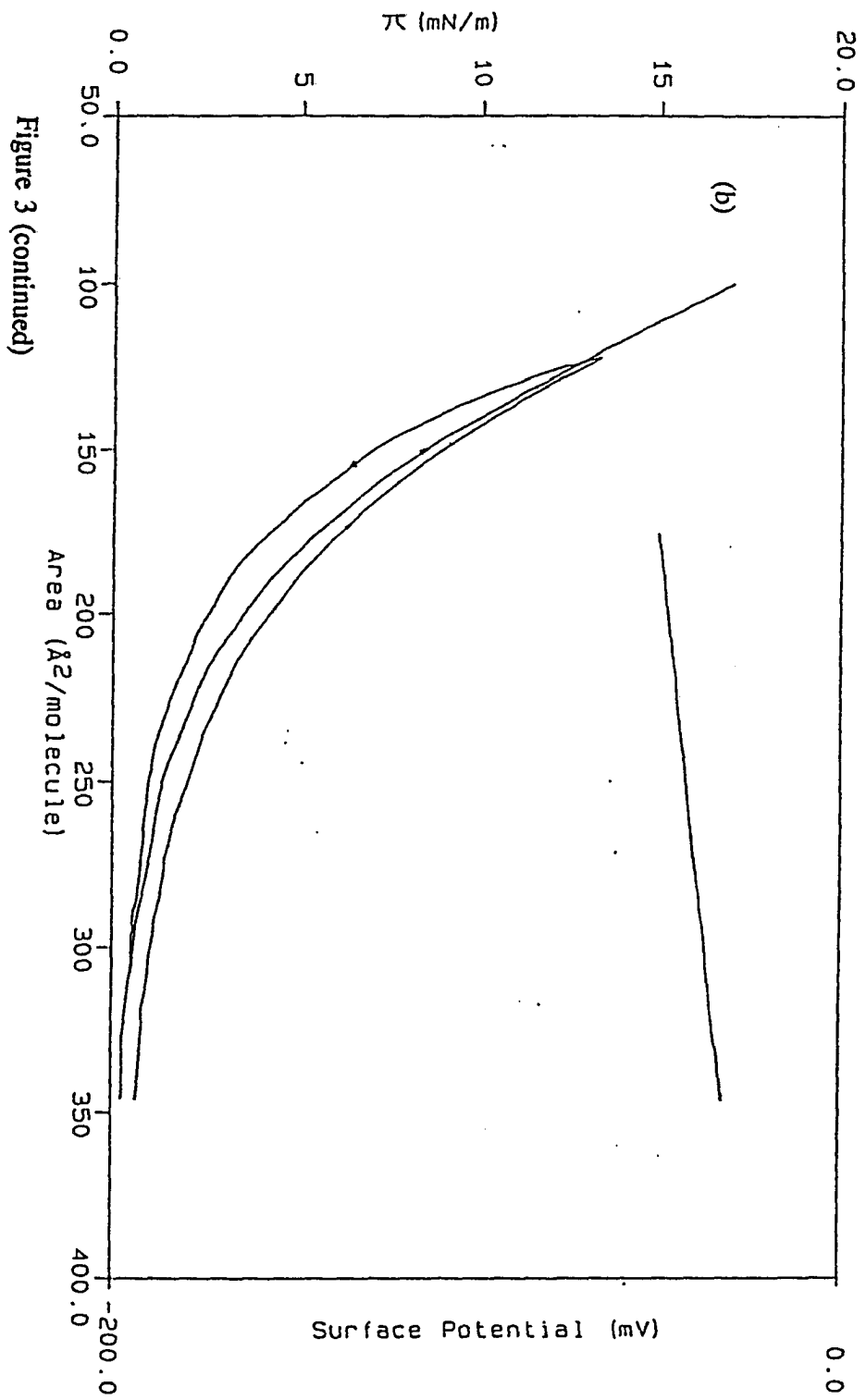
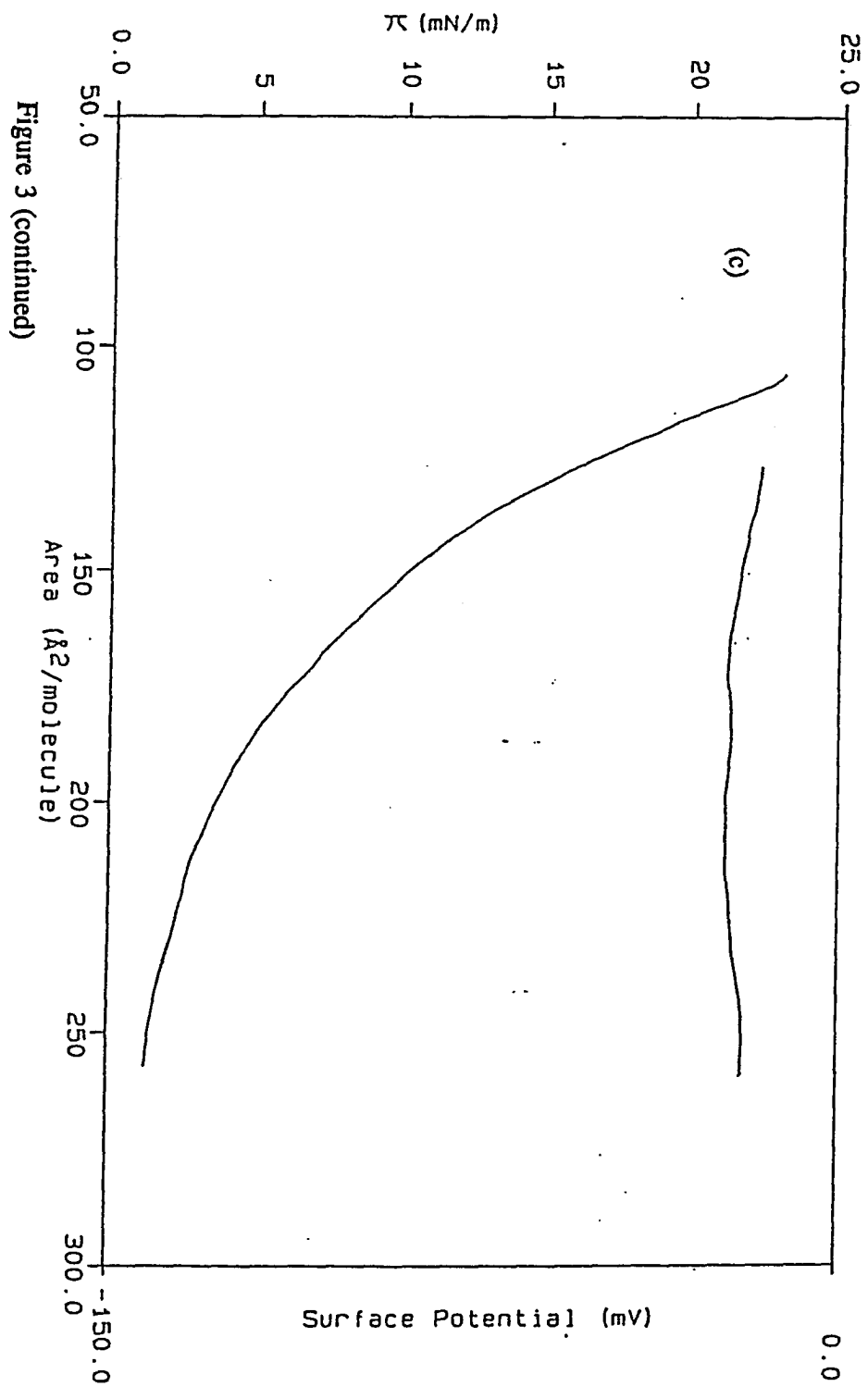


Figure 3 (continued)



compression. The interaction on the diols with the hydroxyl groups of the glycol is probably stronger than in the case of the ketal ring interaction, and tends to anchor the chain more firmly in the subphase.

Neither compound showed these large changes in surface potential at low temperature, possibly because the reduction in thermal energy kT is sufficient to retard the reorientation of chains such that they are lifted off the interface.

It must be assumed that in all cases and at any state of compression (with the qualifications noted above) that the compounds all lie flat or supine at the interface. The estimated area for any isomer, based on CPK models, is 270-280 Å². Any agreement with the values in Table 1 must be taken as fortuitous, however, because of the interplay of two opposing tendencies: first, the obvious appreciable solubility of the monolayers in the subphase (see Table 1), tending to produce values of molecular areas that are too low, and second, an opposing tendency producing values that are too high; the latter effect may be ascribed to two factors.

The structures of these compounds are such that the hydrophilic region(s) is much larger in area than the total cross-section of the alkyl chains. In such a situation the alkyl chains will never be forced into a contacting, close-packed situation regardless of the compression exerted. Assuming that all isomers tend to lie flat in extended positions in the plane of the interface, and that they will all have the same apparent area per molecule, the apparent molecular areas will always be larger than the true area because many of the possible configurational states will include chains in contact in such a manner that occluded

void areas will be present, tending to increase the apparent area. These contorted configurations may tend to be frozen or locked into states which will have voids present even at high compression. Inspection of molecular models indicates that such void areas could amount to 50 \AA^2 or more.

A second important factor which could produce apparent areas larger than the true size arises because of the chiral center present in all these compounds; each compound is a 50:50 mixture of diastereomers because the starting materials for the synthesis were not single enantiomers. The effect of chirality in monolayers has been most extensively explored by the thorough and elegant studies of Arnett and co-workers [8]. They have shown that, in general, the surface isotherms of mixed monolayers of enantiomers will produce larger apparent molecular areas. Compounds composed of one pure enantiomer or the other produce identical isotherms indicating smaller apparent molecular areas than those of isomer mixtures. In the present case, mixtures of diastereomers are present because of different isomers present in the compounds used in the initial synthetic steps. The effects of isomeric mixtures may produce appreciable but indeterminate results for apparent molecular areas. The only way of separating the effects of dissolution into the subphase from the effect of looser enantiomeric packing is to determine surface isotherms for one or both pure enantiomers; these are not available at present.

An additional tendency may be present, the magnitude of which is also indeterminate. It is possible that spontaneous segregation of pure enantiomers could take place in small (but not macroscopic) regions of a mixed monolayer. This would have the effect of decreasing

the apparent molecular areas. Recent evidence that segregation of pure isomers may actually take place in enantiomeric mixed monolayers has been provided by a study of transferred films by atomic force microscopy [9]. For the present compounds, this effect probably could not be pronounced because of the lack of any capacity to form strong, structured and solid monolayers.

Conclusions

Monolayer characteristics were determined for three isomeric cleavable phospholipids **1a**, **1b**, **1c** and the daughter compounds **2a** and **2b**. Surfactants **1a-c** displayed surprisingly high solubility in pure water subphase; stable monolayers could not be formed even at 7-8 °C. Reproducible surface pressure isotherms were obtained for **1a-c**, **2a** and **2b** using a subphase of aqueous 30% polyethylene glycol. The present study suggest that polyethylene glycol provides a satisfactory alternative for those molecules that have very high solubility in pure water. The apparent areas/molecule were larger than expected based on estimates from CPK models, even assuming that all alkyl chains are flat on the interface and are never elevated above it to any appreciable degree, even at high compressions. Surface potential values generally remained constant throughout the range of compression. The disparities between measured and estimated molecular areas are probably due to two effects: chirality in the systems and occlusion of void areas present in many of the planar conformational states.

Acknowledgements

This work was supported by the National Science Foundation (CHE 910482) and the U.S. Army Research Office. This work was also performed in part under contract W-7405-Eng-82, Basic Energy Science, U.S. Dept. of Energy. The Author express appreciation to H. Brockman, Hormel Institute, University of Minnesota, for the acquisition of the surface potential electrode and helpful discussions.

References

- 1 D. A. Jaeger, J. Jamrozik, T. G. Golich, M. W. Clannan and J. Mohebalian, *J. Am. Chem. Soc.*, *111* (1989) 3001.
- 2 D. Ono, A. Masuyama and M. Okahara, *J. Org. Chem.*, *55* (1990) 4461.
- 3 A. Sokolowski, A. Piasecki and B. Burczyk, *J. Am. Oil Chem.*, *69* (1992) 633.
- 4 H. Ringsdorf, B. Schlarb and J. Venzmer, *Angew. Chem., Int. Ed. Engl.*, *27* (1988) 113.
- 5 F. M. Menger, M. G. Wood, S. Richardson, Q. Zhou, A. R. Erlington and M. J. Scherrod, *J. Am. Chem. Soc.*, *110* (1988) 6797.
- 6 F. M. Menger, S. D. Richardson, M. G. Wood, Jr. and M. J. Scherrod, *Langmuir*, *5* (1989) 207.
- 7 J. Richard, A. Barraud, M. Vandevyver and A. Ruadel-Textier, *Thin Solid Films*, *159* (1988) 207.

- 8 P. L. Rose, G. Harvey and E. M. Arnett, in D. Bethell (Ed.), *Advanced in Physical Organic Chemistry*, Vol. 28, Academic Press, New York, 1993, pp. 45-138.
- 9 C. J. Eckhardt, N. M. Peachey, D. R. Swanson, J. M. Takacs, M. A. Khan, X. Gong, J-H. Kim, J. Wang and R. A. Uphaus, *Nature*, 362 (1993) 614.

CHAPTER 5. MONOLAYER AND SPECTROSCOPIC STUDIES OF
BACTERIOCHLOROPHYLL A

A paper prepared for submission to *The Journal of Physical Chemistry*

J. Y. Wang, Jiyu Fang, T. M. Cotton and R. A. Uphaus

Abstract

Monolayers containing Bacteriochlorophyll *a* (BChl *a*) with or without dimyristoylphosphatidylcholine (DMPC) as a matrix material were investigated at the nitrogen-water interface by surface pressure-area and surface potential-area isotherms. These monolayers were transferred to solid supports and characterized by UV-vis absorption spectroscopy and surface enhanced resonance Raman scattering (SERRS). Strong hysteresis in the first compression-expansion cycle was observed for the BChl *a* monolayers. More stable BChl *a* monolayers were formed after subsequent cycles. The configuration of BChl *a* in monolayers was folded: only the ester linkage group was anchored on the water surface, while its phytol chain and bacteriochlorin ring were above the water surface. The lateral interaction between the bacteriochlorin rings resulted in the aggregation of BChl *a* in pure monolayers. When BChl *a* was diluted by DMPC, the miscibility and interaction between the two components in monolayers were found to depend on their molar ratio. At low molar fraction of BChl *a*, homogeneous mixed monolayers were formed and aggregation of BChl *a* was prevented. At high molar fractions of BChl *a*, an immiscible binary mixed monolayer

was formed. The dominant vibrational modes of BChl *a* in monolayers, assigned to C_sC_m , C_sC_b , C_sC_b , C_mH and C_sN stretching bands were observed in the SERRS spectra. In addition, the presence of partially oxidized BChl *a* was also determined from the SERRS spectra.

Introduction

Langmuir monolayers at the air-water interface have been used as biomimetic model systems for studying the interactions between proteins, phospholipids and ions [1]. By transferring protein or protein-lipid mixed monolayers onto solid substrates, it is possible to construct artificial biological membranes. Recently, many studies have emphasized the use of functional protein Langmuir-Blodgett films for device development, such as biosensors [2-3] and molecular electronics [4-5].

Bacteriochlorophyll *a* (BChl *a*) occurs in purple photosynthetic bacteria. It plays an important role in the primary events of the photosynthetic process beginning with the initial capture of light, to energy transfer and, finally, light-energy conversion in the photosynthetic reaction centers [6]. Only one prior investigation of BChl *a* monolayers has been reported [7]. In contrast, chlorophyll *a* (Chl *a*) which occurs in higher plants and in algae has been extensively investigated in monolayers at the air-water interface and on solid supports [8]. The reason for the fewer studies of BChl *a* may be the instability of isolated BChl *a* in the presence of air and light. It has been shown that the properties of BChl *a* monolayers are different from those of Chl *a* monolayers. Therefore, a detailed characterization of the

structure and photoactivity of BChl *a* monolayers is warranted. The present study focuses on BChl *a* monolayers with or without phospholipid as a matrix molecule. The interaction between BChl *a* and phospholipid at the nitrogen-water interface was investigated by surface pressure-area isotherms and by surface potential measurements. The BChl *a* monolayers were deposited onto quartz plates and electrochemically roughened silver electrodes by the Langmuir-Blodgett method and characterized by UV-vis absorption spectroscopy and surface-enhanced resonance Raman scattering (SERRS).

Materials and methods

Materials

BChl *a* used was extracted from chromophores and purified by high performance liquid chromatography (HPLC) according to standard procedures [9]. Dimyristoyl phosphatidylcholine (DMPC) was purchased from Sigma Chemical Co. and used without further purification. The phosphate salts (NaHPO_4 and NaH_2PO_4) were purchased from Fisher Chemical Co. Chloroform (Fisher Chemical Co., HPLC grade) was used as the spreading solvent. All solutions containing BChl *a* were prepared immediately prior to use in order to minimize oxidation in air.

Quartz plates were used as substrates for the measurements of UV-vis absorption spectra. Silver electrodes were electrochemically roughened and used as SERRS substrates. The water used for the subphase was purified by passage through a Milli-Q system,

following a prepurification step using carbon and particulate filtration and reverse osmosis treatment of tap water. The pH value of the subphase was adjusted to 8.0 using phosphate buffer solution.

Methods

A rectangular Langmuir trough equipped with a Wilhelmy plate was used for the surface pressure measurements of the BChl *a* monolayers at the nitrogen-water interface. Surface potentials were determined with a specially designed ionization type surface electrode [10]. The entire trough system was enclosed in a grounded Faraday cage because of the sensitivity of the surface potential electrode to minor ambient electrical fluctuations. The pure and mixed solution were spread onto a phosphate buffer subphase (pH = 8). The temperature of the subphase was kept at 20 °C. Isolated BChl *a* is extremely prone to oxidation when exposed to air and light. The present monolayer studies were performed under a nitrogen atmosphere and in minimal light. The monolayers were transferred onto quartz plates and roughened silver electrodes at a surface pressure of 20 mN/m.

Absorption spectra of BChl *a*-incorporating monolayers were recorded with a Lambda 6 UV/Vis spectrometer (Perkin-Elmer Co.) at room temperature. Kr⁺ and Ar⁺ tunable gas lasers (INNOVA 100-k3, Coherent Radiation, Inc.) were used as excitation sources for Raman spectroscopy. The Raman scattered light was collected in a back scattering geometry and focused onto the slits of spectrometer/spectrograph (Spex, Triplemate 1877). An intensified silicon photodiode array (Princeton Applied Research, Model 1420) was used as

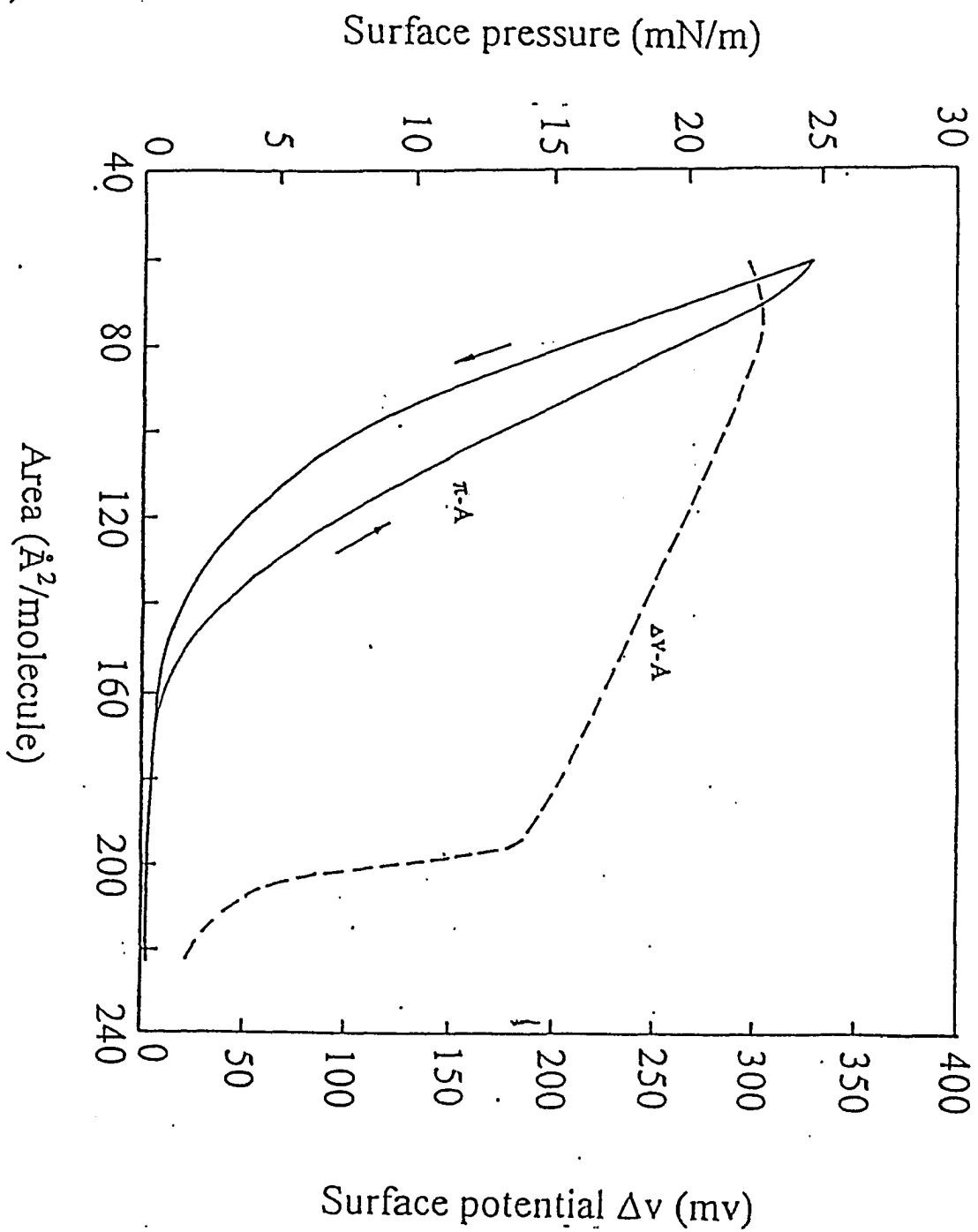
the detector. The signals were acquired and processed using an optical multichannel analyzer (OMA III, Princeton Applied Research). The laser power was kept maintained ≤ 10 mW at the sample. All SERRS spectra were obtained at 77K in a liquid nitrogen cell.

Results and discussions

Monolayer properties of pure components

Figure 1 shows the surface pressure-area (π -A) and surface potential-area (Δv -A) curves for pure BChl *a*. As can be seen, BChl *a* exhibits complex monolayer behavior. The π -A isotherm obtained from the first compression of a freshly spread monolayer is different from subsequent ones. A strong hysteresis is observed in the first compression-expansion cycle. The hysteresis phenomenon is less prominent in the subsequent cycles. In most cases, the cycles become identical after the second compression. The area per molecule is 140 \AA^2 for the first compression and is reduced to 100 \AA^2 for the second compression. Because the area of the flat porphyrin rings is about 200 \AA^2 , it is apparent that the porphyrin ring of BChl *a* molecule has a tiled orientation with respect to the monolayer plane. The difference in area per molecule in the first and subsequent compression cycles may be due to an orientation change of the porphyrin ring of BChl *a* molecule. One possible configuration is that the BChl *a* is folded: at low surface pressures, the ester linkage and the porphyrin are probably anchored at the water surface, with the hydrophobic phytol chain extending away from the water surface. At high surface pressures, strong intermolecular interactions cause the

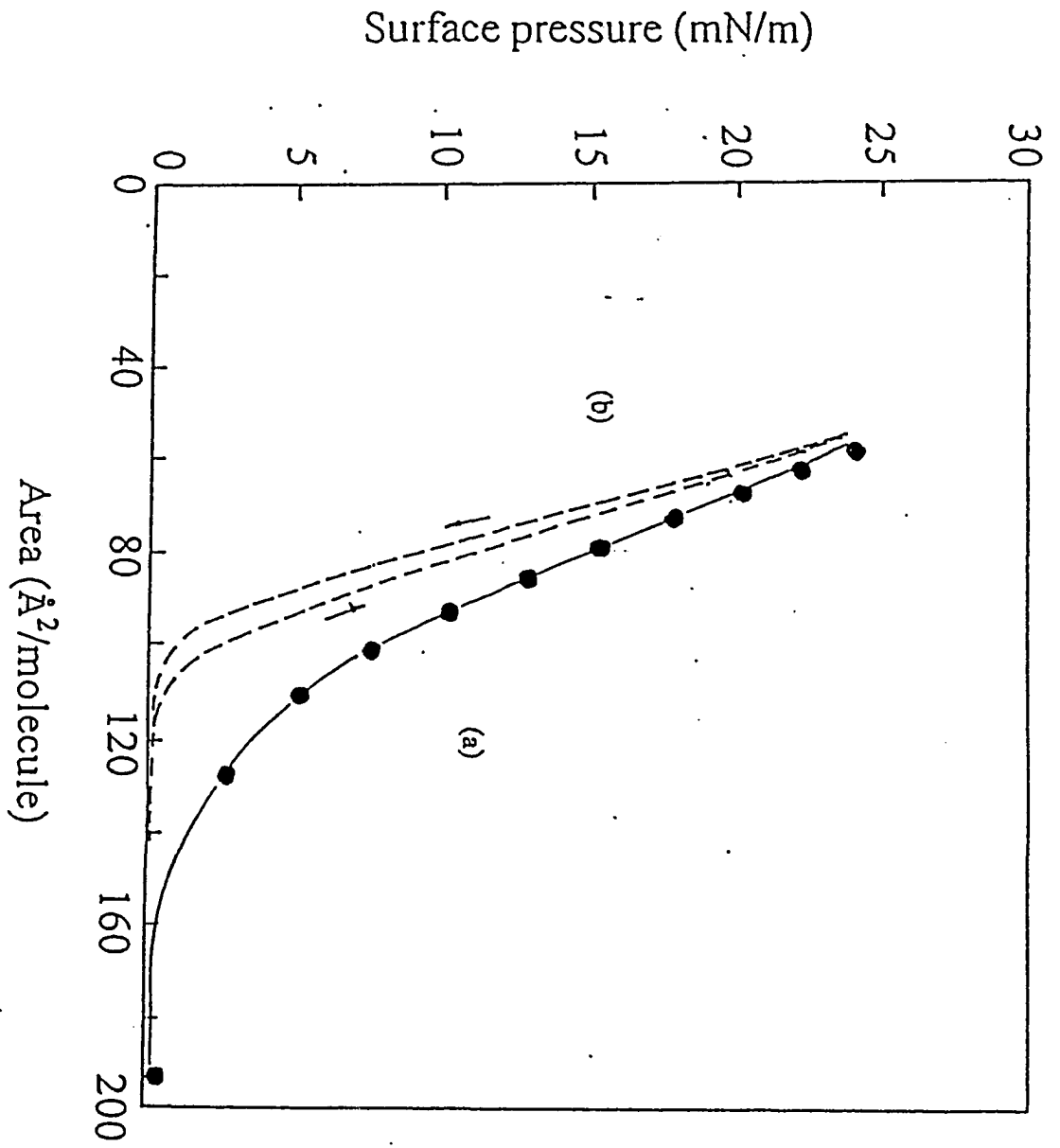
Figure 1. Surface pressure/area isotherms and surface potential changes of pure BChl a monolayers.



porphyrin ring to lift gradually away from the water surface and only the ester linkage is anchored on the water surface. From the Δv -A curve, it is noted that the surface potential jumps from 40 mV at 210 Å²/molecule to 200 mV. The area anchored on the water surface is close to that of the porphyrin ring. Therefore, the abrupt change of surface potential may be due to the fact that the porphyrin ring is extruded from the water surface and oriented at an angle with respect to the water surface. This change in orientation produces a change in the overall dipole moment across the interface and causes the jump in the surface potential. When the monolayer is compressed continuously until collapse occurs at a surface pressure of 25 mN/m, the surface potential exhibits a slow change from 200 to 280 mV. This can be attributed to a change in packing density and/or the tilt angle of the porphyrin rings with respect to the water surface.

The hysteresis in the π -A isotherms reflects the long relaxation time associated with the compression-expansion cycle of BChl *a* monolayers. This indicates that the BChl *a* monolayer can reach an equilibrium phase only after sufficient relaxation time. The relaxation effect can be attributed to the structural changes, such as aggregation of BChl *a* or to a conformational changes, such as folding of the molecules. The equilibrium isotherm for BChl *a* monolayers can be measured by increasing surface pressure at steps of 2 mN/m, as shown in Figure 2. After each surface pressure change, the monolayers were held until they reached equilibrium as indicated by the lack of change in the surface pressure. The area per molecule obtained from the equilibrium isotherm is about 105 Å². The value is close to that obtained from the second compression in the continuous compression mode. After the

Figure 2. Surface pressure /area isotherms of pure BChl *a* monolayers. The isotherm (a) was obtained by increasing surface pressure at a step of 2 mN/m. At each step, monolayers were held 5 min. so that monolayers could reach equilibrium. The isotherm (b) was obtained by continuously compressing monolayers after the equilibrium isotherm was measured.



equilibrium process, the hysteresis in the π -A isotherm becomes much smaller during the compression-expansion cycle.

Figure 3 shows the surface pressure-area and surface potential-area isotherms for DMPC monolayers. Several phases such as the liquid-expanded (LE), liquid-condensed (LC) and solid phase can be obtained by controlling molecular density. The monolayer collapses at a surface pressure of 55 mN/m with an area per molecule of 45 Å². During the monolayer compression, the surface potential changes smoothly until the LE-LC phase transition. After the phase transition, the surface potential of DMPC monolayers rises rapidly and reaches a value of 570 mV in the solid phase. This value is very close to a previously reported result of DMPC monolayers [11].

Interaction of BChl a and DMPC in monolayer systems

In order to study the miscibility and interaction of BChl *a* and DMPC in the mixed monolayer system, the surface pressure-area and surface potential-area isotherms of mixtures with different molar ratios were measured. The dependence of area per molecule on the mole fraction of BChl *a*, measured at a surface pressure of 20 mN/m, is shown in Figure 4. According to the additivity rule for surface pressure [1]:

$$A_{12} = x_1A_1 + x_2A_2 \quad (1)$$

where A_{12} is the average molecular area of the mixture. A_1 , A_2 , and x_1 , x_2 are the molecular

Figure 3. Surface pressure/area isotherms and surface potential curve of pure DMPC monolayers.

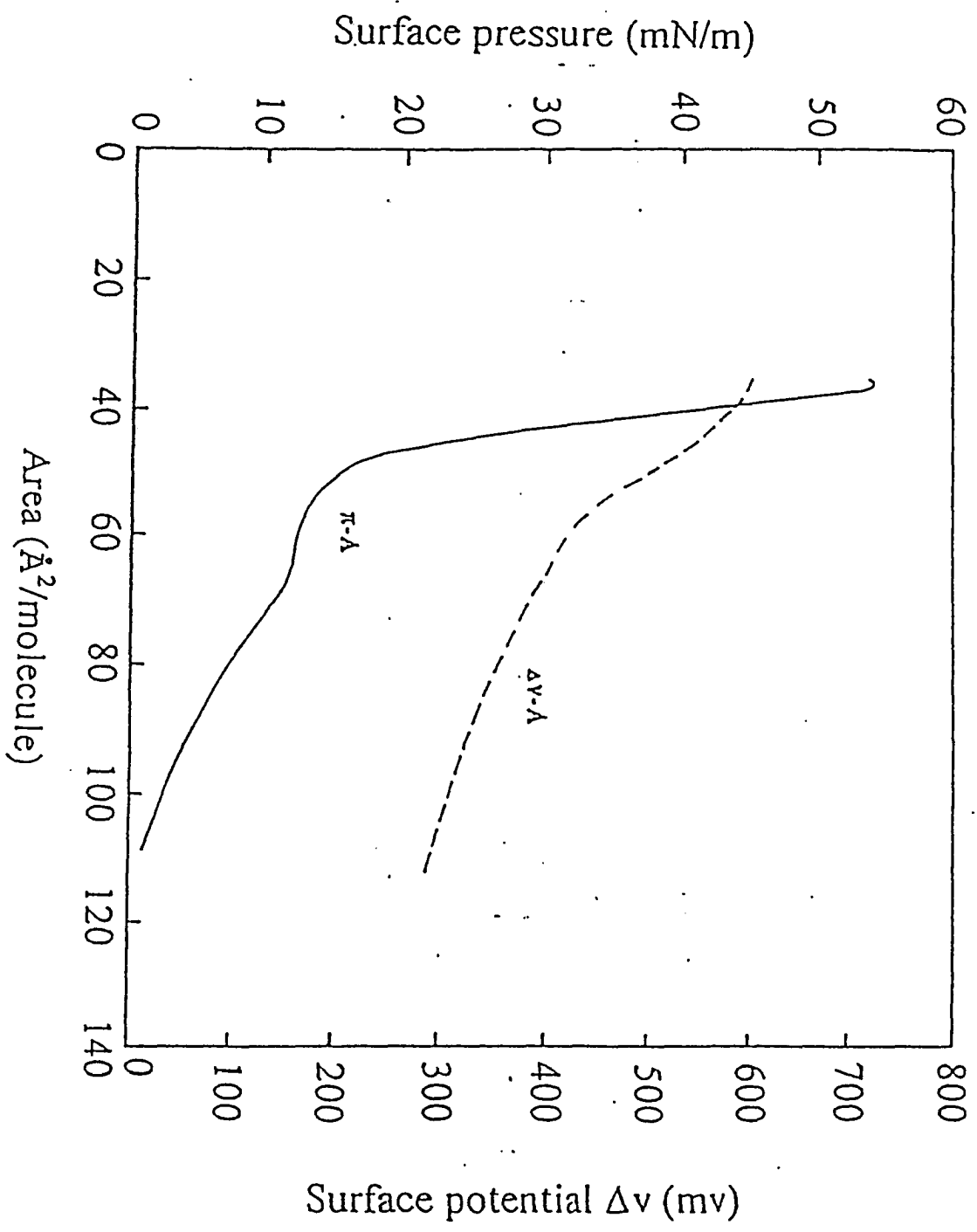
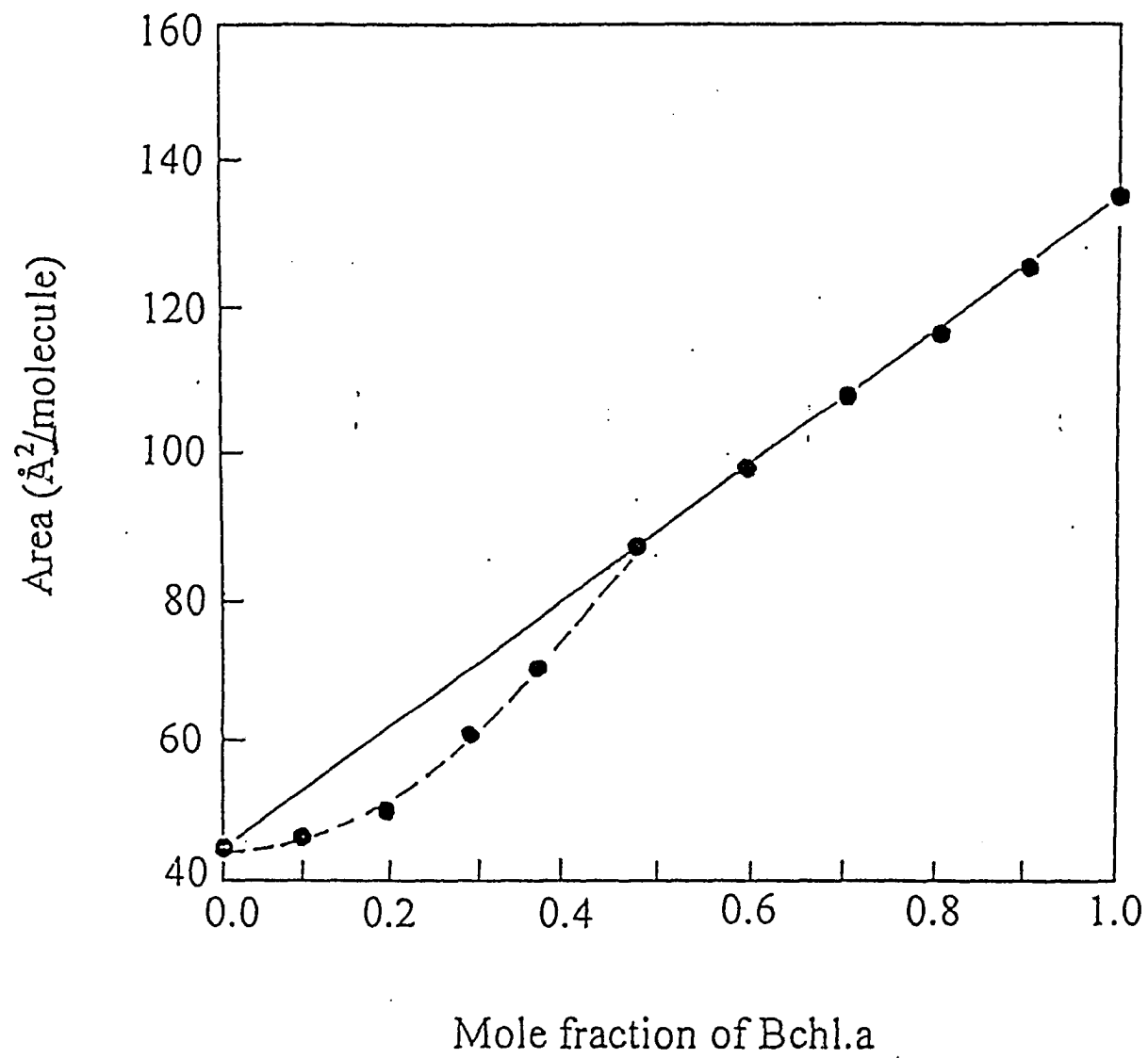


Figure 4. Mean area per molecule vs. BChl a molar fraction for mixed BChl a-DMPC monolayers.



areas and molar fraction of components 1 and 2, respectively. Any deviation of the experimental results from the eqn. 1 is interpreted as evidence for the interaction between the two components. In Figure 4, a negative deviation from this relationship is observed when the mole fraction of BChl α is below 0.4. This implies an interaction occurs between the two components in the mixed monolayers. However, when the mole fraction of BChl α is above 0.4, BChl α and DMPC do not show significant interaction. Therefore, it may be inferred that an immiscible binary phase forms in the mixed monolayers.

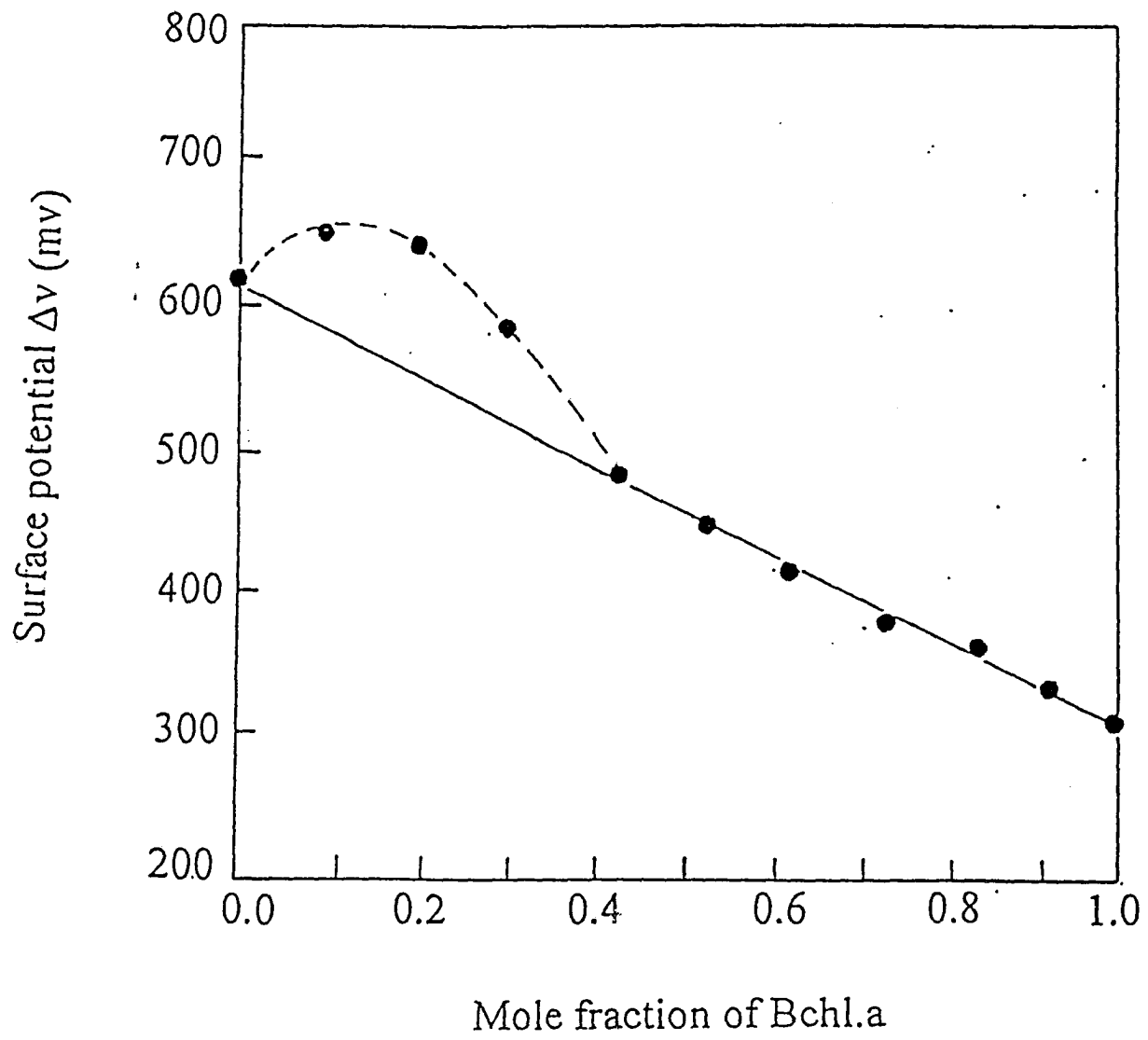
It is well known that the surface potential is also very sensitive to the interaction between two components in mixed monolayers. The additivity rule for the surface potential is as follows:

$$V_{12} = x_1V_1 + x_2V_2 \quad (2)$$

where V_{12} is the average surface potential of the mixture. V_1 , V_2 , and x_1 , x_2 are the surface potentials and mole fractions of components 1 and 2 respectively. In our experiments, evidence for the dependence of the interaction of BChl α and DMPC on their compositions was also obtained from the surface potential measurements, as shown in Figure 5. Deviations from the additivity rule of surface potential is observable only when the molar fraction of BChl α is below 0.4.

The collapse pressure of the BChl α -DMPC monolayers was also measured as a function of monolayer composition, as shown in Figure 6. According to the surface phase

Figure 5. Mean surface potential vs. BChl a molar fraction for mixed BChl a-DMPC monolayers.



rule [1], if the two components are immiscible in monolayers, the collapse pressures are invariant with change in monolayer composition. As can be seen from Figure 6, when the mole fraction of BChl *a* is below 0.4, the collapse pressure depends upon the monolayer composition, exhibiting a distinct maximum when the mole fraction of BChl *a* is 10%.

UV-Vis absorption spectra

Figure 7 shows the absorption spectra of BChl *a* in monolayers with and without DMPC and in solution for comparison. The spectrum of BChl *a* is characterized by an intense Soret band in the near-UV region composed of B_x (396 nm) and B_y (357 nm) components, a band of moderate intensity in the visible region, Q_x (578 nm) and another intense band in the near-infrared, identified as Q_y (780 nm), as shown in Figure 7a. It has been demonstrated that the Q_y band of BChl *a* strongly depends upon its environment [12]. From Figure 7b, it can be seen that the Q_y band of BChl *a* in a monolayer is near 795 nm as compared with that in solution. The red-shifted absorption band indicates that BChl *a* is aggregated in the monolayers. When BChl *a* monolayers are diluted by DMPC, the Q_y band of BChl *a* is shifted back to 780 nm only at low molar fraction of BChl *a*, as shown in Figure 7c. This indicates that aggregation of BChl *a* is prevented in the BChl *a*-DMPC mixed monolayers. However, at high mole fraction of BChl *a* (> 0.4), the red-shift of the Q_y band is still visible. In addition, it can be noted that the B_y/Q_y ratio is 1.25 in solution and 1.17 in monolayers. The slight decrease is probably due to either the partial oxidation of BChl *a* during the monolayer preparation or aggregation of BChl *a* in monolayers.

Figure 6. Collapse pressure vs. BChl a molar fraction for mixed BChl a-DMPC monolayers.

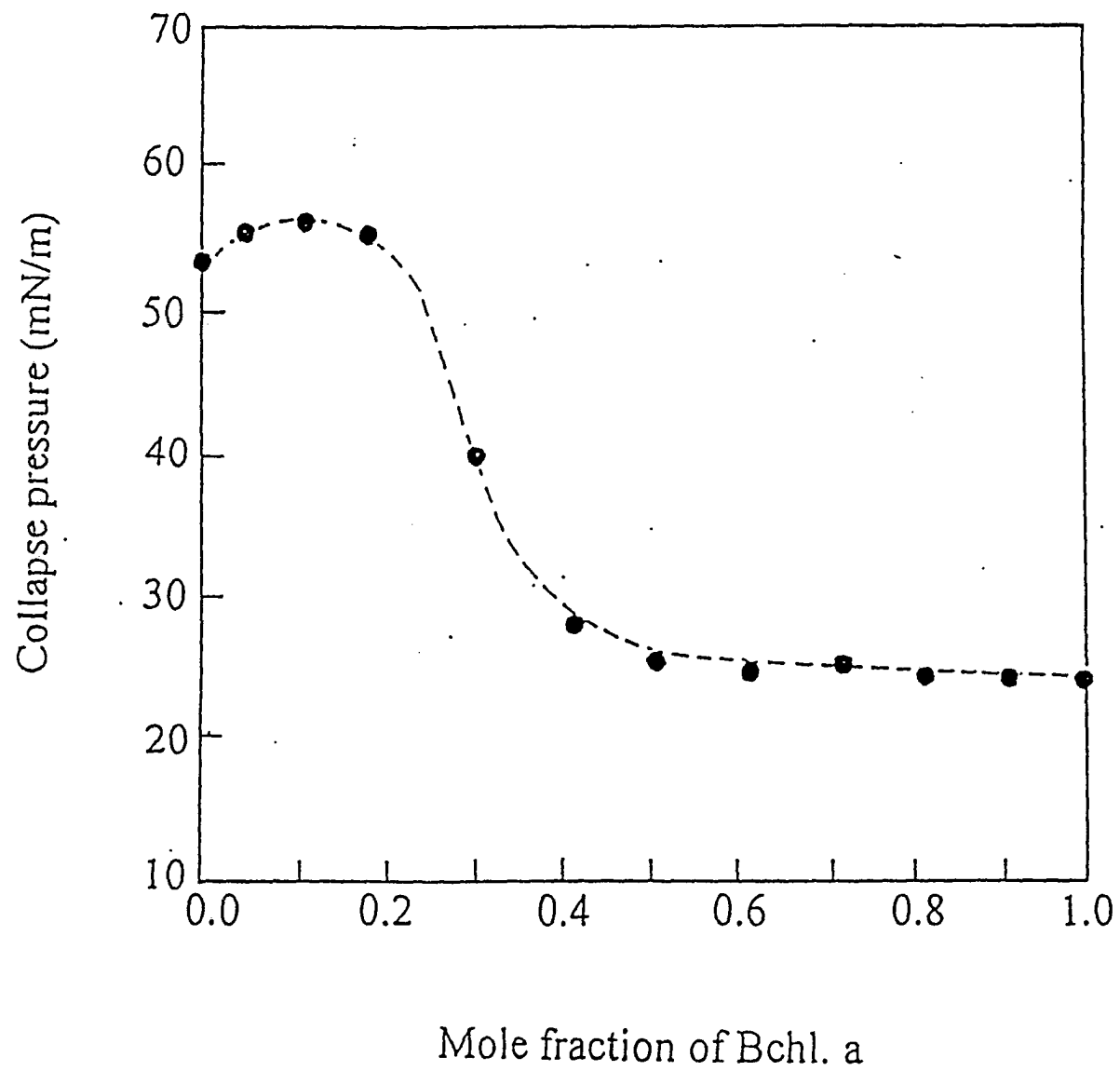
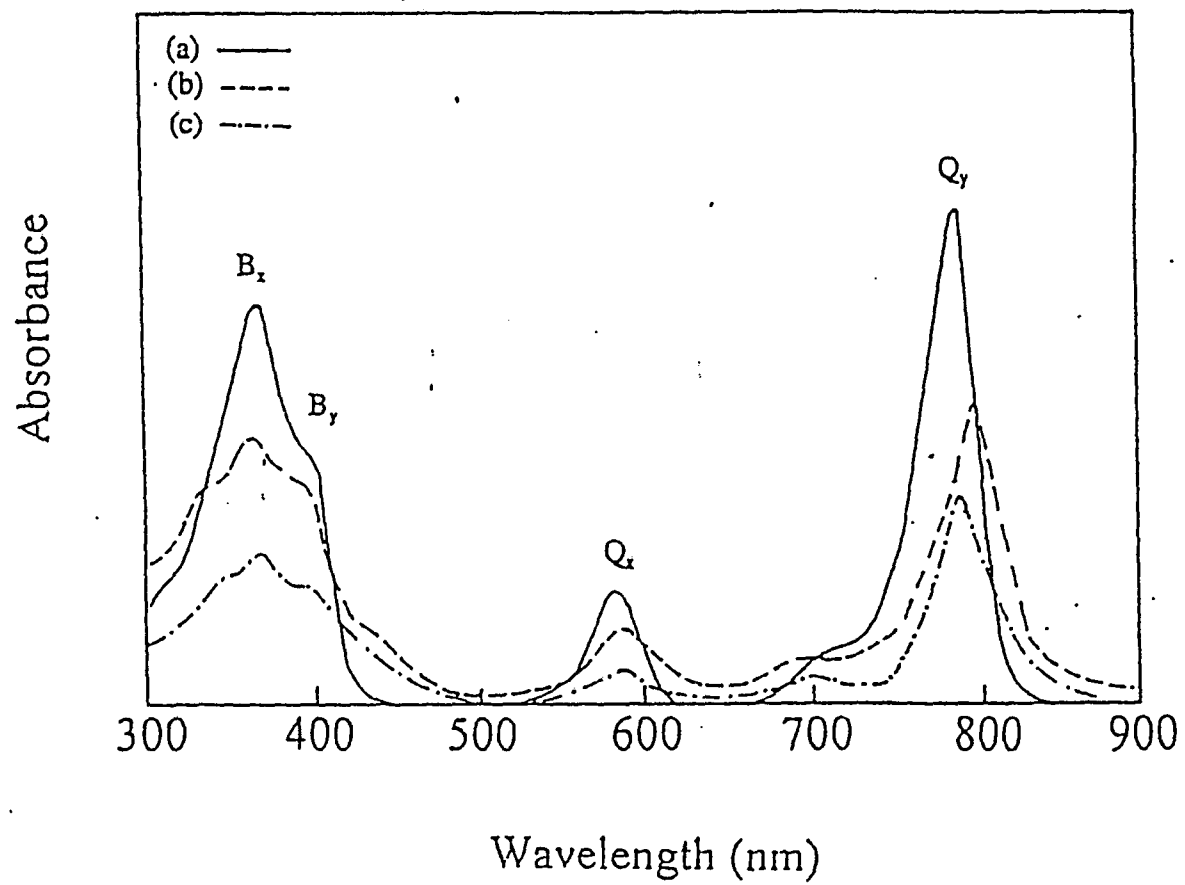


Figure 7. UV-Vis absorption spectra of BChl a in solution (a) and transferred L-s films without (b) and with (c) DMPC matrix molecule (Molar fraction of BChl a = 0.1).



SERRS

It is well known that surface-enhanced resonance Raman scattering (SERRS) is very powerful technique for studying the structure and molecular interactions of biological molecules adsorbed on metal surfaces [12]. SERRS has been successful applied to the study of photosynthetic reaction center monolayers [13]. It allows selective detection of the chromophores or prosthetic groups of the proteins in monolayers, such as chlorophyll and pheophytin.

Figure 8 shows SERRS spectra of BChl *a* in monolayers with and without DMPC excited at 406.7 nm. The Raman spectra exhibit several major bands associated with BChl *a* vibrations at 1610-1611, 1532-1536, 1349-1352 and 1290-1289 cm^{-1} , respectively. These Raman bands are assigned to C_aC_m , C_bC_b , C_aC_b , C_mH and C_aN stretching modes, respectively [14-15]. These major bands of BChl *a* are still visible for BChl *a* /DMPC mixed monolayers. In addition, a weak band due to oxidized BChl *a* is observed at 1555-1556 cm^{-1} for these two different monolayers, indicating the presence of partially oxidized BChl *a*.

Conclusions

BChl *a* has been studied in monolayers both with and without DMPC matrix molecules at the air-water interface by surface pressure-area and surface potential-area isotherms, and on solid supports by UV-Vis absorption spectra and surface-enhanced Raman scattering. The pure BChl *a* monolayers show strong hysteresis in the first compression-

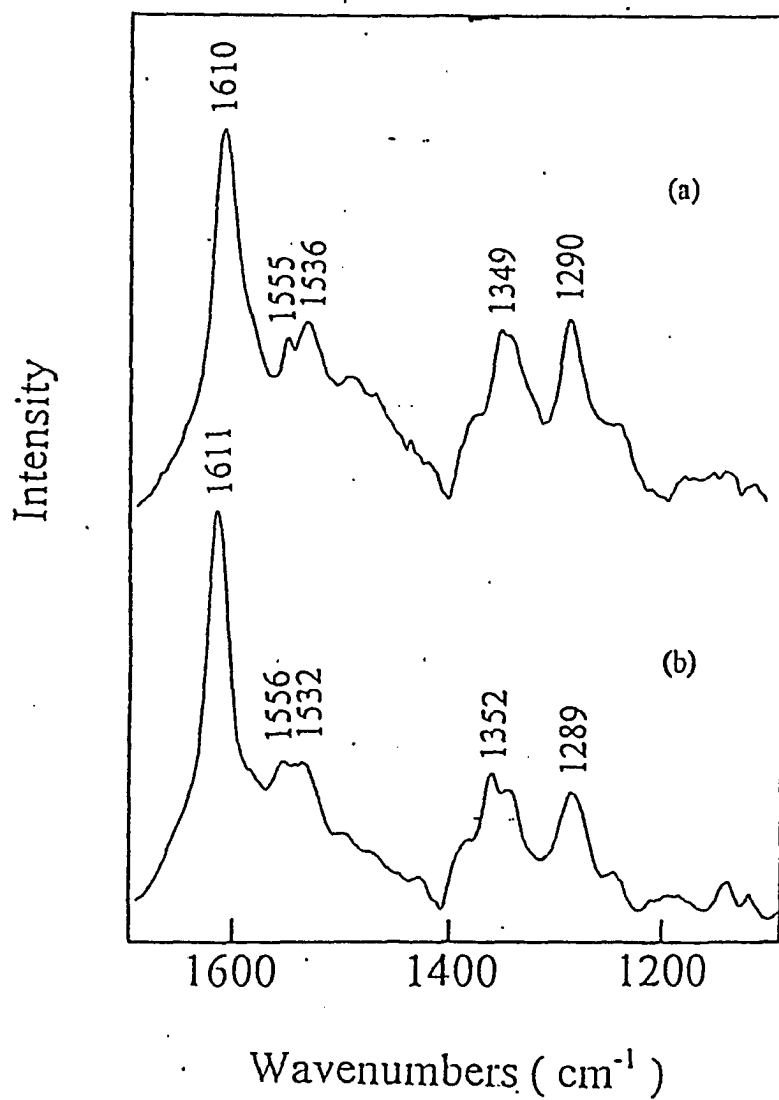


Figure 8. Surface-enhanced Raman spectra of BChl *a* in monolayers with DMPC (molar fraction of BChl *a* = 0.1)(a) and without DMPC (b) matrix.

expansion cycle, but become more stable after the subsequent cycles. The configuration of BChl *a* in the condensed monolayers is a folded molecule: its ester linkage group is anchored at the water surface, and its phytol chain and porphyrin ring are extended away from the water surface. The interaction of BChl *a* and DMPC in the mixed monolayer systems strongly depends on their relative mole fractions. At low molar fraction of BChl *a* (< 0.4), homogeneous mixed monolayer forms. While at high molar fraction of BChl *a* (> 0.4), an immiscible binary monolayer phase forms. UV-Vis absorption spectra show that aggregation of BChl *a* in the monolayers can be controlled using DMPC as a matrix molecule at high molar fractions. The major vibrational bands of BChl *a* in the monolayers, including C_aC_m , C_bC_b , C_aC_b , C_mH and C_aN stretching bands, are clearly observed in SERS spectra. The presence of partially oxidized BChl *a* in monolayers can be detected in these spectra.

References:

1. G. L. Gains, Jr. *Insoluble Monolayers at Liquid-Gas Interfaces*; Wiley, New York, 1972.
2. W. M. Reichert, C. J. Bruckner and J. Joseph, *Thin Solid Films*, 152 (1987) 345.
3. T. Moriizumi, *Thin Solid Films*, 160 (1988) 413.
4. T. Furuno, K. Takimoto, T. Kouyama, A. Ikegami and H. Sasabe, *Thin Solid Films*, 160 (1988) 154.
5. T. Miyasaka, K. Koyama and I. Itoh, *Science*, 255 (1992) 342.

6. M. Y. Okamura, G. Feher and N. Nelson, *In Photosynthesis: Energy Conversion by Plants and Bacteria*; Govindjee, Ed.; Academic Press, New York, 1982; Vol. 1, pp. 179-272.
7. P. Reinach, B. B. Aubrey and S. S. Brody, *Biochim. Biophys. Acta*, 314 (1973) 360.
8. Examples concerning Chl a monolayers at the air-water interface include: (a) A. F. Janzen, J. R. Bolton and M. J. Stillman, *J. Am. Chem. Soc.*, 101 (1979) 6337. (b) K. Iriyama, *J. Membrane Biol.*, 52 (1980) 115. (c) Tancrede, P.; Munger, G.; Leblanc. *Biochim. Biophys. Acta*, 689 (1982) 45. (d) H. Heithier, K. Ballschmiter and H. Mohwald, *Photochem. Photobiol.*, 37 (1983) 201. (e) G. Picard, G. Munger, R. M. Leblanc, R. Le Sage, D. Sharma, A. Siemiarczuk and J. R. Bolton, *Chem. Phys. Lett.*, 129 (1986) 41. (f) J. P. Chauvet, M. Agrawal and L. K. Patterson, *J. Phys. Chem.*, 92 (1988) 4218. (g) G. Picard, J. Aghion, C. Le Crom and R. M. Leblanc, *Thin Solid Films*, 180 (1989) 31. (h) B. Zelent, G. Munger, A. Helluy and R. M. Leblanc, *J. Photochem. Photobiol. A: Chem.*, 57 (1991) 373. (i) D. Frackowiak, B. Zelent, A. Helluy, M. Niedbalska, J. Goc and R. M. Leblanc, *J. Photochem. Photobiol. A: Chem.*, 69 (1992) 213. (j) A. E. Sounni and R. M. Leblanc, *Langmuir*, 8 (1992) 1578.
9. H. H. Strain and W. A. Svec, *The Chlorophylls*, Vernon and Seeley, Eds.; Academic Press, New York, 1966.
10. J. Richard, A. Barraud, M. Vandevyver and A. Ruadel-TeXier, *Thin Solid Films*, 159 (1988) 207.

11. J. C. Watkins, *Biochim. Biophys. Acta*, *152* (1968) 293.
 12. See a review: T. M. Cotton, *In Advances in Spectroscopy: Spectroscopy of Surfaces*.
Clark and Hester. Eds.; Wiley and Sons, New York, 1988, pp. 91-153
 13. G. Chumanov, R. Picorel, S. Toon, M. Seibert and T. M. Cotton, *Photochem. Photobiol.*,
58 (1993) 757.
 14. P. M. Callahan and T. M. Cotton, *J. Am. Chem. Soc.*, *109* (1987) 7001.
 15. N. J. Bolt, R. J. Donohoe, R. R. Brige and D. F. Bocian, *J. Am. Chem. Soc.*, *109*
(1987) 2284.
-

SUMMARY

Monolayers composed of different systems of molecules have been studied in the research of this dissertation. Several different techniques were used to characterize these monolayers. These techniques have made it possible to investigate the morphology of the monolayers on a molecular level.

In Chapter 2, newly discovered Fullerene C_{60} and its derivatives were studied using neutron and X-ray reflection techniques. Because of the nature of neutron and X-ray irradiation, the film thickness and in-plane structure can be ascertained. It was found that C_{60} is highly aggregated at the air-water interface due to its lack of amphiphilic character. However, by introducing amine groups on the fullerene molecules, aggregation was significantly reduced. The neutron and X-ray reflection data can be rationalized by a single model structure defined in terms of the dimensions of an average cell and its chemical composition. For the amine adduct, this model ascribes a total thickness of about 29 Å to the molecular interface layer with the internal structure defined as follows. The fullerenes form a central stratum and the remainder alkyl tails are located close to both the air and the water interfaces. The alkyl moieties close to the aqueous substrate are hydrated. By contrast, neutron reflection and surface pressure vs. area data of spread films of pure C_{60} on aqueous surfaces indicate the formation of inhomogeneous multilayer films with a thickness and a surface roughness exceeding the molecular size. These underivatized fullerenes, thus, do not form monomolecular films.

The formation of nanoscale size particles within a channel protein MIP-26 monolayer was studied in Chapter 3. The synthesis of uniform nanoscale semiconductor particles remains challenging because of the difficulty of controlling the reaction volume. This study demonstrates a new method for preparing nanoscale particles using MIP-26 channel protein as a micro reaction vessel. The cadmium and zinc sulfides were produced in the "quantum dot" size range as evidenced by their markedly blue-shifted optical spectra.

In Chapter 4, monolayer characteristics were determined for three isomeric phospholipids and their daughter compounds. These phospholipids have relatively high solubility in the aqueous subphase and stable monolayers could not be formed under these conditions. Aqueous 30% polyethylene glycol was shown to be appropriate as a non-water subphase. Surface potential measurements were carried out as well as surface pressure/area isotherms. The apparent areas/molecule obtained from the isotherms were larger than expected based on estimates from CPK models, even assuming that all of the alkyl chains lie flat at the interface and are never elevated above it to any appreciable degree, even at high compression. The disparities between measured and estimated molecular areas are probably due to two effects: chirality in the systems and occlusion of void areas present in many of the planar conformational states.

Monolayer and spectroscopic studies of Bacteriochlorophyll *a* (BChl *a*) were performed in Chapter 5. BChl *a* occurs in purple photosynthetic bacteria and plays an important role in the primary events of the photosynthetic process. Surface pressure/area isotherms and surface potential measurements were carried out at the nitrogen-water

interface. Mixed monolayers were prepared using dimyristoylphosphatidylcholine (DMPC) as a matrix material. UV-Vis spectra and surface-enhanced Raman scattering spectra were recorded in order to obtain information about BChl *a* aggregations. The results indicated that pure BChl *a* monolayers show strong hysteresis in the first compression-expansion cycle and become more stable after subsequent cycles. The interaction of BChl *a* and DMPC in the mixed monolayer systems strongly depends on their relative mole fractions. At low mole fractions of BChl *a*, homogeneous mixed monolayers form. In contrast, at higher mole fractions of BChl *a*, an immiscible binary phase forms. UV-Vis absorption spectra show the aggregation of BChl *a* in monolayers can be controlled using DMPC as matrix molecule. The presence of partially oxidized BChl *a* in monolayers was identified in SERRS spectra.

REFERENCES

1. S. Mann, *MRS Bulletin, October* (1992) 32 and references cited therein.
2. C. Jehoulet, Y. S. Obeng, Y-T Kim, F. Zhou and A. J. Bard, *J. Am. Chem. Soc.*, *114* (1992) 4237.
3. D. M. Cox, S. Behal, M. Disko, S. M. Gorun, M. Greaney, C. S. Hsu, E. B. Kollin, J. Miller, W. Robbins, R. D. Sherwood and P. Tindall, *J. Am. Chem. Soc.*, *113* (1991) 2940.
4. P. M. Allemand, A. Koch, F. Wudl, Y. Rubin, F. Diederich, M. M. Alvarez, S. J. Anz and R. L. Whetten, *J. Am. Chem. Soc.*, *113* (1991) 1050.
5. J. W. Arbogast, A. P. Darmany, C. S. Foote, Y. Rubin, F. N. Diederich, M. M. Alvarez, S. J. Anz and R. L. Whetten, *J. Phys. Chem.*, *95* (1991) 11.
6. T. W. Ebbesen, K. Tanigaki and S. Kuroshima, *Chem. Phys. Lett.*, *181* (1991) 501.
7. M. R. Wasielewski, M. P. O'Neil, K. R. Lykke, M. J. Pellin and D. M. Gruen, *J. Am. Chem. Soc.*, *113* (1991) 2774.
8. R. J. Sension, C. M. Phillips, A. Z. Szarka, W. J. Romanow, A. R. McGhie, J. P. McCauley, Jr., A. B. Smith and R. M. Hochstrasser, *J. Phys. Chem.*, *95* (1991) 6075.
9. R. R. Hung, J. J. Grabowski, *J. Phys. Chem.*, *95* (1991) 6073.
10. J. W. Arbogast, C. S. Foote, *J. Am. Chem. Soc.*, *113* (1991) 886.
11. K. Yanigaki, T. W. Ebbesen and S. Kuroshima, *Chem. Phys. Lett.*, *185* (1991) 189.

12. Y. Kajii, T. Nakagawa, S. Suzuki, Y. Achiba, K. Obi and K. Shibuya, *Chem. Phys. Lett.*, **181** (1991) 100.
13. P. V. Kamat, *J. Am. Chem. Soc.*, **113** (1991) 9705.
14. N. M. Dimitrijevic, P. V. Kamat, *J. Phys. Chem.*, **96** (1992) 4881.
15. M. Gevaert and P. V. Kamat, *J. Phys. Chem.*, **96** (1992) 9883.
16. R. E. Haufler, J. Conceicao, L. P. F. Chibante, Y. Chai, N. E. Byrne, S. Flanagan, M. M. Haley, S. C. O'Brien, C. Pan, Z. Xiao, W. E. Billups, M. A. Chiufolini, R. H. Hauge, J. L. Margrave, L. J. Wilson, R. Curle and R. E. Smalley, *J. Phys. Chem.*, **94** (1990) 8634.
17. J. W. Bausch, G. K. Surya Prakash, G. A. Olah, D. S. Tse, D. C. Lorents, Y. K. Bae, and R. Malhotra, *J. Am. Chem. Soc.*, **113** (1991) 3205.
18. J. H. Holloway, E. G. Hope, R. Taylor, G. J. Langley, A. G. Avent, D. T. John, J. P. Hare, H. W. Kroto and D. R. M. Walton, *Chem. Commun.*, (1991) 966.
19. G. A. Olah, I. Bucsí, C. Lambert, R. Aniszfeld, N. J. Trivedi, D. K. Sensharma and G. K. Surya Prakash, *J. Am. Chem. Soc.*, **113** (1991) 9387.
20. T. Suzuki, Q. Li, K. C. Khemani, F. Wudl and O. Almarsson, *Science*, **254** (1991) 1186.
21. F. Wudl, in Amato I: Bucky balls, Hairy balls, Dopey balls, *Science*, **252** (1991) 646.
22. F. Wudl, A. Hirsch, K.C. Khemani, T. Suzuki, P.-M. Allemand, A. Koch, H. Eckert, G. Srdanov and H. M. Webb, in G.S. Hammond and V.J. Kuck(eds.), *Fullerenes, Synthesis, Properties, and Chemistry of Large Carbon Clusters*, American Society, Washington, D. C., 1992, p. 161.

23. Y. S. Obeng and A. J. Bard, *J. Am. Chem. Soc.*, *113* (1991) 6279.
24. G. Williams, C. Pearson, M. R. Bryce and M. C. Petty, *Thin Solid Films*, *209* (1992) 150.
25. J. Milliken, D.D. Dominguez, H. H. Nelson and W. R. Barger, *Chem. Mater.*, *4* (1992) 252.
26. T. Nakamura, H. Tachibana, M. Yumura, M. Matsumoto, R. Azumi, M. Tanaka and Y. Kawabata, *Langmuir*, *8* (1992) 4.
27. J. Guo, Y. Xu, Y. Li, C. Yang, Y. Yao, D. Zhu and C. Bai, *Chem. Phys. Lett.*, *195* (1992) 625.
28. P. Ganguli, D. V. Paranjape, K. R. Patil, S. K. Chaudhary and T. Kshrsagar, *Indian J. Chem.*, *31* (1992) F42.
29. R. Back and R. B. Lennox, *J. Phys. Chem.*, *96* (1992) 8149.
30. M. Iwahashi, K. Kikuchi, Y. Achiba, I. Ikemoto, T. Arki, T. Mochida, S. Yokoi, A. Tanaka and K. Iriyama, *Langmuir*, *8* (1992) 2980.
31. F. Diederich, J. Effing, E. Jones, L. Jullien, T. Plesniviy, H. Ringsdorf, C. Thilgen and D. Weinstein, *Angew. Chem. int. Ed. Engl.*, *31* (1992) 1599.
32. A. Henglein, *Chem Rev.*, *89* (1989) 1861 and references cited therein.
33. J. H. Fendler, *Chem. Rev.*, *87* (1987) 877.
34. S. Mann, A. J. Skarnulis and R. J. P. Williams, *Isr. J. Chem.*, *21* (1982) 3.
35. L. Motte, C. Petit, L. Boulanger, P. Lixon, and M. P. Pileni, *Langmuir*, *8* (1992) 1049.
36. Y. Wang and W. Mahler, *Opt. Commun.*, *61* (1987) 233.

37. A. J. Ekimov and A. Onushchenko, *JETP Lett.*, 40 (1984) 1136.
38. Y. Wang and N. Herron, *J. Phys. Chem.*, 91 (1987) 257.
39. R. Rossetti, R. Hull, J. M. Gibson and L. E. Brus, *J. Chem. Phys.*, 82 (1985) 552.
40. J. G. Brennan, T. Siegrist, P. J. Carrol, S. M. Stuczynski, L. E. Brus and M.L. Steigerwald, *J. Am. Chem. Soc.*, 111 (1989) 4141.
41. D. A. Jaeger, J. Jamrozik, T. G. Golich, M. W. Clannan and J. Mohebalian, *J. Am. Chem. Soc.*, 111 (1989) 3001.
42. D. Ono, A. Masuyama and M. Okahara, *J. Org. Chem.*, 55 (1990) 4461.
43. A. Sokolowski, A. Piasecki and B. Burczyk, *J. Am. Oil Chem.*, 69 (1992) 633.
44. H. Ringsdorf, B. Schlarb and J. Venzmer, *Angew. Chem., Int'l Ed. Engl.*, 27 (1988) 113.
45. Okamura, M. Y.; Feher, G.; Nelson, N. *In Photosynthesis: Energy Conversion by Plants and Bacteria*; Govindjee, Ed.; Academic Press, New York, 1982; Vol. 1, pp 179-272.
46. Reinach, P.; Aubrey, B. B.; Brody, S. S. *Biochim. Biophys. Acta.* 1973, 314. 360.

ACKNOWLEDGEMENTS

I would like to express my appreciation to my research advisors Dr. Cotton and Dr. Uphaus for their support and encouragement throughout the course of this work. I am very grateful for what they have done for me and it was a great pleasure to work with them. I also want to thank Dr. David Vaknin for his patience and guidance. I appreciated his help and support both during the trip to Denmark and at home. My sincere thanks also go to every member of the Cotton research group: Jae-Ho, Jeanne, John, Chengli, Hung, Al, Dale, George, Morgan, Brian G. and Brian C. I enjoyed working with you guys and good luck to all of you in whatever you do in the future.

I also want to thank my friends who helped and encouraged me during the past four years. Finally, I want to thank my parents for their love and support; their encouragement and belief in me made me stronger through my difficult times.